Chapter 12
Precipitation Technologies for Nanoparticle Production

Julien Maincent and Robert O. Williams III

Abstract Precipitation technologies have been widely studied for nanoparticle production because they provide more control over particle size, shape, and morphology as compared to mechanical processes, such as milling and homogenization. Several precipitation processes are discussed in this chapter, with special attention to experimental parameters and typical particle attributes. The chapter also touches on novel nanoparticle recovery techniques that may be coupled with precipitation processes to enable these precipitation technologies to be scaled for commercial applications. The current authors would like to thank and acknowledge the significant contribution of the previous authors of this chapter from the first edition. This current second edition chapter is a revision and update of the original authors' work.

Keywords Milling • Homogenization • Phase separation • Supersaturation • Equilibrium • Compressed fluids • Supercritical fluids (SCF) • Gaseous antisolvent (GAS) • Ultrasonic dispersion devices • Rapid expansion of supercritical solutions (RESS) • Evaporative precipitation into aqueous solution (EPAS) • Controlled precipitation (CP) • Floc • Microprecipitated bulk powder (MBP)

12.1 Introduction

It has been reported that 40 % or more of newly discovered drug candidates are poorly water soluble, often resulting in poor and/or erratic bioavailability (Lipinski 2001, 2002). Consequently, the majority of poorly water-soluble drugs fail to reach the market because their absorption into the body is limited by their slow dissolution rates in bodily fluids (Gardner et al. 2004; Rabinow 2004; Kipp 2004; Crison 2000). Traditional approaches to improving drug dissolution rates have focused on

J. Maincent • R.O. Williams III (✉)
Division of Pharmaceutics, College of Pharmacy, The University of Texas at Austin, 1 University Station A1920, Austin, TX 78712-0231, USA
e-mail: julien.maincent@utexas.edu; Bill.Williams@austin.utexas.edu

R.O. Williams III et al. (eds.), *Formulating Poorly Water Soluble Drugs*, AAPS Advances in the Pharmaceutical Sciences Series 22,
DOI 10.1007/978-3-319-42609-9_12

increasing the drug's solubility, often utilizing solubilizing excipients (CREMPHOR EL[1] (polyethoxylated castor oil) is added to TAXOL),[2] complexing agents (cyclodextrins and polyethylene glycols), or cosolvents (ethanol–water solvent mixtures) (Rabinow 2004; Kipp 2004; Muller et al. 2001). However, the success of these approaches has been limited due to the large quantities of excipients required to achieve sufficient solubilities, which increase the likelihood of adverse side effects in patients and limits drug loading (Rabinow 2004; Kipp 2004; Muller et al. 2001). For example, the marketed product SPORANOX IV[3] requires 400 mg of 2-hydroxypropyl-β-cyclodextrin to solubilize 10 mg of the active ingredient, itraconazole (Sporanox Package Insert). Similar limitations impact the utilization of lipid-based formulations, which employ liposomes and emulsions to address solubility issues (Rabinow 2004). Solubilization of drugs using lipid-based methods leads to drug loadings well below 50 % w/w (Matteucci et al. 2006) and often below ~10 % w/w, especially for high-melting-point compounds, thus restricting their use in high-dose formulations (Rabinow 2004; Kipp 2004; Muller et al. 2001). Consequently, only a small number of commercialized pharmaceutical products are based on these strategies (Muller et al. 2001).

An alternative approach to enhancing the dissolution rates of poorly water-soluble drugs has been to formulate the drugs as nanoparticles, loosely defined in the pharmaceutical industry as structures with a diameter less than 1 μm. According to the Noyes–Whitney equation, which is based on Fick's first law of diffusion, dissolution rates of drug particles may be enhanced by increasing the drug's solubility in aqueous media (C_{Eq}) and/or by reducing particle size, which increases the surface area for adsorption (A) and decreases the boundary layer thickness (h) (Noyes and Whitney 1897):

$$\frac{\partial M}{\partial t} = \frac{DA}{h}\left(C_{Eq} - C_{Bulk}\right), \tag{12.1}$$

where M is the mass of undissolved drug, t is the time, D is the average diffusion coefficient, and C_{Bulk} is the drug concentration in the bulk solution. Nanoparticle formulations offer several advantages over lipid-based solubilization methods for improving drug dissolution rates. Unlike lipid-based techniques, particle formation processes are more amenable to compounds that have low solubility in both water and oils, which is often the case for high-energy crystals (Rabinow 2004). Additionally, by circumventing the need to deliver a dissolved compound, the drug's preferred crystalline state may be preserved during delivery and storage (Rabinow 2004). Furthermore, solid nanoparticles facilitate higher drug loadings than solubilized formulations, which is crucial for high-dose compounds.

Nanoparticles may be produced by top-down or bottom-up approaches. Top-down approaches refer to mechanical processes, such as milling and homogenization,

[1] CREMPHOR EL is a registered trademark of BASF Corporation.

[2] TAXOL (paclitaxel) is a registered trademark of Bristol-Myers Squibb Company.

[3] SPORANOX IV is a registered trademark of Janssen Pharmaceutical Products, LP.

and use high-impact forces to break large particles into smaller particles. Particles with median diameters of 300–400 nm are commonly produced by these methods, and particles smaller than 200 nm have been reported for the poorly water-soluble drugs danazol (average particle diameter of 169 nm) (Liversidge and Cundy 1995) and atovaquone (average particle diameter of 100 nm) (Dearn 1994; Westesen and Siekmann 1998) using top-down methods. However, the high-energy inputs required to achieve these levels of size reduction may subject the drug to chemical degradation, often through thermal degradation, due to the considerable amount of heat that is often generated during milling and homogenization processes (Jacobs et al. 2000; Liversidge et al. 2003; Muller and Bohm 1997). These high-energy methods are also prone to producing partially amorphous drug domains, complicating control of crystalline morphology, and thus drug stability (Chan and Chew 2003). Moreover, these methods often require lengthy processing times, risk contamination with impurities, and are subject to low process yields (Muller et al. 2001). In contrast, bottom-up approaches refer to solution-based precipitation techniques that induce phase separation of the drug (originally in solution) from the solvent. Precipitation is driven by a deviation from phase equilibrium conditions, where typical supersaturation driving forces are gradients in concentration or temperature. This chapter will focus on precipitation processes where supersaturation of a drug solution produces nucleation and growth under controlled conditions to influence particle formation. Supersaturation, S, is defined as the solute concentration (C_{drug}) relative to that under equilibrium conditions ($S = C_{\text{drug}}/C_{\text{eq}}$). Freezing-induced nanoparticle precipitation methods (based on a thermal driving force) are discussed in detail in review articles by Overhoff et al. (2007a, 2009).

In non-freezing-based precipitation techniques, the poorly water-soluble drug is typically dissolved in a solvent and precipitation of the drug is initiated by a reduction in solvent power, by either addition of an antisolvent or solvent evaporation. A reduction in solvent powder leads to supersaturation of the drug and drives nucleation of drug particles. Once nucleation occurs, the particles grow by condensation, in which dissolved drug molecules diffuse to the particle surface and integrate into a solid particle, and/or by coagulation, where multiple particles collide and aggregate to form larger particles (Fig. 12.1) (Weber and Thies 2002). Stabilizers may be added to the system to arrest particle growth.

Particle nucleation and growth are competing processes. The degree of supersaturation, S, significantly impacts nucleation rates, as seen in the equation describing primary nucleation rate, B^0 (Sohnel and Garside 1992)

$$B^0 \propto \exp\left(-\frac{16\pi\gamma^3 V_M{}^2 N_A}{3(RT)^3 \left[\ln(1+S)\right]^2} \right), \tag{12.2}$$

where γ is the interfacial tension, V_{M} is the molar volume, N_{A} is Avogadro's number, R is the ideal gas law constant, and T is the temperature. According to (12.2), nucleation rates increase as the degree of supersaturation increases. However, supersaturation levels decrease as particles grow by condensation, due to a reduction in the solute mass in

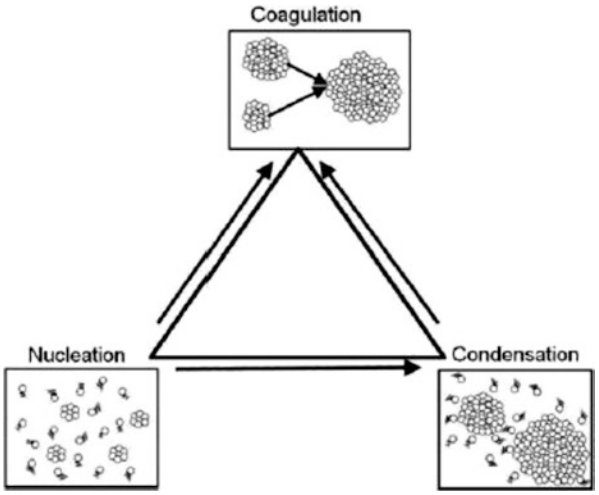

Fig. 12.1 Mechanism of precipitation. Adapted from Weber and Thies (2002)

solution. Hence, condensation competes with nucleation. Furthermore, coagulation competes with condensation by reducing the total number of particles, and thus surface area, in the system (Matteucci et al. 2006). Therefore, final particle properties, including size distribution and morphology, are heavily impacted by the processing parameters that influence nucleation and growth rates (e.g., solvent choice, stabilizer selection, and mixing rates). Rapid generation of supersaturation over a narrow time interval facilitates more narrow PSDs. Therefore, faster nucleation rates, relative to growth, favor the production of uniformly smaller particles.

Relative to top-down approaches (milling and homogenization processes), precipitation technologies are typically more controlled, in terms of consistently producing particles with similar morphologies, and offer the ability to achieve higher drug loadings (Matteucci et al. 2006, 2007; Overhoff et al. 2007a, b; Engstrom et al. 2007, 2008; Rasenack and Muller 2002; Rogers et al. 2004; Shoyele and Cawthorne 2006; Vaughn et al. 2005; Young et al. 2000). Precipitation processes are often easier to scale-up and require less particle handling than milling and homogenization operations, resulting in higher process yields and lower impurity risks, as well as simplified cleaning and sterilization procedures (Rogers et al. 2001a). Additionally, precipitation technologies may be operated as continuous or semicontinuous processes, whereas milling and homogenization operations are batch processes (Rogers et al. 2001a). This chapter will focus on several different approaches to nanoparticle precipitation that are relevant to pharmaceutical drug development, highlighting key advances and important processing parameters for various active pharmaceutical ingredients (API). Precipitation processes utilizing compressed or supercritical fluids, as well as aqueous media, as antisolvents, will be summarized. Furthermore, novel modifications to conventional precipitation processes will be discussed, in addition to several techniques that have been used to harvest the resultant nanoparticles after precipitation, including flocculation-based processes.

12.2 Precipitation Processes Utilizing Compressed or Supercritical Fluids

Compressed fluid and supercritical fluid (SCF) antisolvent precipitation processes offer several advantages over more conventional liquid antisolvent processes. The antisolvent may be completely removed via pressure reduction to the gaseous phase, resulting in improved product purities and reduced environmental and toxicity concerns. A SCF is a fluid that has been compressed beyond its critical pressure (P_c) or heated above its critical temperature (T_c). An important feature of SCFs is that their densities can change significantly with small changes in pressure. These density changes give rise to variations in diffusivity and viscosity, as well as the solubility of other solvents and small solutes. Typical diffusivities of SCFs are on the order of 10^{-3} cm^2/s (~100 times greater than that for liquids) and their viscosities are on the order of 10^{-4} g/cm/s (~100 times lower than that for liquids). These favorable mass transfer properties facilitate rapid diffusion of the SCF antisolvent into a liquid solvent, which enables rapid supersaturation and nucleation, thus favoring the production of small particles.

Several commonly used SCFs are listed in Table 12.1 (Sekhon 2010). Of these fluids, carbon dioxide (CO_2) is the most prevalently used in pharmaceutical applications because it is inexpensive, nonflammable, and nontoxic. Figure 12.2 shows how small changes in pressure and temperature result in significant changes in the density of CO_2, which in turn, largely affects the solubility of small molecules in CO_2 (Fig. 12.3). The density of CO_2, as a function of pressure (P) and temperature (T), may be obtained from the NIST Standard Reference Database (http://webbook.nist.gov) or calculated as follows (Jouyban et al. 2002):

Table 12.1 Critical constants for select supercritical fluids (SCF)

SCF	T_c (°C)	P_c (bar)	Safety hazard
Trifluoromethane (fluoroform)	25.9	47.5	
Chlorotrifluoromethane	28.9	39.2	
Ethane	32.3	48.8	Flammable gas
Carbon dioxide	31.1	73.7	
Dinitrogen monoxide (laughing gas)	36.5	72.6	May enhance combustion of other substances
Sulfur hexafluoride	45.5	37.6	
Chlorodifluoromethane (HCFC 22; R22)	96.4	49.1	Combustible under certain conditions
Propane	96.8	43.0	Extremely flammable
Ammonia	132.4	112.7	Flammable and toxic
Trichlorofluoromethane (CFC 11; R11)	198.0	44.1	
Water	374.0	220.5	

Adapted from Gupta (2006)

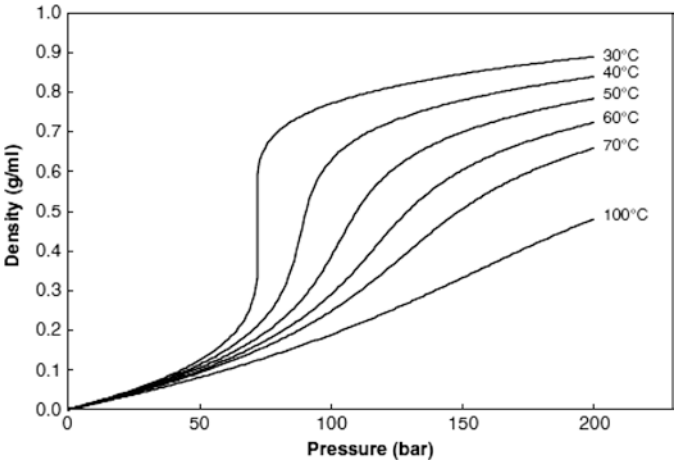

Fig. 12.2 Dependency of CO_2 density on pressure and temperature. Data from NIST Standard Reference Database (http://webbook.nist.gov/chemistry)

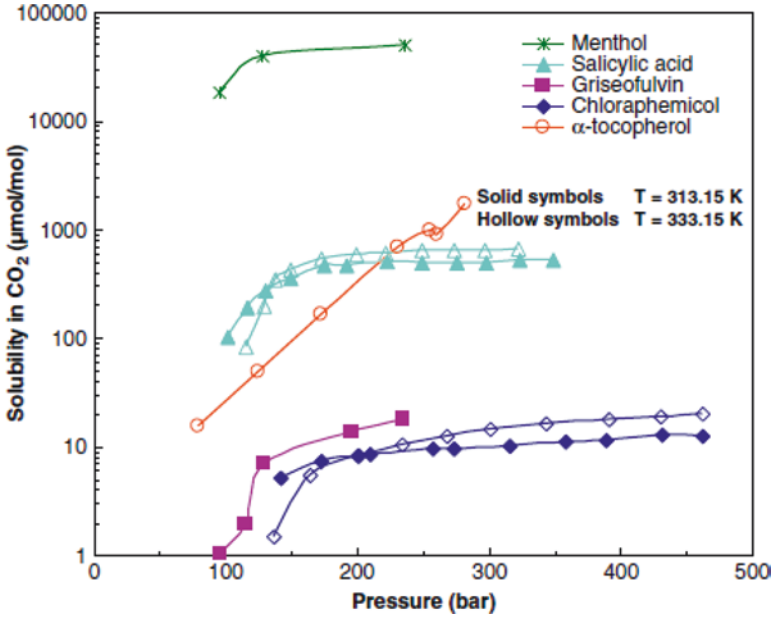

Fig. 12.3 Solubility of several drug compounds in CO_2 at varying pressures and temperatures. Data adapted from Gupta (2006)

$$\rho_{CO_2} = \frac{1}{44}\exp\left(-27.091 + 0.609\sqrt{T} + \frac{3966.170}{T} - \frac{3.445P}{T} + 0.401\sqrt{P}\right), \tag{12.3}$$

where ρ_{CO_2} is in moles/mL, T is in Kelvin, and P is in bars.

In addition to CO_2 density, a drug's solubility in supercritical CO_2 ($scCO_2$) is dependent upon the drug's vapor pressure and drug–CO_2 interaction. The following empirical correlation for drug solubility in CO_2 was developed by Mendez-Santiago and Teja (1999):

$$\gamma_2 = \frac{10^6}{P}\exp\left(\frac{A}{T} + \frac{B\rho_1}{T} + C\right), \tag{12.4}$$

where γ_2 is in μmol/mol, P is in bars, T is in Kelvin, ρ_1 is the CO_2 density in mols/mL, and the constants A, B, and C are empirical constants (values for various drug molecules are listed in Table 12.2). Accurate knowledge of a drug's solubility in CO_2 is necessary to reliably produce adequate process yields.

SCF precipitation techniques fall into three major categories (1) gas antisolvent precipitation (GAS), (2) precipitation with a compressed antisolvent (PCA), and (3) rapid expansion from supercritical solutions (RESS). PCA processes are also commonly referred to as aerosol solvent extraction system (ASES), solution-enhanced dispersion by supercritical fluids (SEDS), and supercritical antisolvent (SAS). The differences between these different precipitation techniques are discussed in the following sections of this chapter.

12.2.1 Precipitation with a Gaseous Antisolvent (GAS)

GAS precipitation is a batch process, in which the SCF antisolvent, often CO_2, is added to an organic solution containing dissolved API. Typical operating pressures for this process are 5–8 MPa, in the range where CO_2 is highly soluble in most organic solvents (Martin and Cocero 2008). As the CO_2 dissolves into the solute-rich liquid phase, the solvent strength decreases. Consequently, the API's solubility in the solvent decreases which generates supersaturation of the API and promotes nucleation and precipitation. In some cases, additional excipients may also be dissolved in the organic drug solution to precipitate the API within an excipient matrix. In order to induce rapid drug nucleation, which favors the production of small particles, CO_2 must be readily soluble in the organic solvent and the API must have low solubility in CO_2. Excessive solubility of the API in CO_2 would facilitate particle growth. Under optimal operating conditions, CO_2's high solubility and favorable transport properties in the organic solvent facilitate homogenous supersaturation conditions more rapidly than can be achieved using liquid

Table 12.2 Values of empirical constants used to determine drug solubility in CO_2 using (12.4)

Drug	*A*	*B*	*C*
7-Azaindole	–8412	87,110	20.66
Behenic acid	–4473	61,240	6.8
Biphenyl	–10,200	132,800	25.75
Brassylic acid	–10,860	146,100	21.01
Capsaisin	–7172	70,830	19.54
Cholecalciferol	–9784	172,500	18.42
Diphenylamine	–18,720	397,100	33.4
Eicosanoic acid	–15,990	161,600	36.97
1-Eicosanol	–14,530	122,500	36.15
Endrin	–9912	167,800	20.29
Ergocalciferol	–1092	173,500	21.51
Flavone	–11,430	110,100	27.38
D(–)-Fructose	–871.2	10,740	–4.29
D(+)-Glucose	847.1	2471	–9.12
3-Hydroxyflavone	–9746	81,530	21.31
Ketoprofen	–12,090	157,500	24.72
Medroxyprogesterone acetate	–10,270	186,100	17.77
Methoxychlor	–12,670	184,100	27.38
Monocrotaline	–10,440	8057	20.28
Mystiric acid	–17,250	173,100	44.84
Naproxen	–9723	122,900	18.11
Narasin	–8529	124,900	13.86
Nifedipine	–10,020	168,500	15.92
Nimesulide	–13,820	186,900	28.14
Nitrendipine	–9546	151,400	15.91
Octacosane	–19,860	123,000	52.555
1-Octadecanol	–17,290	141,000	45.32
Palmityl behenate	–8378	59,180	18.44
Penicillin V	–6459	73,730	13.29
Phenylacetic acid	–13,730	14,450	35.78
Piroxicam	–10,560	18,130	17.57
Progesterone	–12,090	21,040	23.43
t-Retinol	–8717	168,900	16.6
Salinomycin	–18,990	185,500	42.05
Stigmasterol	–13,010	169,000	25.23
Testosterone	–14,330	238,300	26.42
Theobromine	–7443	114,000	8.31
Theophylline	–6957	94	760
Triacontane	–22,965	199,800	57.22
Trioctylphosphine oxide	–9378	211,900	17.65
Vanillin	–7334	136,500	14.53

Data from Gupta (2006)

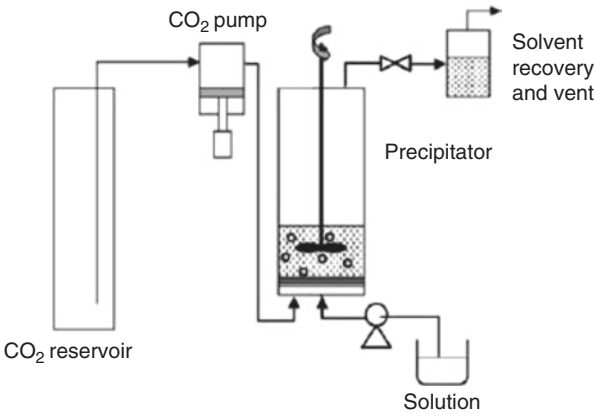

Fig. 12.4 Schematic of GAS process. Schematic adapted from Martin and Cocero (2008)

antisolvents. When precipitation is complete, the CO_2–organic solvent solution is flushed from the system and the precipitate, i.e., the drug powder, remains in the precipitation vessel. The drug powder may then be washed with fresh CO_2 to remove excess organic solvent. A schematic of the GAS precipitation system is shown in Fig. 12.4. The primary drawback of the GAS precipitation process is the difficulty in harvesting the precipitate drug particles from the organic solvent solution while minimizing particle growth and agglomeration. Furthermore, in cases where elevated temperatures are need to sufficiently expand the SCF into the organic solvent, thermal degradation of the API may occur.

Because GAS precipitation is driven by the antisolvent capabilities of CO_2 in the organic solution, appropriate processing conditions may be selected based on optimizing thermodynamic criteria, specifically by understanding the volumetric expansion of the organic solvent due to CO_2 solubilization, and thus solubility of the solute in the solvent–CO_2 mixture. In a study by de la Fuente et al., volumetric expansion of the organic solvent was correlated to the difference between the partial molar volumes (v) of the organic solvent under operating conditions versus atmospheric pressure, as shown in the following equation (de la Fuente Badilla et al. 2000):

$$\frac{\Delta v}{v} = \frac{v(T,P) - v_0(T,P_0)}{v_0(T,P_0)}, \tag{12.5}$$

where T is the operating system's temperature, P_0 is the atmospheric pressure, and v_0 is the partial molar volume at the operating system's temperature and atmospheric pressure. Studies have shown that (12.5) adequately predicts drug solubilities in a solvent–CO_2 solution for naphthalene and phenanthrene in a toluene–CO_2 system, and thus is capable of predicting their success in forming satisfactory particles by

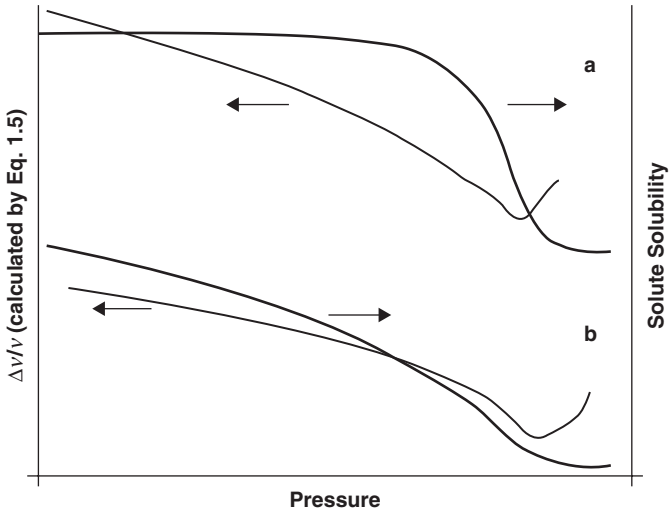

Fig. 12.5 Relative volumetric expansion of toluene, defined as the difference between the partial molar volumes (v) of toluene under operating and atmospheric conditions, and solute solubility in a (**a**) CO_2–toluene–naphthalene and (**b**) CO_2–toluene–phenanthrene system. Reprinted from Martin and Cocero (2008). Copyright (2008), with permission from Elsevier

GAS precipitation (Fig. 12.5) (Martin and Cocero 2008; de la Fuente Badilla et al. 2000; de la Fuente et al. 2004). The likelihood of a specific solute to successfully form small, uniform particles by GAS precipitation is indicated by a steep decrease in its solubility at some CO_2 concentration. More specifically, a high sensitivity of the solute's solubility to CO_2 concentration indicates that precipitation will occur rapidly and homogenously once a critical concentration is reached. On the other hand, systems that demonstrate only a slow decrease in solubility as CO_2 concentration is increased will likely not yield small, uniform particles, as precipitation will take place continuously as CO_2 is fed into the precipitation vessel. de la Fuente et al. hypothesized that optimum GAS precipitation conditions exist at the minimum of the solvent's volumetric expansion curve, as defined in (12.5). According to Fig. 12.5, naphthalene was predicted to be successfully precipitated using the GAS technique while phenanthrene was not (de la Fuente Badilla et al. 2000). This model has also been verified experimentally for a salicylic acid–propanol–CO_2 system (Shariati and Peters 2002).

Typical particle sizes of poorly water-soluble drugs prepared by GAS precipitation are on the order of 1–10 μm (Martin and Cocero 2008), although submicron particle sizes have been achieved in some cases (Turk 2009). GAS precipitation processes have also been reported to be successfully scaled from a 300-mL to 1-L batch size (Muhrer et al. 2003; Muhrer and Mazzotti 2003). However, when processes are scaled to larger volumes, a stirrer was needed to improve mixing between the organic solvent and CO_2 (Martin and Cocero 2008). Key process parameters that control final particle size and morphology include the pressure

and temperature of the precipitation process, solvent selection, and the CO_2 addition rate to the organic solution (Muhrer et al. 2003; Fusaro et al. 2004; Subramaniam et al. 1997; Mueller et al. 2000). As mentioned previously, changes in pressure and temperature largely influence the mass transfer properties of CO_2. Solvent selection and the rate of CO_2 addition affect supersaturation levels and, thus, nucleation and crystallization rates. In a study by Muller et al., GAS precipitation of a proprietary poorly water-soluble drug yielded amorphous spheres when precipitated from ethanol, whereas a crystalline form was obtained when acetone or acetonitrile was chosen as the solvent, even though all other operating conditions were identical (Mueller et al. 2000). Likewise, an amorphous solid dispersion of oridonin stabilized with PVP K17 exhibiting a dramatic increase in bioavailability was obtained from ethanol solution (Li et al. 2011). Additional studies by Muller et al. reported that the average particle size of their proprietary poorly water-soluble drug, when precipitated from an ethanol solution, could be reproducibly adjusted to sizes between ~200 nm and 10 μm by varying the addition rate of CO_2 over two orders of magnitude (Muhrer et al. 2003; Mueller et al. 2000). The CO_2 addition rate (Q_A) was defined as the ratio between the CO_2 flow rate and the initial volume of organic solution, in order to normalize for different batch sizes. Moreover, the particle-size distribution (PSD) was unimodal for "slow" ($Q_A \leq 0.04$ min^{-1}) and "fast" ($Q_A \geq 1.54$ min^{-1}) CO_2 addition rates, but was bimodal for "intermediate" addition rates ($0.1 \leq Q_A \leq 0.5$ min^{-1}) (Muhrer et al. 2003). In another example where paracetamol (aqueous solubility ~12 mg/mL) was precipitated from an acetone solution by GAS, the mean particle size decreased threefold (250–87 μm) with an increase in Q_A by a factor of three (0.1–3.33 min^{-1}) (Fusaro et al. 2004). Similarly, nanoparticles of 5-fluorouracil precipitated from dimethylsulfoxide was highly dependent on the processing variables such as anti-solvent addition rate, pressure, temperature, and solution concentration (Esfandiari and Ghoreishi 2013a, b). In contrast, GAS precipitation of lysozyme from dimethyl sulfoxide (DMSO) did not demonstrate a significant change in particle size with varying CO_2 addition rates (Muhrer and Mazzotti 2003). Additionally, for the studies using paracetamol and lysozyme, a unimodal PSD was obtained regardless of Q_A, which was varied from "slow" to "fast" (Fusaro et al. 2004; Muhrer and Mazzotti 2003).

In light of these conflicting reports relating experimental parameters to final particle properties, a better understanding of the GAS process, specifically the sensitivity of CO_2 addition rates on resultant particle size, has been sought through the development of theoretical models to describe the GAS process. Muhrer et al. presented a model that couples population balance theory with thermodynamic equilibrium to relate nucleation rates to final particle size (Muhrer et al. 2002). Solution thermodynamics and particle formation and growth are accounted in the model based on assumptions of isothermal conditions and instantaneous vapor–liquid phase equilibrium upon addition of the antisolvent, thus neglecting any mass transfer resistance. Particle growth, however, is described by an empirical correlation, which does not discern between the different mechanisms of condensation and coagulation (Martin and Cocero 2008; Dodds et al. 2007). In a study

recently published by Kikic et al., the impact of the organic solvent selection, the ratio of CO_2/solution and pressure on drug solubility was estimated using Peng-Robinson's equation of state. Ternary diagrams were obtained enabling an initial screening for optimal processing conditions. These estimations are also valid for the SAS process detailed in the following Sect. 12.2.2 (Kikic et al. 2010).

In the Muhrer et al. model, systems in which primary nucleation (generation of nuclei resulting from supersaturation, in the absence of drug crystals) is dominant to secondary nucleation (occurs in the presence of existing drug crystals) tend to be more susceptible to variations in CO_2 addition rates. Therefore, in systems dominated by primary nucleation, average particle sizes and PSDs may be tuned by controlling CO_2 addition rates. An increase in Q_A elevates supersaturation levels, facilitating higher nucleation rates and thus promoting the formation of more nuclei, which results in a larger population of smaller particles. The relationship, as determined by Muhrer's model (Muhrer et al. 2002), between supersaturation ratio, S, and average particle size, as a function of Q_A, is illustrated in Fig. 12.6. The supersaturation ratio was calculated as the ratio of the fugacity of the solute in the liquid phase to the fugacity of the pure solid. Muhrer's model also demonstrated that in cases where secondary nucleation is dominant, the mean particle size is largely unaffected by changes in the rate of CO_2 addition, whereas systems with intermediate secondary nucleation rates

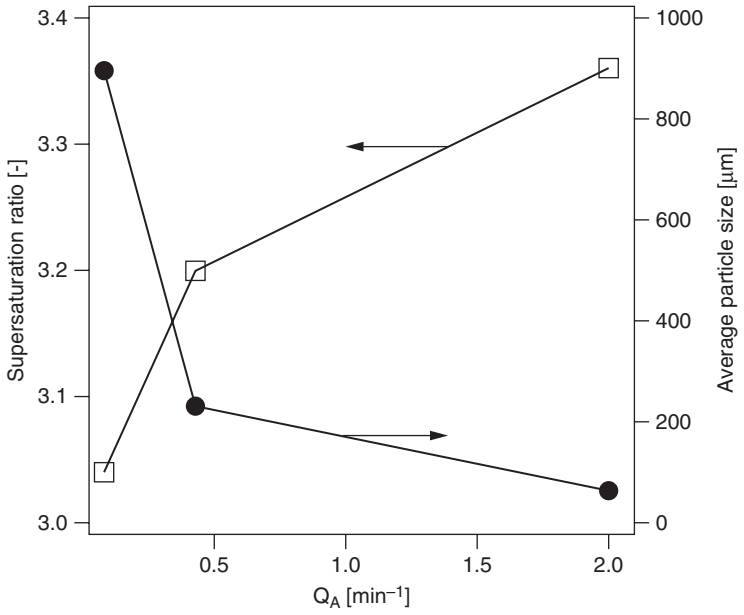

Fig. 12.6 Effect of CO_2 addition rate, Q_A, on the supersaturation ratio, S, and the average size of particles produced by GAS precipitation for a model phenanthrene–toluene–CO_2 system. Reprinted with permission from Fusaro et al. (2005). Copyright (2005) American Chemical Society

were predicted to be moderately affected by variations in Q_A and possessed bimodal distributions. Good quantitative agreement with this model was obtained in two studies where phenanthrene was micronized using GAS precipitation (Muhrer et al. 2002; Bakhbakhi et al. 2005). However, because this model was developed primarily to explain the effect of Q_A on final particle size, minor deviations between the model and experimental results were observed when examining the role of initial drug concentration on particle size for a poorly water-soluble drug–ethanol–CO_2 system. The discrepancies were attributed to the fact that the model neglects mass-transfer resistances, and thus did not account for the increasing viscosity of the organic solution due to higher drug concentration. In response, Elvassore proposed a population balance model that accounted for particle nucleation, growth, aggregation, as well as settling, where nucleation and growth were described by the McCabe model (Elvassore et al. 2003, 2004). The model was validated with experimental measurements for the GAS precipitation of poly(L-lactide) acid (PLLA). While a good correlation was achieved, several model parameters could not be experimentally determined and were assumed in order to fit the model to the experimental data. The results of this model indicated that aggregation rates should not be neglected and that they strongly influence the attainment of unimodal (low aggregation rates) versus bimodal (high aggregation rates) distributions, in contrast to Muhrer's model which did not account for aggregation rates. Dodds et al. developed another model that used solution thermodynamics and crystallization kinetics to examine particle growth in GAS processes (Dodds et al. 2007). The Dodds et al. model showed good agreement with experimental results for GAS precipitation of naphthalene, phenanthrene, cholesterol, and beclomethasone dipropionate (Dodds et al. 2007). In a recent study by Esfandiari et al., mathematical modeling of the GAS process was used to determine nucleation and growth rate parameters. The model was validated by comparison with experimental data and was successful in predicting particle size distribution (Esfandiari and Ghoreishi 2013a, b). Also, Erriguible et al. published an approach to model a case of co-crystallization with naproxen and nicotinamide as co-former. Their modeling accounted for the liquid vapor equilibrium and its impact on solubility of naproxen and nicotinamide, and also the nucleation and growth of the co-crystal. The experimental size distribution was in agreement with the one predicted (Erriguible et al. 2015). While all of the models contributed to an enhanced understanding of the underlying mechanisms driving GAS precipitation, further validation is required to understand their applicability to additional drug–solvent systems. It should be noted that predicting physical properties of particles produced by GAS precipitation has not been trivial and currently appears to be highly dependent on a specific system due to the complexities that arise from multiple interactions within the system (drug–solvent, solvent–CO_2, and drug–solvent/CO_2 solution). It is also important to note that GAS precipitation generally does not produce nanoparticles, as it is typically limited by the mixing and thus nucleation rates that can be achieved in this system.

12.2.2 Precipitation with a Compressed Liquid or Supercritical Fluid (PCA, ASES, SEDS, and SAS)

The physical properties of drug powders produced by precipitation methods are greatly influenced by the process arrangement. In contrast to GAS precipitation, the PCA process atomizes the drug solution into the SCF antisolvent. In PCA, the organic solution containing the API is atomized into a vessel that has been pressurized with the compressed liquid or SCF, often CO_2. Unlike the batch GAS process, PCA is a semicontinuous technique because the $scCO_2$ is continuously fed throughout the atomization process to promote more rapid mixing with the organic solvent. Upon removal of the residual solvent, the pressure in the vessel is reduced to atmospheric pressure and the drug particles are collected by a filter at the bottom of the vessel. Similar to the GAS process, additional excipients may also be dissolved in the organic drug solution to produce composite API/excipient particles. A schematic of the PCA system is shown in Fig. 12.7. The PCA process typically operates at 9–15 MPa, slightly higher than GAS processes, in order to achieve higher supersaturation values and sufficient mixing between the CO_2 and organic solution feed streams (Martin and Cocero 2008).

Atomization of the drug–CO_2 solution into the antisolvent, as opposed to bubbling the CO_2 solution, facilitates more rapid mass transfer between the drug solution and the antisolvent, which makes the PCA process more conducive to the production of smaller particles compared to GAS precipitation. (Rogers et al. 2001a; Martin and Cocero 2008; Fusaro et al. 2004) The high surface area of atomized droplets increases the area of intimate contact between the drug solution and the antisolvent to facilitate mixing, thus promoting rapid supersaturation and precipitation. Upon atomization, the organic solvent diffuses into the CO_2 phase and the CO_2

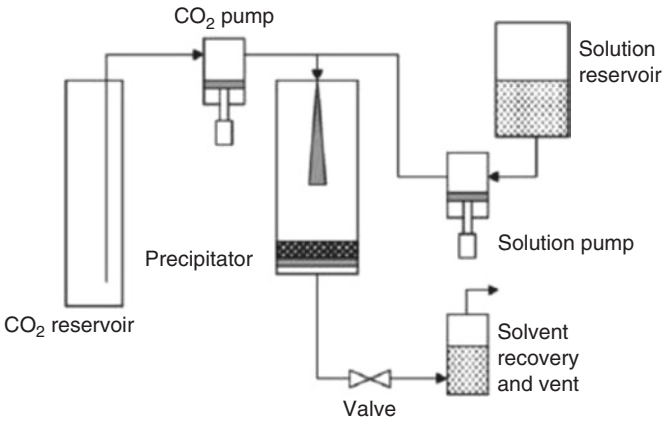

Fig. 12.7 Schematic of PCA process. Reprinted with permission from Martin and Cocero (2008). Copyright 2008 with permission from Elsevier

diffuses into the organic droplets, resulting in a more efficient, bidirectional mass transfer of CO_2 and organic phase, in contrast to the unidirectional mass transfer in GAS precipitation (Rogers et al. 2001a; Martin and Cocero 2008).

The mass-transfer efficiency between the CO_2 and organic solvent phase may be further increased by adjusting operating parameters of the PCA process, including increasing the miscibility between the solvent and CO_2 or by tuning the degree of atomization of the organic solution into the CO_2 phase. Increased miscibility between the solvent and CO_2 and more intense atomization, which yields higher surface area droplets, enhance mass-transfer efficiency (Rogers et al. 2001a; Fusaro et al. 2004). For systems in which the solvent and CO_2 are fully miscible (supercritical conditions), experimental parameters that affect mixing rates between the solvent and CO_2 streams, such as degree of atomization, are less likely to influence precipitation results for some nozzle designs, thus suggesting that mixing rates between the solvent and CO_2 are faster than precipitation rates (Reverchon et al. 2003a, b, 2007). However, for systems where solvent and antisolvent are only partially miscible (subcritical conditions), mixing parameters significantly influence precipitation results. Furthermore, changes in particle morphology, as well as an increased propensity for particle agglomeration, are frequently observed at subcritical conditions, indicating that mixing of the CO_2 and solvent is not complete and occurs simultaneously with precipitation during droplet formation (Martin and Cocero 2008). An increase in atomization intensity facilitates solvent–CO_2 mixing during droplet formation. For subcritical conditions, the degree of atomization may be quantified by the Weber number, N_{We}, a dimensionless ratio of inertial to surface tension forces, which is given by

$$N_{We} = \left(\rho_A v^2 D_{drop}\right) / \sigma, \tag{12.6}$$

where ρ_A is the antisolvent density, v is the relative velocity, D_{drop} is the droplet diameter, and σ is the interfacial tension. Higher-intensity atomization is characterized by larger N_{We} values for a given Reynolds number (Re) (Lengsfeld et al. 2000). However, for supercritical conditions, the surface tension of the organic solvent decreases to zero over a distance shorter than that of characteristic jet break-up lengths, calculated based on classic jet break-up theory (Lengsfeld et al. 2000). Thus, distinct droplets do not form and the solvent stream forms more of a gaseous plume (Bristow et al. 2001). Therefore, atomization for miscible fluids were analyzed using gaseous mixing theory and mixing rates, using mixing length scales for turbulent mixing (Shekunov et al. 1999; Jarmer et al. 2003).

Atomization intensity may be increased using ultrasonic dispersion devices, coaxial nozzles, or two-component jet nozzles to enhance the interaction between the solvent and antisolvent in a mixing chamber prior to atomization. Schematics of different nozzle types are shown in Fig. 12.8. Ultrasonic dispersion devices vibrate at an ultrasonic frequency to enhance mass-transfer efficiency by increasing mixing rates between the solvent and antisolvent, as well as to atomize the feed solution into smaller droplets. Final particle sizes may be tuned by controlling vibration

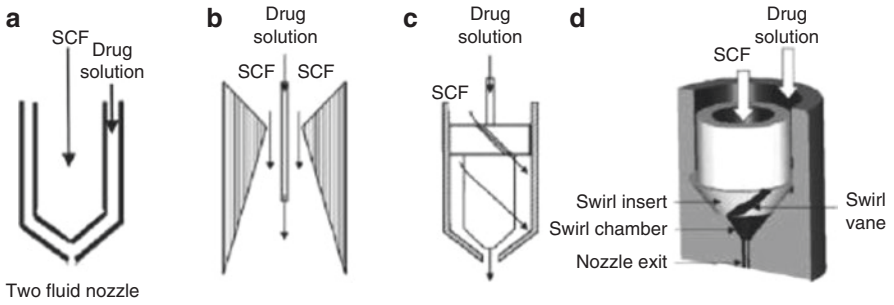

Fig. 12.8 Schematics of different nozzles used in SCF precipitation processes: (**a**) coaxial nozzle (Okamoto and Danjo 2008), (**b**) coaxial nozzle with a converging–diverging annulus (Fusaro et al. 2005), and (**c**, **d**) two configurations for a two-component jet nozzle (Fusaro et al. 2005; Jarmer et al. 2003). Reprinted with permission from Okamoto and Danjo (2008) (Copyright 2008 with permission from Elsevier), Fusaro et al. (2005) (Copyright 2005 American Chemical Society), and Jarmer et al. (2003) (Copyright 2003 with permission from Elsevier)

intensity of the dispersion device. For coaxial (or two-fluid) nozzles (Fig. 12.8a), the organic drug solution is fed through one axis and the $scCO_2$ is fed through the other. As the two feeds meet, intense mixing of the two streams facilitates rapid nucleation and particle precipitation upon atomization from the nozzle. Primary particle sizes may be controlled by adjusting the relative velocities of the two streams, which regulates the intensity of mixing between the solvent and antisolvent phase. Several configurations for coaxial nozzles have been utilized, with optimal designs heavily dependent on the particular drug system. In some cases, a converging–diverging nozzle is employed to rapidly disperse the liquid feed during atomization to facilitate nanoparticle production (Fig. 12.8b). In two-component jet nozzles, the antisolvent is introduced at a sharp angle into the mixing chamber to enhance turbulence of the fluids during mixing (Fig. 12.8c, d). Studies have shown that turbulent mixing of the solvent and antisolvent greatly impacts supersaturation homogeneity, allowing for more control of the PSD during PCA by tuning precipitation kinetics (nucleation and growth rates) (Jarmer et al. 2003). Primary particle sizes ranging from 200 to 1000 nm for poorly water-soluble drugs, and as low as 50 nm for water-soluble molecules, have been achieved using these technologies (Table 12.3) (Gupta 2006).

Scalability of the PCA technology has been demonstrated for the production of paracetamol particles at laboratory scales ($1–8 \times 10^{-4}$ kg/s CO_2 + ethanol + paracetamol flowrates) to small manufacturing plant scales ($0.9–1.5 \times 10^{-2}$ kg/s CO_2 + ethanol + paracetamol flowrates) (Baldyga et al. 2010). In terms of batch sizes, 1 kg nanoparticles/day have been produced at pilot plant scale using PCA (Gupta 2006). However, it is important to note that strategies for scaling up PCA processes differ when operating under subcritical or supercritical regimes. Subcritical operating conditions exhibit higher sensitivities to certain parameters, such as nozzle design. PCA precipitation of PLLA at both laboratory and pilot plant scales, under conditions of partial solubility of CO_2 in the solvent, was heav-

Table 12.3 Drug nanoparticles produced by PCA

Drug	Solvent	*P* (bar)	*T* (K)	Atomization conditions	Particle size (nm)
Albumin (Bustami et al. 2000)	Water/ethanol	N/A	N/A	Coaxial nozzle	50–500
Amoxicillin (Reverchon et al. 2000, 2003b; Reverchon and Della Porta 1999)	*N*-Methylpyrrolidone	150	313	Coaxial nozzle with coaxial injector	120–1200
Gentamicin/PLA (Falk et al. 1997)	Methylene chloride	85	308	US nozzle, vibrating at 120 kHz	200–1000
Hydrocortisone (Weber et al. 1999)	Dimethyl sulfoxide	100	308		600
Ibuprofen (Weber et al. 1999)	Dimethyl sulfoxide	100	308		500–1000
Insulin (Bustami et al. 2000)	Water/ethanol			Coaxial nozzle	50–500
Naltrexen/l-PLA (Weber et al. 1999)	Methylene chloride	85	308	US nozzle, vibrating at 120 kHz	200–1000
Nicotinic acid (Falk et al. 1997)	Ethanol			Coaxial nozzle	400–750
RhDNase (Hanna and York 1998)	Ethanol			Coaxial nozzle	50–500
Salbutamol (Bustami et al. 2000)	Methanol/acetone	100	333	Coaxial nozzle	500
Naloxone/l-PLA (Hanna and York 1998)	Methylene chloride	85	308	US nozzle, vibrating at 120 kHz	200–1000
Dexamethasone phosphate (Falk et al. 1997)	Methanol	102	313	US nozzle, power = 90 W	175
Griseofulvin (Thote and Gupta 2005)	Dichloromethane	96.5	308	US nozzle, power = 90–180 W	310–510
Griseofulvin (Chattopadhyay and Gupta 2001a)	Tetrahydrofuran	96.5	308	US nozzle, power = 120–180 W	200–280
Lysozyme (Chattopadhyay and Gupta 2002)	Dimethyl sulfoxide	96.5	310	US nozzle, power = 12–90 W	190–730
Lysozyme (Rodrigues et al. 2009)	Ethanol	180–250	318–333	Coaxial nozzle	100–5000
Tetracycline (Chattopadhyay and Gupta 2001b)	Tetrahydrofuran	96.5	310	US nozzle, power = 30–120 W	110–270

US ultrasonic. Data adapted from Gupta (2006)

ily influenced by nozzle design. While PCA processes operating at higher *Re* are more likely to be successfully scaled up, maintenance of a constant *Re* or constant jet velocities at the antisolvent inlet does not guarantee scalability between laboratory and pilot plant batches (Jarmer et al. 2006). One criterion that enables process scalability is the maintenance of a constant energy dissipation rate in the nozzle. Nozzle design significantly influences the propagation of secondary nucleation mechanisms, and thus impacts energy dissipation rates during solvent atomization. Another option to achieve scalability is to target a constant suspension density and residence time within the mixing chamber by adjusting solvent flow rates through the nozzle, which maintains mixing quality and, thus, promotes comparable nucleation and growth rates. When either of these conditions was met, PLLA particles with similar PSDs were obtained at both laboratory and pilot scales of production (Martin and Cocero 2008; Jarmer et al. 2006). When operating in the complete miscibility regime, PCA precipitation of amoxicillin conducted at both laboratory and pilot plant scales yielded very similar results, in terms of particle size and morphology, regardless of nozzle design and residence time in the precipitation vessel (Martin and Cocero 2008; Reverchon et al. 2003b). The same trends were observed in a study by Wubbolts et al., where acetaminophen and ascorbic acid particles were produced by PCA under subcritical versus supercritical conditions (Wubbolts et al. 1999). When an acetaminophen–ethanol solution was atomized into CO_2 under subcritical conditions, the droplets did not fully evaporate and a solvent-rich region was observed at the bottom of the precipitation vessel. This subcritical operating condition resulted in ~200-μm acetaminophen particles. The large particle sizes were attributed to the growth of nucleated crystals in the solvent-rich phase at the bottom of the vessel. In contrast, an ascorbic acid–ethanol–CO_2 system under supercritical conditions yielded ~1–5-μm particles, in which particle size was virtually insensitive to temperature and pressure changes while in the supercritical regime.

Reverchon et al. further investigated the span of particle properties produced by PCA when operating under supercritical conditions (Reverchon et al. 2007). More than 20 compounds, spanning a wide range of materials including superconductor and catalyst precursors, dye pigments, polymers, and pharmaceuticals, were examined in this study (Reverchon et al. 2007). Nanoparticles were formed only under supercritical conditions and when the solute was virtually insoluble in the antisolvent–solvent mixture. In agreement with previous studies, particle size was not dependent on nozzle design for these experiments, which were operated at supercritical conditions (Martin and Cocero 2008; Reverchon et al. 2003a, b; Wubbolts et al. 1999). However, the initial solute concentration in the organic solvent did influence final particle size. Increased concentrations of the solute in the organic solvent resulted in larger particles (Reverchon et al. 2007). In fact, Fig. 12.9 shows that, for the entire range of compounds that were tested, average particle sizes scaled linearly with the relative concentration of solute in the feed organic solvent, C_R, for a given operating temperature, pressure, and mole fraction of antisolvent, where $C_R = C_{drug}/C_{eq}$ and C_{drug} is the concentration of solute in the organic solvent. This linear relationship between feed drug concentration and particle size indicates that the particle sizes produced by PCA depend primarily on the differential

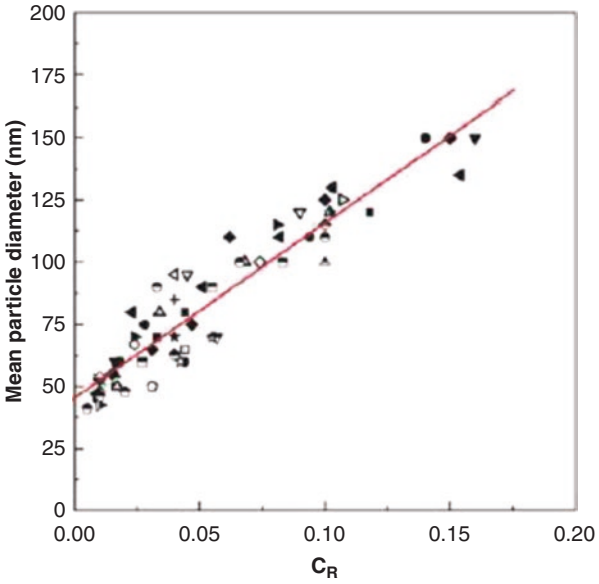

Fig. 12.9 Mean particle diameter, as a function of relative solute concentration in feed, C_R ($C_R = C_{drug}/C_{eq}$), of various materials, including metal acetates, pharmaceuticals, polymers, and dye pigments, processed by PCA under supercritical conditions ($P = 150$ bar and $T = 40$ °C). Reprinted from Reverchon et al. (2007). Copyright 2007 with permission from Elsevier

between the solute concentration in organic solvent and the saturated concentration, not necessarily on the properties of a specific solute. Additionally, wider PSDs were observed for higher solute concentrations. Extrapolation of the linear relationship between particle size and relative solute feed concentration suggests that the smallest average diameter of particles produced by PCA is 45 nm, which is in accordance with what has been observed in literature. The smallest average particle sizes reported for PCA processes are on the order of 40–50 nm for several compounds, including lysozyme, rifampicin, and polyvinyl alcohol (PVA). Growth of particle sizes from systems with higher feed solute concentrations may be attributed to an increased concentration of nuclei, which increase collisions rates. In the cases where the SC fluid is not a strong anti-solvent, it was reported that another driving force for recrystallization could be obtained by operating in non-isothermal conditions (e.g., solution warmer than SC fluid). Indeed, due to solubility increasing with temperature, a higher supersaturation level was achieved when solution and SC fluid were mixed (Erriguible et al. 2013).

The PCA manufacturing technique coupled with an appropriate formulation (usually an amorphous state stabilizer) can change the crystalline state of the drug (Lim et al. 2010). Indeed, amorphous solid dispersion nanoparticles of sirolimus, PVP and surfactant were produced, and they exhibited improved solubility, dissolution properties and stability. These results were confirmed in vivo in mice where enhanced bioavailability of sirolimus nanoparticles was observed (Kim et al. 2011).

HPMC/PVP was shown to decrease the dissolution rate of amorphous telmisartan due to a gel layer formation, therefore a balance between amorphous state stabilization and dissolution rate must be defined (Park et al. 2013). Rossman et al. demonstrated that paracetamol crystal polymorphism could be modified by varying the ethanol/acetone content in the drug solution. It was also found that varying the solvent led to primary or secondary structure of paracetamol. Low levels of supersaturation led to larger crystals due to prolonged crystal growth phase (Rossmanna et al. 2013).

PCA processing was also successfully used to produce sub-micron co-crystals of several drug models demonstrating the ability of this technique to rapidly screen pharmaceutical co-crystals (Padrela et al. 2010).

In order to gain a more fundamental understanding of how different operating conditions influence particle properties, several theoretical models have been developed to describe particle formation and growth in the PCA process. Many of the models focus on calculating the rate of mass transfer of antisolvent into the solvent phase because this is believed to be a key factor dictating particle size and morphology. Werling and Debenedetti proposed a model for two-way mass transfer between a droplet of organic solvent and compressed antisolvent that accounts for both subcritical and supercritical conditions (Werling and Debenedetti 1999, 2000). The model assumes that the droplet of organic solvent is stagnant; thus, only mass transfer by diffusion is considered. For subcritical conditions, the solvent droplet initially swells due to the diffusion of antisolvent into the droplet. As the pressure in the system is increased, the lifetime of the solvent droplet decreases because the droplet shrinks as the CO_2–solvent mixture evaporates to induce precipitation. However, as the system tends toward near-critical conditions, the lifetime of the solvent droplet increases drastically because CO_2 diffusivity tends toward zero near the critical point. Longer droplet lifetimes may lead to larger particle sizes because droplet coalescence, and thus particle growth, is more likely. Because distinct droplets do not form under supercritical conditions, a hypothetical interface, based on the density gradient between the solvent-rich and antisolvent-rich regions, was assumed in the model. Modeling results indicated that solvent droplets would swell if the density of the organic solvent was higher than that of the antisolvent. Likewise, the solvent droplets would shrink if the solvent density was lower than that of the antisolvent. The extent of droplet swelling or shrinking is dependent on the system's temperature and pressure, as it affects density and diffusivity differences between solvent-rich and antisolvent-rich domains. In systems near their critical point, solvent droplets undergo greater swelling and experience longer lifetimes, and are more sensitive to operating conditions than systems far from the critical point. Elvassore et al. expanded upon Werling and Debenedetti's model by including the effects of the solute on the diffusivity and density of the SCF into the mass-transfer calculations (Elvassore et al. 2004). The assumption of a stagnant droplet of organic solvent is maintained and the diffusion flux in the solute–solvent–antisolvent system was calculated using Maxwell–Stefan relationships. In this model, slowly diffusing solutes, such as polymers, were found to increase droplet lifetimes by as much as one order of magnitude for high solute concentrations, compared to solutes with

faster diffusivities. The extent of a solute's solubility in the solvent–antisolvent mixture also influenced the particles' morphologies, as the evolution of the precipitation front was found to be significantly different for highly soluble and poorly soluble compounds (Elvassore et al. 2004). Perez de Diego et al. proposed a model that accounted for the convective motion of CO_2 (Perez de Diego et al. 2006). Martin et al. has adapted the mass-transfer model developed by Werling and Debenedetti (1999, 2000) to simulate the formation of protein particles by PCA (Martin et al. 2007). More recently, a numerical model utilizing computational fluid dynamics (CFD) calculations (Martin and Cocero 2004) more accurately modeled supercritical systems using a turbulent, gaseous plume to simulate the organic feed stream, instead of the hypothetical spherical droplet used by Werling and Debenedetti (1999, 2000). While each new model includes an additional degree of the PCA process's complexity to impart further insight, all of the models express similar trends. Droplet lifetimes are shorter for supercritical systems than subcritical systems and shorter growth periods are more likely to lead to smaller particle sizes. When operating in the supercritical condition, the most important mechanism affecting final particle size is primary nucleation, and thus process parameters that facilitate more rapid and higher nucleation rates tend to form smaller particles. Reverchon and De Marco proposed an explanation of morphology and particle size for differentiating nanoparticles and spherical microparticles. For instance, they explained that surface tension vanishing at supercritical conditions and liquid jet break up, two precipitation mechanisms in competition influenced the morphologies and final particle size. They demonstrated that two mechanisms were involved in crystal formation: (1) droplet drying followed by fast crystallization which led to spherically shaped crystals and (2) precipitation from an expended liquid which led to different morphologies and particle size depending on the interaction with the solvent. This knowledge allows selection of the particle size of the precipitated particles (Reverchon and De Marco 2011). Additionally, it is important to design systems away from the critical point of the antisolvent because the near-zero diffusivities at this condition lead to droplets with longer lifetimes, which have a propensity to result in larger particle sizes. However, current models are still not able to universally quantify the dependence of particle size on process parameters for a range of drug–solvent–antisolvent systems. As mentioned previously, multiple interactions within the system (drug–solvent, solvent–CO_2, and drug–solvent/CO_2 solution) significantly affect thermodynamics, hydrodynamic, mass transfer, and mixing and precipitation kinetic behavior, and thus make it difficult to generalize results for a wide range of systems.

12.2.3 Rapid Expansion of Supercritical Solutions (RESS)

In contrast to GAS and PCA processes, the rapid expansion of supercritical solutions (RESS) process utilizes the SCF as a solvent, not an antisolvent. The solute is dissolved directly into the SCF phase in the extraction unit. Then, the system is

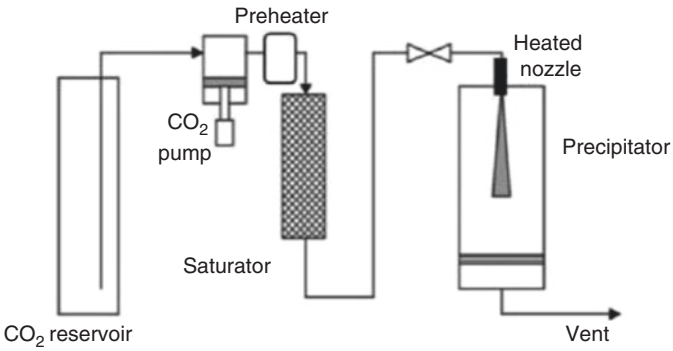

Fig. 12.10 Schematic of RESS process. Schematic adapted from Martin and Cocero (2008)

depressurized across a nozzle into a collection chamber at atmospheric conditions. The sudden depressurization causes evaporation of the SCF, resulting in a significant reduction in solvent power, and thus promotes rapid nucleation and precipitation of the solute. As with the other particle formation techniques discussed previously, additional excipients may be dissolved in the SCF, typically CO_2, to produce composite particles of drug and excipients (Turk 2009). A schematic of the RESS process is shown in Fig. 12.10. Intense atomization of the drug–CO_2 stream is desirable to achieve nanoparticles from the RESS process. Therefore, depressurization of the CO_2 feed stream from the nozzle is designed to be extremely rapid, with typical CO_2 flow rates exiting the nozzle at the speed of sound, creating supersaturation levels on the order of 10^5–10^6 within a time frame 10^{-6}–10^{-4} s (Debenedetti et al. 1993). The intense turbulence generated by rapid depressurization of CO_2 distributes the newly generated supersaturation regions almost instantaneously and homogenously throughout the fluid, which facilitates the production of small particles with narrow PSDs. This rapid dissipation of energy is highly endothermic, and thus the nozzle is generally heated to prevent freezing of CO_2 during atomization, which can cause clogging.

Several process parameters of RESS that have been reported to affect final particle characteristics include the temperature and pressure in the extraction unit, the temperature and pressure of the SCF–drug solution just before atomization, termed as pre-expansion temperature ($T_{\text{pre-exp}}$) and pressure ($P_{\text{pre-exp}}$), respectively, as well as post-expansion temperature (T_{postexp}) and pressure (P_{postexp}). These conditions determine the process path along the pressure–temperature (P–T) diagram for the SCF. The P–T diagram for CO_2 is shown in Fig. 12.11. Depending on initial P–T conditions, the expansion pathway may intersect the vapor–liquid saturation line, which may result in significant changes in particle morphology (Martin and Cocero 2008). When the expansion path intersects the solid–liquid saturation line, solid, frozen CO_2 forms during atomization, requiring the nozzle to be heated during operation to prevent clogging. Nozzle design is another parameter that has reportedly influenced final particle properties, as the geometry of the nozzle influences the timescale over which depressurization occurs and, thus, the degree of atomization (Martin and Cocero 2008; Rogers et al. 2001a).

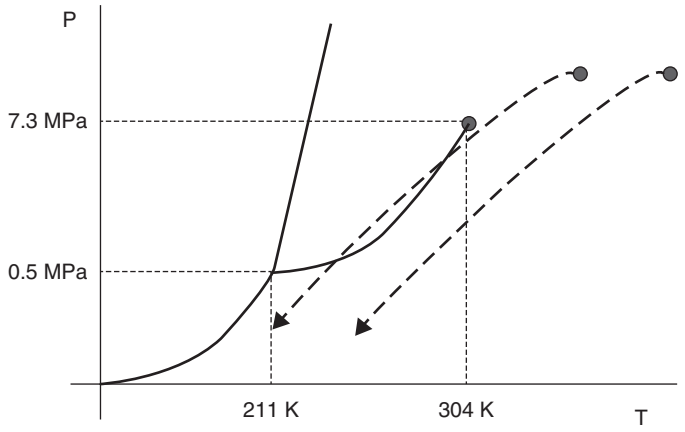

Fig. 12.11 *P–T* diagram of CO_2. *Dashed lines* illustrate pathways that may be taken during CO_2 depressurization from nozzle in PCA. Reprinted from Martin and Cocero (2008). Copyright 2008 with permission from Elsevier

To date, however, a definitive relationship between experimental process parameters and particle properties has not been established and, in some cases, experimental results have been inconsistent. For example, for a given $P_{\text{pre-exp}}$, an increase in $T_{\text{pre-exp}}$ from 350 to 425 K resulted in an increase in the size of benzoic acid particles produced by RESS (diameter increased from 0.2 to 1.3 μm), while the particle size of cholesterol remained unchanged (~0.25 μm) (Fig. 12.12). Similarly, an increase in $P_{\text{pre-exp}}$ resulted in a decrease in particle size of benzoic acid, while the size of cholesterol particles again remained essentially constant. Numerous studies have been conducted to better understand which process parameters most strongly and consistently influence final particle size. The RESS process commonly produces particles in the 1–5-μm size range, although submicron particles have been produced under specific operating conditions (Gupta 2006). Several RESS studies have been highlighted in Table 12.4. Clearly, process temperatures and pressures and nozzle geometry significantly influence particle size and shape, and, in some cases, morphology (Turk and Bolten 2010). Relatively small adjustments to just one of these operating conditions may significantly impact particle diameter by an order of magnitude, as well as completely alter the particle shape from a sphere to a needle shape, as seen in the cases for salicylic acid and griseofulvin particles produced by RESS (Table 12.4). Based on reports from literature, including those listed in Table 12.4, several trends in processing conditions have been identified to facilitate nanoparticle production (Turk 2009).

- Influence of $T_{\text{pre-exp}}$: An increase in $T_{\text{pre-exp}}$ typically leads to larger particle sizes. For a given operating pressure, even though elevated temperatures may increase drug solubilities and thus increase supersaturation and nucleation rates (Liu and Nagahama 1996), the higher temperatures also tend to increase turbulence within the mixing chamber, leading to higher instances of particle coagulation (Franklin

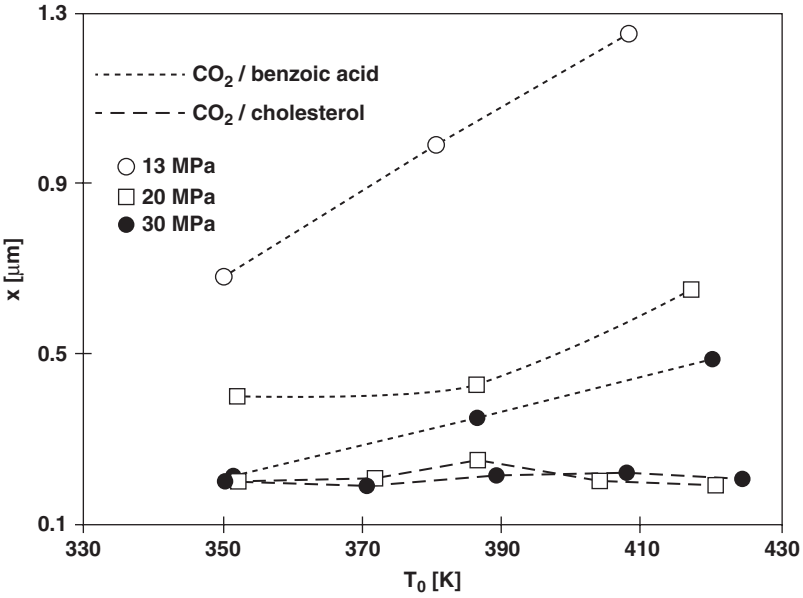

Fig. 12.12 Influence of pre-expansion conditions on particle sizes of benzoic acid and cholesterol prepared by RESS. Reprinted from Turk (2000). Copyright 2000 with permission from Elsevier

et al. 2001). The increased rate of particle coagulation appears to outweigh the benefits of enhanced nucleation rates achieved by elevated $T_{\text{pre-exp}}$ conditions.

- Influence of $P_{\text{pre-exp}}$: An increase in $P_{\text{pre-exp}}$ typically leads to smaller particle sizes because a higher pressure results in an increased mass flow rate of CO_2, which decreases the residence time of the particles in the expansion chamber, reducing the time for particle growth. The reduction in residence time also facilitates the production of more spherical particle shapes, by limiting the time available for additional growth along one axis.
- Influence of nozzle: Nozzles with smaller length-to-diameter (L/D_{noz}) ratios have been found to produce smaller particles, as larger nozzle diameters facilitate increased CO_2 mass flow rates (for a given $T_{\text{pre-exp}}$ and $P_{\text{pre-exp}}$). Additionally, nozzles with smaller L/D_{noz} ratios allow for the pressure drop to occur closer to the free jet (Rogers et al. 2001a; Weber et al. 2002). As the L/D_{noz} ratio is increased, there is an increased propensity for an initial burst of particle nucleation to occur near the nozzle exit. A second round of nucleation occurs upon full expansion of the SCF, resulting in larger particles as well as broader PSDs. Typically, nozzle diameters range from 10 to 50 μm i.d. and length-to-diameter ratios range from 5 to 100 (Young et al. 2000).

It is important to note that these reported trends reflect a considerable portion of the studies in literature, but are not exclusively observed. Deviations from these observed trends, as in the case of cholesterol particles produced by RESS, have been associated with extremely low solute solubilities in SCF and/or solutes that significantly influence the surface tension of the SCF (Turk 2000).

Table 12.4 Drug particles produced by RESS

Drug	P (bar)	$T_{pre\text{-}exp}$ (K)	$T_{post\text{-}exp}$ (K)	Particle size (μm)[a]	Nozzle parameters L/D_{noz}, D_{noz} (μm)
Aspirin (Domingo et al. 1997)	160–200	403	NR[b]	Nonspherical: 2–5	5, 40
Caffeine (Ksibi et al. 1995)	150	380	300	Needles: 3–5/1	20, 220
	150	380	350	Needles: 15–20/1	20, 220
Ibuprofen (Kayrak et al. 2003; Charoenchaitrakool et al. 2000)	150	361	298	Nonspherical: 2–9	44.4, 180
	190	308	298	Nonspherical: 2.5–5	20–40,50
Cholesterol (Turk 2009)	200–300	353–422	298	Nonspherical: 0.2–0.3	7.8, 45
Salicylic acid (Reverchon et al. 1993; Turk and Lietzow 2008)	200	373	263–273	Spheres: 1–5	20, 40
	200	373	293–303	Needles: 5–30/1–3	20, 40
	200	328	298	Spheres: 0.13–0.23	1, 50
Griseofulvin[c] (Reverchon and Pallado 1996; Turk et al. 2002)	200	423	298	Spheres: 0.9–1.4	20, 40
	200	323	298	Needles: 13–36/1.0–1.3	20, 40
	200	348–418	298	Spheres: 0.25	1, 50
β-sitosterol (Turk et al. 2002)	200–300	348–418	298	Spheres: 0.18–0.23	1, 50
Paclitaxel (Yildiz et al. 2007)	150–250	323	283	Nonspherical: 0.3–2.8	70, 50
Naproxen (Turk 2009)	200	363	NR[b]	Shape not reported: 0.66	NR[b]
Fenofibrate (Hiendrawan et al. 2014)	200	308	NR	3.04	D_{noz} : 200
Raloxifene (Keshavarz et al. 2012)	177	323	NR	Spheres: 0.016	D_{noz} : 30

Unless otherwise noted, CO_2 was the solvent

[a]For needle-shaped particles: length/diameter; for spherical particles: diameter; nonspherical refers to particles that do not possess an aspect ratio typical of needle-shaped particles, but deviate significantly from an aspect ratio of unity (i.e., rectangle with aspect ratio ~2). Sizes for nonspherical particles correspond to effective diameters

[b]NR indicates a value that was not reported

[c]Solvent was CHF_3

In response to the seemingly conflicting experimental results surrounding the RESS process, several theoretical models have been postulated to gain fundamental knowledge about the RESS process in order to better target optimal process parameters suitable for nanoparticle production. Many of the models focus on the expansion of the SCF in the nozzle to qualify the impact of nozzle design on final

particle characteristics. The models show that sonic velocities are achieved at the nozzle outlet and the resultant supersonic jet exiting the nozzle immediately experiences a steep drop in pressure and temperature, causing solute precipitation. Thus, nucleation occurs primarily during free jet expansion. Calculations estimate that nuclei formed in the free jet are as small as 5–10 nm for poorly water-soluble drugs (Gupta 2006; Reverchon and Pallado 1996; Turk et al. 2002). However, intense turbulence within the supersonic free jet often results in significant coagulation between particles before the SCF in the droplets completely evaporates (Franklin et al. 2001; Helfgen et al. 2003). Thus, controlling-expansion conditions may be tuned to facilitate SCF evaporation and minimize droplet coagulation. For example, expansion chamber geometries that minimize the formation of turbulent eddies are desirable to lower the probability of particle coagulation (Helfgen et al. 2003). Additionally, the introduction of an air flow jet into the expansion chamber resulted in smaller particles by reducing the residence time of the drug particles in the expansion chamber (Helfgen et al. 2003). In addition to the work focused on nozzle design, other models have examined particle formation and growth within an SCF. The theories used to describe particle growth in gaseous and liquid phases were also found to be applicable, with minor adjustments, for supercritical precipitation processes. Debenedetti (1990) and Turk (2000) calculated nucleation rates achieved in the RESS process using a modified definition for supersaturation, S, which was adjusted to account for the highly nonideal behavior of SCF by including fugacity, f, as a thermodynamic correction factor.

$$S = \frac{C_{drug}}{C_{eq}} \frac{f\left(T,P,C_{drug}\right)}{f\left(T,P,C_{eq}\right)}. \tag{12.7}$$

Helfgen et al. applied the modified supersaturation term in conjunction with the general dynamic equation for aerosols, commonly used to describe particle growth in aerosols (Pratsinis 1988), to predict particle nucleation and growth rates in RESS. Results from the model indicated that the majority of particle precipitation and growth took place in the free jet and that turbulent coagulation in the free jet is the primary mechanism of particle growth (Franklin et al. 2001; Helfgen et al. 2003). Relatively good agreement between the model and experimental results were demonstrated for the production of benzoic acid, griseofulvin, and β-sitosterol by RESS (Helfgen et al. 2003). While trends relating particle size to experimental parameters such as nozzle design and pre- and postexpansion conditions identified by various models have been in accordance with experimental observations, quantitative determination of nucleation and growth rates for a wide range of drug systems remains challenging because reasonable values for some model parameters cannot be determined experimentally and must be assumed.

Recently, Mullers et al. used RESS as a method to combine micronization and co-crystallization in a single manufacturing step. Pure co-crystals of ibuprofen and nicotinamide were obtained due to the very fast precipitation conditions and the absence of organic solvents. The solubility difference between ibuprofen and

nicotinamide in the supercritical fluid was a concern because it influences supersaturation and thus nucleation. As previously reported (Vemavarapu et al. 2009), the authors stated that a simultaneous precipitation of both components was plausible due to high affinity of the co-former for the drug compared to the solvent. Ibuprofen dissolution rate was significantly increased and was explained by the higher surface area (Mullers et al. 2015).

RESS does not require organic solvents, does not involve milling and may be operated at moderate temperatures (typically below 80 °C). However, the primary drawback of RESS is low process yields. Most organic solids possess low solubility in $scCO_2$ due to the low polarizability of CO_2. Therefore, large amounts of SCF are required to produce relevant batch sizes. For example, the solubility of griseofulvin in $scCO_2$ is only 18 ppm. Therefore, the production of 18 mol (~6 kg) of griseofulvin by RESS would require one million moles (~44,000 kg) of CO_2. In order to overcome the low throughput rates due to low solubility of drug in the SC fluid, closed loop recirculation of the fluid could be incorporated in the manufacturing process. Recovery of the resultant particles is also challenging, as efficient filtration is required to remove such large volumes of solvent (Gupta 2006). To increase drug loading, extraction temperatures and pressures may be increased. The addition of cosolvents, such as methanol, acetone, and ethanol, to $scCO_2$ has also been used to increase drug solubility. However, this tactic is not always recommended as it may lead to solubilization of the particles in the cosolvent. Additional methods to increase process yields and reduce particle coagulation for RESS-based techniques are discussed in the next section.

12.2.4 Modified RESS Processes

RESS into aqueous solutions: Rapid Expansion from Supercritical to Aqueous Solution (RESAS) and Rapid Expansion of a Supercritical Solution into a Liquid Solvent (RESOLV)

To address the significant particle growth that occurs in the RESS process due to particle collisions during free jet expansion, the process was modified by directing the atomized drug–SCF solution into an aqueous solution to provide a barrier against particle growth. This modified RESS process was coined RESAS, also known as RESOLV. In RESAS/RESOLV, the supercritical solution is atomized through a nozzle directly into an aqueous solution containing a stabilizer, typically a surfactant. A schematic for the RESAS/RESOLV process is shown in Fig. 12.13. The nozzle is placed below the surface of the aqueous solution to promote intimate contact between the newly formed nuclei exiting the nozzle and the stabilizers dissolved in the aqueous media. Because the turbulent expansion of CO_2 in a surfactant solution produces considerable amounts of foam, nitrogen is streamed above the aqueous solution to disrupt the foam and facilitate drainage back into the bulk liquid phase (Young et al. 2000).

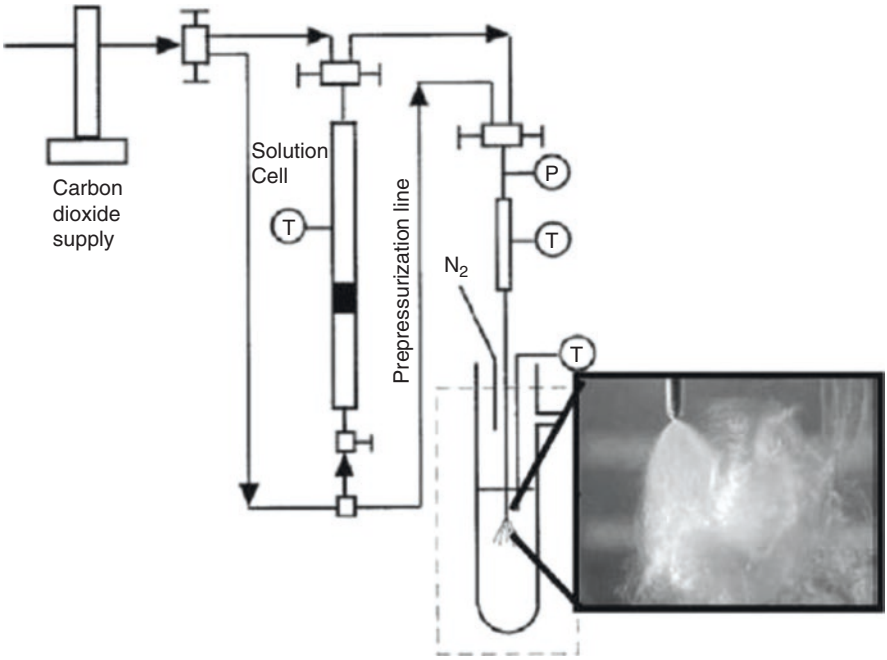

Fig. 12.13 Schematic of RESAS process, inset is a photograph of the spray of the CO_2 solution stream expanding through a tapered elliptical nozzle with a flow rate of 2.5 mL/min at 345 bar. Adapted from Young et al. (2000, 2003)

By atomizing the SCF stream into a surfactant solution, particle growth in the free jet may be arrested by the rapid adsorption of surfactant molecules to the newly formed particle surfaces. Young et al. demonstrated the ability of the RESAS process to produce ~500-nm particles of the poorly water-soluble drug, cyclosporin A (CsA), using Tween 80 as a stabilizer (Young et al. 2000). In contrast, CsA particles produced by RESS, where the $scCO_2$ solution was sprayed into air instead of a Tween 80 solution, were 3–50 μm in diameter. As a control, the $scCO_2$ solution was also sprayed into water containing no surfactant to validate the role of Tween 80 in impeding particle coagulation and growth. Resultant particle sizes ranged between 0.23 and 4.10 μm. Therefore, inhibited CsA particle growth in the RESAS process is attributed to the rapid diffusion of Tween 80 to particle surfaces and its ability to provide steric stabilization to the particles.

The successful production of drug nanoparticles by RESAS/RESOLV has also been demonstrated for ibuprofen (40–80 nm in diameter when stabilized by Tween 80 (Turk 2009) or polyvinylpyrrolidone (PVP_{40K}) (Pathak et al. 2004, 2006), naproxen (64 nm when stabilized by PVP_{40K}) (Turk 2009), and paclitaxel (200–530 nm when stabilized by PVP_{40K} or PVP_{360K}) (Pathak et al. 2007). However, for these cases, the drug/polymer ratio was typically $<<1$, ~0.08–0.2. To better understand how to efficiently increase the drug potency of RESAS particles while

still maintaining submicron particle sizes, the critical processing parameters for the RESAS process were investigated by Young et al. (2000, 2003, 2004). Experimental parameters such as surfactant selection, temperature of the aqueous reservoir, and final drug concentration, in addition to the operating parameters known to influence particle properties in RESS, were varied to manipulate the efficiency of surfactant molecules to stabilize nanoparticles (Young et al. 2000). Nonionic surfactants, Pluronic F127 (also known as poloxamer 407) and Myrj 52, in addition to Tween 80, were explored in efforts to stabilize CsA particles. CsA particles stabilized by Pluronic F127 and Myrj 52 were about twice as large (>840 nm in diameter) as those stabilized by Tween 80 (500 nm in diameter) when produced at similar operating conditions, emphasizing the importance of selecting stabilizers with sufficient affinity for the drug particle surface and adequate chain length to provide steric repulsion. In contrast, a phospholipid-based surfactant produced CsA particles with a mean diameter of 220 nm, about half the size of the Tween 80-stabilized particles produced by RESAS at similar operating conditions. However, higher amounts of phospholipid were necessary to stabilize the smaller CsA particles compared to Tween, only achieving a drug/surfactant ratio of 0.1 compared to 0.65 for Tween-stabilized particles. In the case of phospholipids, the bulk of the surfactant arranges to form vesicles. The aggregation number of surfactant molecules is much larger for vesicles than for micelle-forming surfactants such as Tween, which explains the lower drug/surfactant ratios observed for phospholipid stabilizers. The temperature of the aqueous reservoir is also a key parameter for the RESAS process, as it influences the surfactant assembly and thus the rate at which the surfactant is able to reach the particles' surface. Phospholipid stabilizers are especially sensitive to temperature because vesicles tend to become rigid at temperatures below 25 °C. Hence, phospholipids are more effective stabilizers when heated to higher temperatures and facilitate the stabilization of smaller particles. Under optimized conditions ($T_{\text{aqueous bath}} = 80$ °C, CsA concentration in $CO_2 = 54$ mg/mL, CO_2 flow rate through nozzle = 2.5 mL/min, and pressure drop across nozzle = 345 bar), a phospholipid surfactant mixture stabilized ~500-nm CsA particles (31 % w/w drug) at drug suspension concentrations up to 5.4 % w/w (Young et al. 2004). The increase in drug suspension concentration resulted in slightly increased particle sizes, compared to the 220-nm CsA particles when suspension concentrations were held to 1.3 % w/w (Young et al. 2004).

The RESAS process was shown to successfully produce smaller particles of water-insoluble materials than was achieved by RESS due to particle stabilization within an aqueous surfactant solution. In the case of mild particle aggregation after RESAS precipitation, a high-pressure homogenization step has been added to the end of the RESAS process to promote more uniform PSDs and to break up any aggregates that may have formed. This process train has been patented by RTP Pharmaceuticals Inc., and was later licensed by Baxter Healthcare Corporation for incorporation into their NANOEDGE technology (Hu et al. 2004; Keck and Mueller 2006). The primary limitation of RESAS, as in the RESS process, is that the solute must possess moderate solubility in an SCF.

12.2.4.1 Rapid Expansion of Supercritical Solutions with Solid Cosolvents (RESS-SC)

In the RESS-SC process, a cosolvent that solidifies upon atomization from the nozzle is used to enhance the solubility of solutes in $scCO_2$, as well as provide a barrier for coagulation in the free jet during $scCO_2$ expansion (Thakur and Gupta 2005). In contrast to RESS, where the nuclei tend to coagulate during free jet expansion, the excess amounts of solid cosolvent added during the RESS-SC process surrounds the nuclei to create a physical barrier to reduce coagulation. The cosolvent may be removed later by lyophilization. A schematic representing the RESS-SC technique, in contrast to RESS, is shown in Fig. 12.14.

In addition to the typical operating parameters that are important in RESS, clearly, the selection of the solid cosolvent is a key parameter in the RESS-SC process. The solid cosolvent must be nonreactive with the drug and CO_2, possess good solubility in $scCO_2$, be in the solid state at the nozzle exit, have a reasonably high vapor pressure to facilitate removal by sublimation, and, preferably, inexpensive since excess amounts are needed to maintain submicron particle sizes. Thus far, menthol has been the most prevalently used solid cosolvent for RESS-SC applications. Menthol is a natural product extracted from mint-flavored plants, possesses a melting point of 42 °C, and satisfies all the criteria listed above. Menthol enhanced the solubility of the poorly water-soluble drug griseofulvin 28-fold in sc-CO_2, enabling the production of 50–250-nm particles by RESS-SC, which is an order of magnitude smaller than those produced by RESS, at a 28-fold increase in payload. Aminobenzoic acid (80-nm mean diameter) and phenytoin (120-nm mean diameter) particles have also been produced using the RESS-SC process (Thakur and Gupta 2005, 2006a, b). The RESS-SC technique broadens the applicability of the RESS process to more drugs, as well as facilitates the production of higher payloads compared to RESS. Yet, stability and reproducibility of the nanoparticles are a concern; Uchida et al. successfully overcame poor particle size

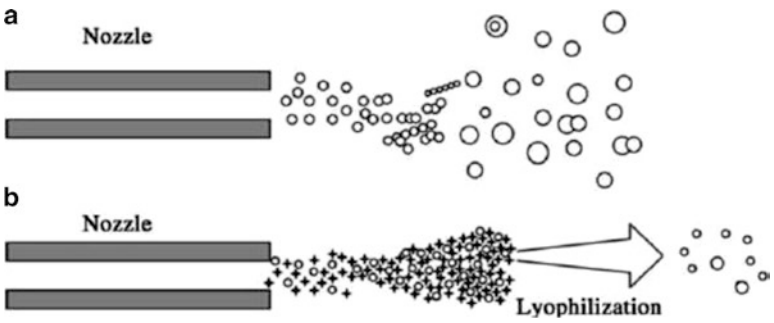

Fig. 12.14 (**a**) Schematic of the RESS process and (**b**) RESS-SC process. *Circles* represent drug particles and *stars* represent solid-cosolvent particles. Reprinted with permission from Thakur and Gupta (2005). Copyright (2005) American Chemical Society

and morphology reproducibility occurring with menthol co-solvent, by replacing it with vanilline (Uchida et al. 2015). However, not all drugs exhibit increased solubility with the presence of solid co-solvents and thus RESS-SC is not a universal solution for all drug systems.

12.2.4.2 Particles from Gas Saturated Solutions (PGSS) Process

The PGSS process flow is similar to RESS, but differs in the case that CO_2 does not act as a solvent. In PGSS, the CO_2 is dissolved in a melted solid and the mixture is depressurized through a nozzle. Expansion of the dissolved CO_2 results in intense atomization and cooling of the molten solid, and thus precipitation of particles. This process is suitable for materials with a large solubility in CO_2, such as PEGs and oils (Martin et al. 2010; Perrut et al. 2005). Benefits of this process are that it consumes less CO_2 than the previously discussed SCF technologies, may be operated under moderate pressures (10–15 MPa), and solubility of the drug in the CO_2 is not necessary to achieve high process yields, as the drug can be dispersed in the melted solid (Martin et al. 2010; Perrut et al. 2005). Therefore, this precipitation process is optimal for polymer encapsulation and is capable of particle micronization, typically yielding micron-sized particles, larger than achieved by RESS (~3–60 μm for theophylline and PEG 6000 (Martin et al. 2010; Rodrigues et al. 2004). Theoretical models that describe the PGSS process, which were built upon existing RESS models, suggest that the larger particles produced by PGSS compared to RESS are due to significant coagulation in the free jet region (Martin and Cocero 2008; Li et al. 2005). Recently, PGSS has been used as a manufacturing technique for lipid based microparticles in order to improve their dissolution. Fenofibrate solid dispersion in Gelucire 50/13 was obtained and exhibited improved dissolution profile (Pestieau et al. 2015).

12.2.5 Comparison of Precipitation Processes Utilizing Supercritical Fluids

SCF precipitation technologies have demonstrated the ability to produce submicron particles of poorly water-soluble drugs. However, the creation of submicron particles is not considered typical for any of the processes, as 1–5-μm particles are commonly produced. The experimental research in this area has been predominantly descriptive, rather than predictive, with the conclusions heavily dependent upon the materials and conditions of that specific study. The inability to develop generalized models that accurately predict final particle sizes with respect to different operating parameters over a wide range of drug systems is due to the simultaneous influence of the operating parameters on multiple particle formation and growth factors, such as thermodynamics, fluid mechanics, mass transfer, and mixing and precipitation

Table 12.5 Comparison of micronization techniques using compressed fluids

Process	Temperature (°C)	Organic solvent required	Compressed fluid as solvent	Compressed fluid as antisolvent	Yields poorly water-soluble nanoparticles
GAS	25–80	Yes	No	Yes	Yes
PCA/SAS/ASES/ SEDS	25–80	Yes	No	Yes	Yes
RESS	≤100	No	Yes	No	Yes
RESAS	25–80	No	Yes	No	Yes
PGSS	~25–40	No	No	No	No

Adapted from Rogers et al. (2001a) and Perrut et al. (2005)

kinetic behavior. Despite case-specific results, general attributes of the different processes may be identified to provide general guidelines as to the capabilities of each process. Comparisons between the different SCF micronization options are shown in Table 12.5.

Generally, GAS processes produce larger particles than PCA processes, primarily due to the higher mass-transfer rates achieved in PCA. Characteristic mass-transfer times (τ_{mt}) for GAS and PCA processes have been calculated based on models developed by Lin et al. and Werling and Debenedetti (Fusaro et al. 2005; Werling and Debenedetti 1999, 2000; Lin et al. 2003).

$$\tau_{mt}^{GAS} = M_0 / M_{CO_2}, \tag{12.8}$$

$$\tau_{mt}^{PCA} = t_{\max} V_0 / \left(V_{\max} - V_0\right). \tag{12.9}$$

where M_0 is the initial amount of solvent, M_{CO_2} is the CO_2 addition rate, t_{max} is the time for the solvent droplet in the PCA process to swell to its maximum diameter, V_0 is the original volume of the solvent droplet prior to swelling, and V_{max} corresponds to the volume of the solvent droplet at its maximum diameter. In the GAS process, the mass-transfer rate is a function of the CO_2 addition rate. In PCA, the mass-transfer rate is correlated to the change in volume of the solvent droplet due to the mass transfer of CO_2 into the droplet. Figure 12.15 illustrates the effect of characteristic mass-transfer times on particle size, based on Lin's model. The estimated range of mass-transfer times for PCA is about two orders of magnitude smaller than that for the GAS process, further validating the theory that the primary difference between these two processes is the mass-transfer rates that can be achieved. These mass-transfer rates correlate directly with rates of generation of supersaturation, and thus give an indication of characteristic nucleation times. These estimates were confirmed experimentally by the precipitation of the poorly water-soluble drug paracetamol using both GAS and PCA. Mean particle sizes ranging

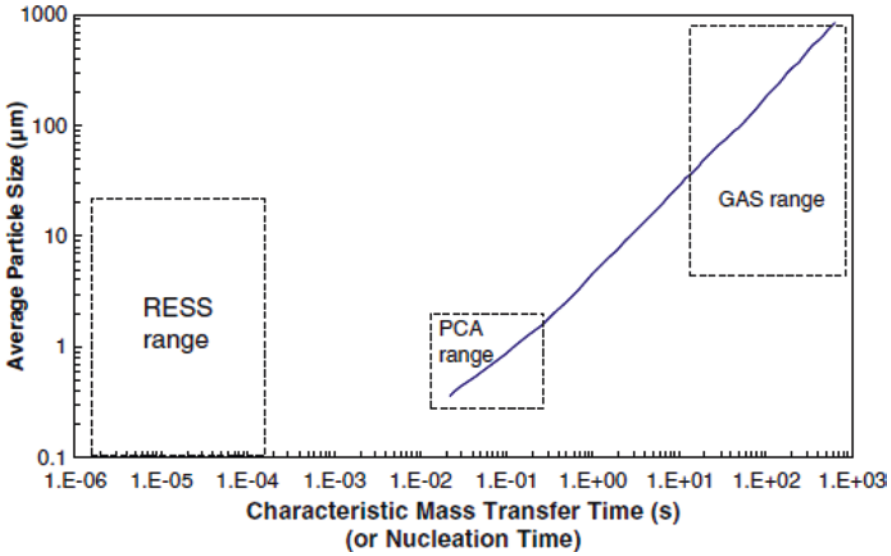

Fig. 12.15 Average size of particles produced by SCF-based precipitation technologies (GAS and PCA) as a function of the characteristic mass-transfer time calculated using the model presented in Lin et al. (2003). If the characteristic mass-transfer time is believed to correlate directly with characteristic nucleation times, then the RESS process may also be quantitatively compared to GAS and PCA. Adapted from Fusaro et al. (2005). Copyright 2005 with permission from Elsevier

from 90 to 250 μm were produced by GAS precipitation, in comparison to 1.3–2.5 μm for PCA. Corresponding mass-transfer times were 20–900 s and 0.04–0.12 s for GAS and PCA, respectively, in the range predicted in Fig. 12.15.

In contrast to GAS and PCA, precipitation by RESS results from a sudden change in pressure, which causes a decrease in solvent power, and thus prompts nucleation and precipitation of particles. Depressurization of CO_2 during RESS has been reported to occur at the speed of sound, corresponding to timescales on the order of 10^{-6}–10^{-4} s (Debenedetti et al. 1993). Because the timescale over which depressurization occurs may be correlated to the timescale during which nucleation occurs, one may expect RESS to be capable of producing smaller nanoparticles, compared to PCA and GAS. However, collisions in the free jet lead to particle growth and similar particles sizes, unless a solvent containing a stabilizer is utilized as in RESAS and RESOLV or RESS-SC. Additionally, RESS does not utilize organic solvents and therefore minimizes environmental and toxicity concerns regarding residual solvent levels. PGSS requires neither organic solvents nor the solute to possess high solubility in CO_2, thus facilitating large process yields. The primary drawback to PGSS is that significant coagulation between primary particles occurs during processing, resulting in typical particle sizes greater than several microns.

12.2.6 Evaporative Precipitation into Aqueous Solution (EPAS)

To address the solubility restrictions that have limited the applicability of SCF precipitation technologies for nanoparticle production, the evaporative precipitation into aqueous solution (EPAS) process was developed based upon similar operating principles as RESAS. In EPAS, the drug is dissolved in an organic solvent and then atomized into a heated aqueous solution. Stabilizers may be incorporated into the organic or aqueous phase, or both. A schematic representing the EPAS process is shown in Fig. 12.16. The elevated temperature of the aqueous solution facilitates rapid evaporation of the organic solvent, which induces supersaturation and subsequent nucleation of the drug. The large interfacial area produced by the nucleating surfaces provides a strong driving force for the adsorption of the stabilizers to the newly formed particles. Passivation of the particle surface by stabilizers hinders particle growth via condensation and coagulation. The resultant particles may be harvested by filtration, lyophilization, or spray drying of the drug dispersion (Sarkari et al. 2002). Because organic compounds generally possess significantly higher solubilities in organic solvents as compared to SCFs, particularly CO_2, the EPAS process is more amenable to a wider variety of APIs and can achieve higher process yields, compared to RESAS.

The key operating parameters that impact particle size and morphology in the EPAS process are similar to those mentioned for RESAS, as EPAS parallels RESAS

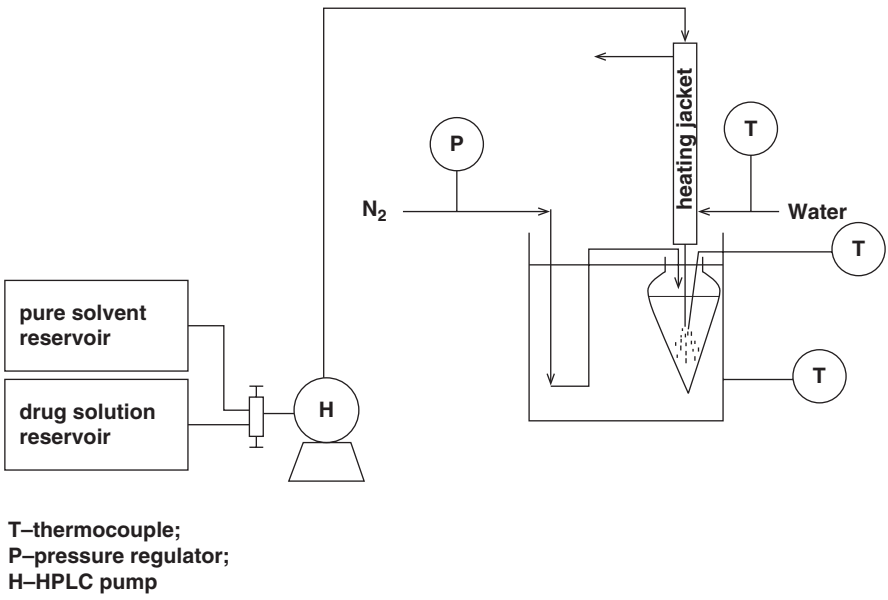

Fig. 12.16 Schematic of EPAS. Reprinted from Chen et al. (2002). Copyright 2002 with permission from Elsevier

in many aspects. However, the evaporation of CO_2 droplets is more rapid than for an organic solvent. Droplet formation is well defined in RESAS because CO_2 is only slightly miscible with water. In EPAS, dichloromethane (DCM) has been chosen as the organic solvent because of its similar low miscibility with water in addition to its ability to solubilize a variety of organic compounds. Minimizing the miscibility of the organic solvent with the aqueous solution reduces particle growth via Ostwald ripening and limits the tendency of the organic solvent to interfere with the capabilities of the surfactant to coat the particles and provide steric stabilization. For CsA particles stabilized with Pluronic F127, smaller particles were produced when DCM was chosen as the organic solvent versus diethyl ether (mean particle diameter of 423 nm versus 1218 nm using DCM and diethyl ether, respectively) (Chen et al. 2002). Both solvents possess similar volatilities and heats of vaporization (Carl 1999). However, at the aqueous reservoir temperature of 75 °C, the solubility of DCM in water is 4 mg/mL, compared to 12 mg/mL for diethyl ether.

Due to the similar particle formation mechanisms of EPAS and RESAS, key EPAS operating parameters also include nozzle design, process temperature, stabilizer selection and concentration, and final suspension concentration in the aqueous phase. The nozzles used in EPAS processes are similar to those for RESAS, targeting intense atomization of the organic solution into the aqueous bath to facilitate rapid nucleation, as well as rapid diffusion of the stabilizers to the particle surfaces. In terms of process temperature, the organic solution is often heated to improve the solute solubility in the organic solution, in addition to promoting more rapid evaporation of the solvent and, thus, supersaturation and nucleation. For similar reasons, the aqueous reservoir is also typically heated, to accelerate evaporation, and, thus, nucleation rates. Higher temperatures in the aqueous reservoir also promote the diffusion of the stabilizers to the particle surface. Chen et al. (2002) showed that the size of polyvinylpyrrolidone (PVP)-stabilized CsA particles decreased from 1354 to 803 nm when the temperature of the aqueous solution was increased from 55 to 85 °C. However, the opposite trend was observed for CsA particles stabilized with Tween 80 where, under the same operating conditions, mean particle size increased from 308 to 774 nm for the same temperature increase. In the case of ethoxylated surfactants, such as Tween 80, high temperatures weaken the hydrogen bonding between the ethylene oxide groups and, thus, hinder steric stabilization (Blankschtein et al. 1986). High temperatures also have an adverse effect on some triblock copolymers, such as Pluronic F127, in which the solution viscosity increases for elevated temperatures, resulting in longer diffusion times (Sinswat et al. 2005). Therefore, the effect of temperature on stabilizer performance should be considered during stabilizer selection. Another parameter that must be addressed, due to its influence on supersaturation levels, is the drug concentration in the feed solution. Unlike RESAS, in which the drug concentration is limited by low solubility in CO_2, feed concentration may be varied in EPAS due to the larger solubilities of drugs in organic solvents. When the feed CsA concentration was increased from 1 to 5 % w/v, the average size of CsA particles decreased by at least 40 %, down to submicron particles, when stabilized by several different surfactants (Chen et al. 2002). The higher drug concentrations in the feed

generated higher degrees of supersaturation during solvent evaporation, leading to smaller particles.

Typical particle sizes generated by EPAS, as determined by light scattering, are in the range of 1–10 μm. However, analysis of the particles by microscopy and Brunauer–Emmett–Teller (BET) surface-area measurements suggests that the micron-sized entities are actually aggregates of smaller, submicron particles (Vaughn et al. 2005; Sinswat et al. 2005). As the solvent evaporates and nucleation occurs, the nuclei become more concentrated as the organic droplet shrinks, which increases the probability of coagulation. Thus, effective stabilization after nucleation is necessary to maintain small particle sizes. The selected stabilizer should diffuse rapidly in the appropriate solvent, have sufficient chain length to provide steric stabilization, and have a high affinity for adsorption of the drug surface. In general, larger-molecular-weight (MW) stabilizers take longer to diffuse to particle surfaces, compromising final particle size. On the other hand, the greater radius of gyration provides better steric stabilization. Therefore, the need for rapid diffusion to the particle surface must be balanced with the need for a surfactant with sufficient MW to provide effective steric stabilization. Several studies have compared the steric capabilities of various surfactants. For example, CsA particles prepared by EPAS using Tween 80 or Myrj 52 were ~500–600 nm in diameter, compared to ~1100 nm when stabilized using higher MW PVP 40 T under the same operating conditions. However, PVP 40 T was found to be a better stabilizer for danazol particles produced by EPAS, compared to lower MW surfactants such as Pluronic F127, sodium lauryl sulfate (SLS), and sodium deoxycholic acid (DCA). PVP-stabilized danazol particles were 10–17 μm in diameter, compared to 22–30-μm particles when stabilized by the lower MW surfactants (Chen et al. 2004a). It is interesting to note the large disparity between the sizes of the CsA and danazol particles stabilized with PVP 40 T, under similar operating conditions. PVP-stabilized CsA particles produced by EPAS ranged between 600 and 1100 nm in diameter for final dispersion concentrations between 1 and 5 % w/v, whereas PVP-stabilized danazol particles were 10–17 μm when prepared at a 2 % w/v aqueous dispersion (Chen et al. 2002, 2004a). This difference in size highlights the fact that stabilizer selection is highly dependent upon the affinity of a stabilizer to adsorb on a particular drug surface, in addition to growth rates for particular drugs.

In EPAS, another factor to consider when selecting the appropriate surfactant is whether to incorporate the stabilizer into the organic phase, in addition to the aqueous phase. The addition of effective amounts of stabilizers to the SCF phase was not plausible in RESAS due to the low solubility of many stabilizers, especially high-MW polymers, in SCFs. The addition of a stabilizer to the organic phase in EPAS has enabled the production of smaller particles, compared to systems where the stabilizer is only present in the aqueous phase, because less time is required for the surfactant to diffuse to the particle surface, as it does not need to cross the aqueous/solvent boundary. The average diameter of carbamazepine (CBZ) particles prepared by EPAS stabilized using Pluronic F127 was ~20 % lower when the Pluronic was integrated into the organic phase versus the aqueous phase (mean

diameter of 13 and 16 μm, respectively) (Sarkari et al. 2002). When stabilizers were added to both the organic and the aqueous phases, even smaller particles were created, about 40 % lower than when Pluronic was added only to the aqueous phase. The ability to reduce particle sizes by including stabilizers in both the organic and aqueous phases during EPAS precipitation was also demonstrated for danazol and itraconazole (Itz) particles, where particle-size reductions up to one order of magnitude were achieved, down to submicron levels, depending on the selected combination of stabilizers (Vaughn et al. 2005; Sinswat et al. 2005).

Interestingly, high-potency particles, greater than 50 % w/w drug, may still be produced by EPAS despite increasing the concentration of stabilizers in both the organic and aqueous phases. As mentioned previously, particle growth is impeded by the adsorption of stabilizers to the particle surface. Because the hydrophilic portions of the surfactant favor the drug–water interface, relative to the hydrophobic particle interior, the surfactant selectively orients itself at the particle surface (Matteucci et al. 2007). Upon passivation of the particle surface, the loading of surfactant is limited by the equilibrium adsorption. Therefore, the most effective strategy for stabilizing particles produced by EPAS is to accelerate surfactant adsorption to the nucleating surfaces through surfactant selection and placement and to use excess amounts of surfactant. Unadsorbed surfactant may be removed by centrifugation after precipitation (Vaughn et al. 2005; Sinswat et al. 2005). EPAS production of Itz yielded particles with a BET surface area of 6.31 m^2/g (~731 nm in diameter, assuming a spherical geometry) and 93.8 % w/w potency when the stabilizer, Pluronic F127, was added to both the organic and aqueous phases (Sinswat et al. 2005; Chen et al. 2004b). When Itz was stabilized using PVP-K15 by EPAS, particles as small as 500 nm in diameter were achieved for a drug-to-excipient ratio of 0.79 (Chen et al. 2004b). It should be noted, however, that slightly larger particle sizes are generally observed as the drug/surfactant ratio (i.e., drug potency) is increased (Chen et al. 2002, 2004b, 2006). For the precipitation of CsA particles with Tween 80 as the stabilizer, the mean particle size increased from 338 nm to 523 nm to 921 nm when the drug-to-excipient ratio was increased from 0.33 to 0.72 to 2.50, respectively (Chen et al. 2002).

Contact-angle measurements verified that the hydrophilic stabilizer sufficiently coated the surface of the particles, as expected, given the colloidal stability. For these measurements, the drug dispersions produced by EPAS were centrifuged to remove unadsorbed surfactant, dried, and the resultant powder was compacted into a tablet. The contact angle observed for a droplet of water on the tablet surface was then measured. The contact angle for Itz tablets prepared from EPAS powder was ~32 % smaller than that for a tablet prepared from a physical mixture of the identical composition, validating the claim that the EPAS process tends to orient the stabilizers to the particle surface (Sinswat et al. 2005). Additional studies have verified these results, where high-potency particles of carbamazepine and danazol produced by EPAS, composed of at least 50 % w/w drug, possess smaller contact angles than identical formulations prepared as a physical mixture (Vaughn et al. 2005; Sarkari

et al. 2002). The lower contact angles of the EPAS particles also indicate enhanced wettability over the physical mixtures, which is especially important to achieve favorable dissolution rates for poorly water-soluble drugs. Because the EPAS process preferentially concentrates the surfactant at the particle surface, where steric and wetting capabilities are maximized, only small amounts of surfactant are required to stabilize particles with high drug potency and to improve wettability for enhanced dissolution. EPAS has also demonstrated advantages with respect to quercetin chemical stability in nanosuspension compared to solution. This was explained by surface coverage by the surfactant coupled with a nanosuspension, which offered only the outer surface for degradation. It was also mentioned that due to protection of the stabilizer layer, even the outer surface was protected from degradation (Gao et al. 2011).

Due to the ability of EPAS to produce particles with good surfactant coverage, high drug suspension concentrations can be obtained, typically between 15 and 50 mg/mL, which is highly attractive for parenteral applications (Vaughn et al. 2005; Sarkari et al. 2002; Sinswat et al. 2005). However, for higher suspension concentrations, larger particle sizes, as well as broader PSDs, are observed. When higher suspension concentrations are desired, it is often beneficial to increase the surfactant concentration in the system, to ensure sufficient coverage of the drug particles. An additional benefit of the well-stabilized EPAS particles is that after drying the drug dispersion, the powders have been shown to redisperse to sizes similar to those present in the original dispersion, indicating good stabilizer coverage of the particles (Chen et al. 2004a). Moreover, the EPAS process was shown to produce both crystalline and amorphous particles, depending on the stabilizers chosen. Rapid stabilization of particles, before molecules are able to rearrange into the crystalline structure, leads to higher amorphous content in the particle. Table 12.6 summarizes some particle properties achieved through precipitation by EPAS.

The advantages of EPAS and emulsion templating have been combined in order to develop a more robust precipitation process called Advanced EPAS. Indeed, replacing the organic solution with an oil-in-water emulsion allowed for better control over the particle size than compared with an organic solution as used in EPAS. The evaluation of the influence of processing parameters demonstrated independence with regards to particle size proving the robustness of the process. Furthermore, Advanced EPAS overcomes the limitation of EPAS in terms of scale up as the requirement for consistent atomizing nozzle is eliminated (Bosselman et al. 2012).

12.3 Antisolvent Precipitation Using Organic Solvents (AP)

The AP process, in which organic solvents make up the solvent phase, is one of the most common bottom-up approaches for particle formation. AP processes are relatively simple, cost effective, and may be operated continuously, facilitating scale-up. The scalability of AP processes has been demonstrated by Novartis for the production of hydrosols and by Soliqs/Abbott for Nanomorph products (Keck and

Table 12.6 Drug particles produced by EPAS

Drug	Stabilizer	API/ stabilizer	Mean particle diameter (μm)	Dispersion loading (mg/mL)	Amorphous
Itz (Chen et al. 2004b; Sinswat et al. 2005)	PVP-K15	0.9–0.7	~0.51 (BET: 9 m^2/g)	10	No
	Pluronic F127				
	Combination				
	Tween80	9.5–15	~730–1500 (BET: 3.1–6.3 m^2/g)	15	No
	PVP-K15				
	Pluronic F127 Combination				
CsA (Chen et al. 2002)	l-α-Phosphatidyl-choline	0.14–0.35	0.25–0.47	14–35	Yes
	Brij	0.3–0.5	0.033–1.04	5–50	Yes
	Myrj				
	Tween				
	PEGs	0.3–0.5	0.077–1.39	5–50	Yes
	PVPs				
CBZ (Sarkari et al. 2002)	Dooxycholic acid	0.45–0.83	12–19	9–40	Yes
	PVP-K15				
	Sodium dodecyl sulfate				
	Pluronic F127				
Danazol (Chen et al. 2004a; Vaughn et al. 2005)	PVPs	0.5–4	12–30	5	No, but ~20 % reduced crystallinity
	Sodium dodecyl sulfate				
	Dooxycholic acid				
	Pluronic F127				
	Combination				
	PVP-K15	1	0.62 (BET: 7.41 m^2/g)/~0.15–0.5 μm drug domains in 7–10 μm aggregates	Not reported	Yes
Riccardin D (Liu et al. 2012)	Poloxamer 188	0.33	~0.18	100	No
	HPMC				
	PVP K30				
	Combination				

Mueller 2006). Similar to EPAS, larger process yields are generally obtained from AP operations, as compared to SCF-based techniques, because organic compounds possess higher solubilities in organic solvents than in SCFs. Additionally, many of the same particle formation mechanisms discussed for EPAS apply to AP

technologies. In AP, the poorly water-soluble drug is first dissolved in an organic solvent and then the drug solution is mixed with an antisolvent, often water. As the two phases mix, the drug solubility decreases, resulting in supersaturation of the drug, which drives nucleation. Unlike EPAS, an organic solvent that is miscible with the antisolvent is selected to facilitate mixing between the two phases. Diffusion of the organic solvent into the aqueous phase tends to spread the nuclei apart, reducing coagulation rates compared to EPAS, in which droplet shrinkage during solvent evaporation tends to promote coagulation of nuclei. Stabilizers may be added to the solvent or antisolvent phases to further mitigate particle growth by condensation and coagulation. The hydrophilic segments of the stabilizer preferentially extend toward the aqueous environment and, thus, the stabilizer adsorbs at the drug–water interface and not within the interior of the particle. Passivation of the particle surface by the stabilizers hinders particle growth. The selective orientation of the stabilizer at the particle surface facilitates the production of stable, high-potency drug particles with a minimum stabilizer to drug ratio. An illustration of the driving mechanism for the AP process is shown in Fig. 12.17.

In the previously discussed precipitation-based particle formation techniques, micron-sized particles are more commonly produced than submicron particles. In AP, process and formulation parameters can often be manipulated to yield submicron particles. A contributing factor to the higher propensity for AP to form nanoparticles is the miscibility between the solvent and antisolvent, which facilitates both rapid supersaturation as well as efficient adsorption of stabilizers to nucleating drug particles. Additionally, atomization of a partially miscible drug solution into the aqueous phase is not necessary to achieve small particles because the solvent and antisolvent are fully miscible. Therefore, a critical determinant of final particle size is the efficiency of mixing between the antisolvent and solvent phases. The impact of mixing on particle formation may be described by the Damkohler number (*Da*), defined as the ratio of mixing time (τ_{mix}) to precipitation time (τ_{prec}).

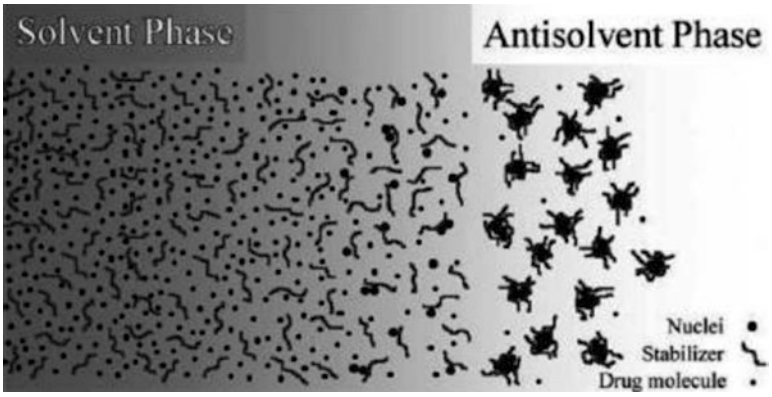

Fig. 12.17 Schematic of antisolvent precipitation (AP) of drug particles in the presence of amphiphilic stabilizers. Reprinted with permission from Matteucci et al. (2006). Copyright (2006) American Chemical Society

$$Da = \tau_{mix} / \tau_{prec}. \tag{12.10}$$

τ_{prec} is a function of condensation time, τ_{cond}, and coagulation time, τ_{coag} (refer to Fig. 12.1). Poor mixing conditions (i.e., large τ_{mix}, resulting in a large *Da*) lead to low, and often nonuniformly distributed, levels of supersaturation, which subsequently result in slower nucleation rates, relative to particle growth rates. These poor mixing conditions tend to produce large polydisperse particles.

Favorable operating conditions promote rapid mixing, and thus facilitate the production of smaller particles, as characterized by *Da* values near unity. A reduction in *Da* may be accomplished by generating greater supersaturation via more rapid nucleation (to reduce τ_{mix}) and/or by extending the time for condensation and coagulation via the addition of stabilizers (to increase τ_{prec}). When *Da* is equal to unity, the particle formation process is insensitive to further reductions in mixing time. Figure 12.18 illustrates this concept, where the size of β-carotene particles was found to decrease with increased jet velocity, which influences mixing intensity, until a threshold value was reached (Johnson et al. 2006). Above this threshold, the particle size remained constant with further increases in jet velocity.

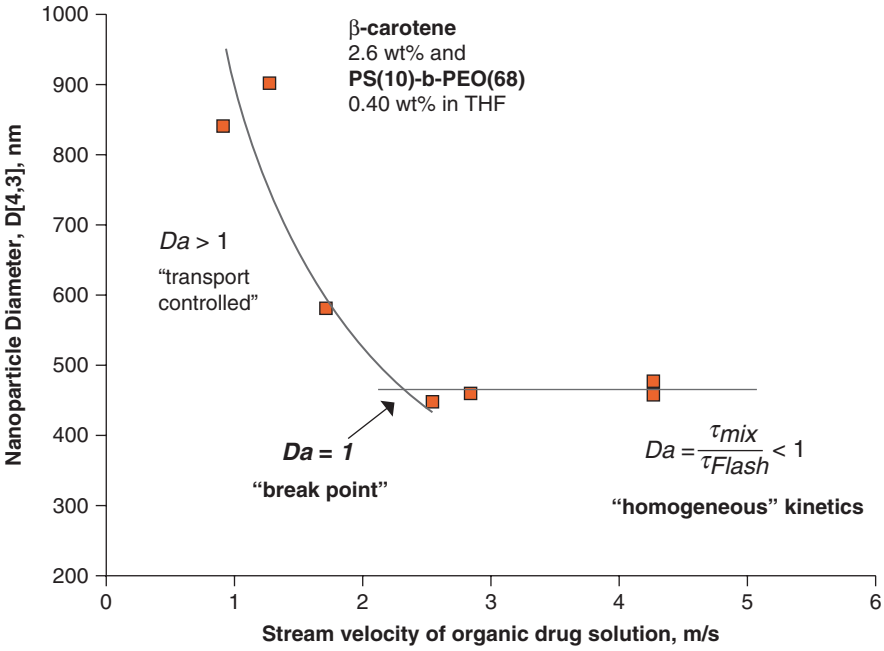

Fig. 12.18 Diameter of β-carotene particles produced by AP, as a function of the stream velocity of the organic drug solution into an aqueous antisolvent. An increase in stream velocity results in a decrease in particle size until the break point is reached. Adapted and reprinted with permission from Johnson et al. (2006). Copyright (2006) American Chemical Society

Therefore, when $Da > 1$, the particle formation process is "transport controlled," signifying that mixing times may be optimized to achieve smaller particles. However, if conditions correspond to a $Da \leq 1$, the process conditions have already been optimized to minimize particle size and only a reduction in drug concentration or a change in solvent or stabilizer selection may offer further improvements for particle size reduction.

The limits of AP processing parameters were thoroughly investigated by Matteucci et al. to gain a solid understanding of the impact of process parameters on the mechanisms driving particle formation and stabilization, primarily for cases where high drug loadings are desired. In the study, Itz, the model poorly water-soluble drug, was stabilized using the amphiphilic polymer Pluronic F127 (P127). Process parameters including stabilizer concentration, the phase in which the stabilizer is added, process temperature, and mixing intensity between the organic and aqueous phases were examined. As in EPAS, higher concentrations of stabilizers resulted in smaller particles when prepared by AP, as expected. Additionally, for a given amount of stabilizer, smaller particles were obtained when the stabilizer was added to the organic versus the aqueous phase. Therefore, for P127-stabilized-Itz particles of similar sizes, a 50 % w/w drug loading can be achieved when P127 is added to the organic phase, compared to only a 25 % w/w Itz loading when P127 is incorporated in the aqueous phase. Another important process parameter for both EPAS and AP is the final suspension concentration. As in EPAS, increased suspension concentrations, which were achieved by increasing feed drug concentrations, generally led to larger particle sizes during AP unless stabilizer levels were also increased accordingly. However, upon reaching a threshold stabilizer level, Itz drug loadings up to 86 % w/w were produced at minimal cost to particle size. In fact, the PSD did not change significantly when the solid loading in the final suspension was varied between 1.8 and 8.9 mg/mL. Matteucci et al. calculated nucleation and growth rates using a population balance model in conjunction with the mixed-suspension, mixed-product-removal crystallization (MSMPR) model to characterize nucleation and growth kinetics (Jarmer et al. 2004), in order to justify the differences in PSD for different experimental parameters.

The temperature of the aqueous bath, into which the organic drug solution is introduced, was also shown to heavily influence final particle size. Matteucci et al. reported that the average particle size of Itz particles stabilized with P127 increased only 15 % when the temperature was raised from 3 to 10 °C. However, particle sizes increased by a factor of 40 when the temperature of the aqueous reservoir was set near room temperature, at 20 °C. The operating temperature influences several aspects of the particle formation process. While higher temperatures generally increase diffusion rates to allow stabilizers to quickly reach growing particle surfaces, they also tend to cause an increase in drug solubility in the solvent/water mixture, which reduces supersaturation and nucleation rates and increases the propensity for Ostwald ripening, all of which leads to larger particle sizes. Additionally, elevated temperatures tend to desolvate amphiphilic molecules due to weakened hydrogen bonding with water, which may reduce steric stabilization. Unlike EPAS, where higher temperatures are needed to facilitate solvent evaporation

and, thus, subsequent supersaturation, smaller particle sizes are expected when the aqueous reservoir is maintained at lower temperatures during antisolvent precipitation. For Itz particles stabilized with P127, Matteucci et al. recommended operating at a precipitation temperature of 3 °C (Matteucci et al. 2006).

To examine the role of mixing energies, characterized by *Re*, on final particle size, the intensity by which the organic solution was introduced to the aqueous phase was adjusted by varying nozzle diameters and jet velocities. Not surprisingly, smaller nozzle diameters and higher jet velocities, which create higher *Re* conditions, tended to yield smaller particle sizes. However, Matteucci et al. found that particles with sizes similar to those produced under high *Re* conditions could still be produced under low or moderate mixing energies by adjusting other experimental parameters to push the *Da* back toward unity, such as increasing the flow rate of the organic solution (decreases τ_{mix}) and/or increasing the stabilizer concentration in the aqueous bath (increases τ_{prec}). Therefore, compensation for a nonoptimal mixing intensity by tuning another process parameter toward a more-optimal setting allows a targeted *Da* condition of unity to be achieved and thus facilitates the production of submicron particles even at lower mixing intensities, which require lower energy inputs (Matteucci et al. 2006). A summary of how different process parameters can compensate for lower *Re* conditions to yield submicron particles is shown in Table 12.7.

Table 12.7 Compensation variables that may be adjusted to maintain a low Damkohler number

Nozzle type	Organic flow rate (mL/min)	*Re*	Stabilizer concentration (% w/w)	Stabilizer location	PSD[a] (μm) D_{50}/D_{90}
Organic flow rate vs. Re					
0.047″ i.d.	130	3400	75	Aqueous	0.24/0.56
Crimped[b]	10	6300	50	Aqueous	0.23/0.52
Stabilizer concentration vs. Re					
0.0025″ i.d.	10	5000	14	Aqueous	0.27/28
0.03″ i.d.	10	410	67	Aqueous	0.27/2.9
0.03″ i.d.	10	410	75	Aqueous	0.23/0.69
Crimped[b]	10	6300	14	Aqueous	0.23/0.52
Stabilizer concentration vs. location					
0.03″ i.d.	10	410	75	Aqueous	0.23/0.69
0.03″ i.d.	10	410	50	Organic	0.24/0.59
Stabilizer location vs. Re					
0.047″ i.d.	10	410	14	Organic	0.29/4.4
0.03″ i.d.	130	3400	14	Aqueous	0.24/0.56
0.0025″ i.d.	10	5000	14	Aqueous	0.27/28

Adapted from Matteucci et al. (2006)

[a]D_{50} and D_{90} refer to the diameter at which the cumulative sample volume was under 50 % and 90 %, respectively

[b]Crimped nozzle refers to a 0.03″ i.d. stainless-steel tubing that was crimped and then filed at the cut end until a stable atomized flow was achieved, as described in Young et al. (2000)

Table 12.8 Impact of the method by which the organic phase is introduced to the aqueous phase on the size of Itz particles prepared by AP and stabilized with P127

Organic introduction technique	*Re*	Organic flow rate (mL/min)	PSD (μm) $D_{10}/D_{50}/D_{90}$	% < 1 μm	Nucleation rate: 10^{-20} n^0	Growth rate: 10^2 Gτ
Pouring	Low	~340	0.12/0.39/8.4	67	1.6	6.2
Drop-wise addition	Low	~11	0.14/0.83/14	52	1.6	6.2
Syringe (0.047″ i.d.)	3400	~130	0.1/0.24/0.56	97	2.0	6.0
High-velocity jet (0.0025″ i.d.)	5300	10	0.13/0.27/28	86	1.8	6.1

In each case, an Itz loading of 86% w/w and a suspension concentration of 8.9 mg/mL was achieved, with the P127 placed in the aqueous phase only (1.67 mg/mL). Adapted from Matteucci et al. (2006)

Matteucci et al. further explored the range of mixing intensities capable of producing Itz nanoparticles stabilized with P127, ranging from simply pouring the organic into the aqueous solution to drop-wise addition to syringe injection, in addition to the use of high-velocity jets. In all cases, the aqueous phase was mixed using a magnetic stir bar (~500 rpm) to enhance heat and mass transfer during mixing of the organic and aqueous phases. As shown in Table 12.8, submicron particles may still be produced when the organic phase is poured or added drop-wise into the aqueous phase, although a sizable percentage of micron-sized particles were also obtained. These lower-energy, and thus poorer-mixing, conditions likely produce smaller degrees of local supersaturation, resulting in slower nucleation compared to the syringe and high-velocity jet addition techniques. This hypothesis is corroborated by the lower calculated nucleation rates for the lower-energy mixing techniques, as determined using the MSMPR/population model. Interestingly, the addition of the organic solution by syringe at a high organic flow rate of 130 mL/min yielded particles of comparable size to those produced using high-velocity jets, where the organic flow rate was 10 mL/min. Additionally, because the same solvent/stabilizer system was used in all cases, growth rates were relatively similar, with slightly lower calculated growth rates for the syringe and high-velocity jet techniques, attributed to more efficient particle stabilization due to enhanced diffusion of stabilizers to particle surface.

The ability of the AP process to form nanoparticles using low-energy mixing intensity methods has been further demonstrated in several other reports. Rasenack and Muller (2002) showed that, despite the organic drug solution being merely poured into the aqueous phase, Itz nanoparticles were produced when the appropriate stabilizer was selected. In the case of Itz, stabilizing agents containing cellulose ethers with alkyl-substituents, such as methyl cellulose (MC), methylhydroxyethylcellulose (MHEC), and hydroxypropylmethylcellulose (HPMC), effectively protected against particle growth to maintain submicron particle sizes. On the other hand, more hydrophilic stabilizers, such as dextran,

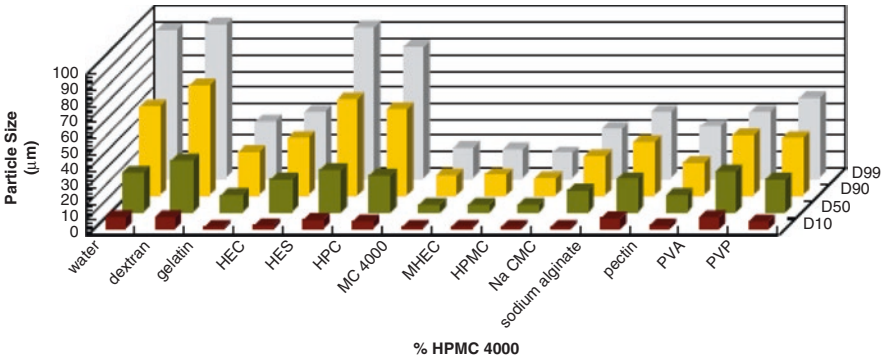

Fig. 12.19 Particle size of itraconazole (Itz) particles produced by AP stored as a dispersion 24 h after precipitation. Concentration of stabilizer in water was 0.025 % w/w. Data from Rasenack and Muller (2002)

polyvinylalcohol, polyvinylpyrrolidone, hydroxyethyl starches (HES), and polar substituted cellulose ethers (hydroxyethyl celluloses (HEC) and hydroxypropyl celluloses (HPC)), yielded micron-sized particles under similar operating conditions (Fig. 12.19). These results indicate that the stabilizer must interact sufficiently with the newly formed surface of the poorly water-soluble compound in order to provide an efficient barrier to particle growth. In the cases of MHEC and MC, the methoxyl and hydroxy propyl groups adsorb onto hydrophobic surfaces (Daniels and Barta 1994). Although HPMC is relatively hydrophilic, it is sufficiently hydrophobic to facilitate adsorption onto hydrophobic particle surfaces (Chang and Gray 1978). The ability of HPMC to efficiently stabilize Itz nanoparticles was further explored by examining the range of HPMC concentrations required for stabilization. A minimum HPMC concentration of 0.025 % in the aqueous reservoir was required to stabilize 600-nm Itz particles under the experimental conditions used by Rasenack and Muller (~30/1 HPMC/Itz, organic solution poured into aqueous solution). Higher HPMC concentrations did not further reduce particle sizes due to the nature by which particles are stabilized in AP, where passivation of the particle surface indicates maximum stabilization (Fig. 12.20). Similar results were observed when HPMC was used to stabilize ketoconazole particles produced by AP under similar operating parameters (Rasenack and Muller 2002). Fenofibrate (~320 nm in diameter) stabilized by a combination of sodium dodecyl sulfate (SDS) and HPMC (Hu et al. 2011) and spirolactone nanoparticles (200–400 nm in diameter) stabilized with HPMC have also been prepared by AP (Dong et al. 2009), where the organic solution was rapidly injected into the aqueous phase using a pipette or syringe. In both studies, the organic and aqueous phases were also pumped into a static mixer, which consists of a chamber containing several baffles to facilitate mixing between entering fluids (Hu et al. 2011; Dong et al. 2010; Gassmann et al. 1994). Resultant fenofibrate and spirolactone particles were of comparable size, although slightly larger, than those prepared when the organic phase was introduced by injection (~330 and 500 nm for fenofibrate and spirolactone, respectively), indicating

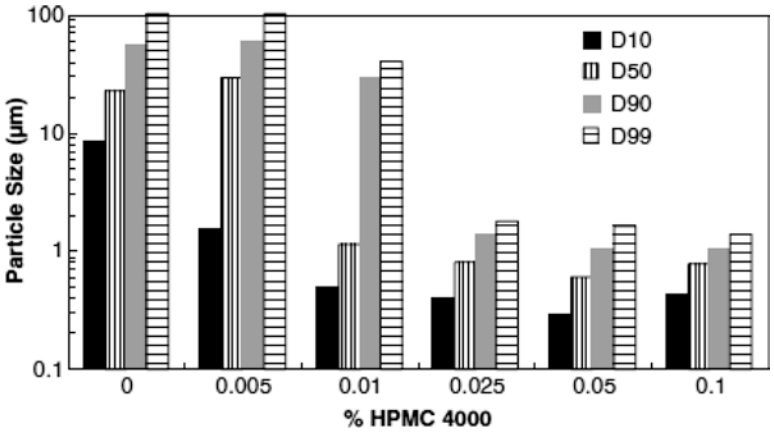

Fig. 12.20 Influence of different concentrations of HPMC 4000 on the size of itraconazole (Itz) particles produced by AP. Particles were stored as a dispersion and sizes were measured 24 h after precipitation. Data from Rasenack and Muller (2002)

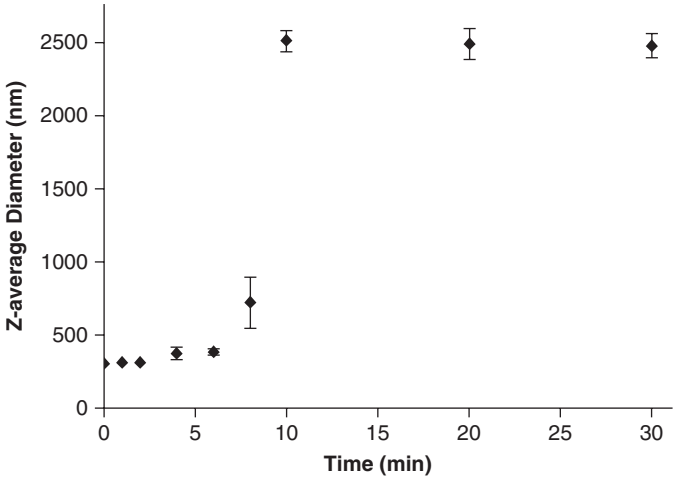

Fig. 12.21 The effect of aging time on the size of freshly precipitated fenofibrate drug particles in dispersion under stirring conditions at the rate of 600 rpm. Reprinted from Hu et al. (2011). Copyright 2011 with permission from Elsevier

relatively efficient mixing within the static mixer. In the case of the fenofibrate particles, continued monitoring of particle size showed that the freshly precipitated particles grew over time if left in the suspension, up to four times the initial size in just 10 min (Fig. 12.21) (Hu et al. 2011). The particle growth may be driven by condensation of dissolved drug molecules and/or Ostwald ripening due to the organic solvent still present in the aqueous suspension. In response to these challenges, modifications to the AP process have been developed to facilitate nanoparticle production as well as to maintain particle size after precipitation by minimizing particle growth and are discussed in the next section.

12.3.1 Recent Trends in AP Processes

12.3.1.1 Flash Nanoprecipitation (FN) Process

To facilitate the production of amorphous nanoparticles for enhanced dissolution of poorly water-soluble drugs, flash nanoprecipitation (FN) aims to minimize mixing times between the solvent and antisolvent, down to millisecond timescales, using a custom-designed confined impinging jet (CIJ) mixer. In a CIJ mixer, a solvent stream and an antisolvent stream are introduced into a mixing chamber at turbulent jet velocities, in such a manner that the two streams are collinear and thus collide with each other. Mixing within impinging jets produces a region of high-energy dissipation, as the kinetic energy of the jet streams is converted to turbulent motion through collision and redirection of fluid flow within a confined volume. These high-energy dissipation regions rapidly reduce the scale of segregation between the two fluid streams, thus facilitating rapid nucleation. The mixing chambers in the FN process must be large enough for the high-energy dissipation regions to form, but limited in volume to avoid significant bypassing of any fluid from intense mixing (Johnson et al. 2006; Johnson and Prud'homme 2003a, b, c). A schematic of the FN process is shown in Fig. 12.22.

Mixing energies characterized by *Re* up to 3000 have been reported for CIJ mixers, corresponding to a characteristic mixing time, τ_{mix}, of 5 ms, when jet diameters,

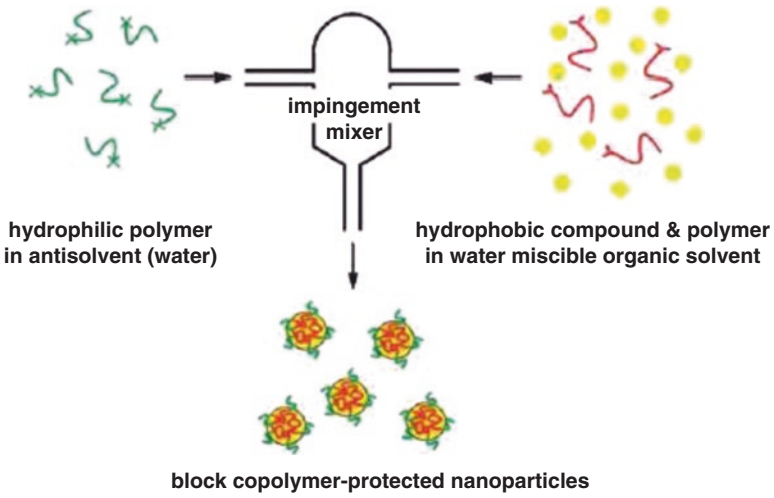

Fig. 12.22 Schematic of confined impinging jet (CIJ) apparatus: A solvent jet, in which the poorly water-soluble drug and stabilizers are dissolved, and an antisolvent jet containing stabilizers are impinged against each other to facilitate mixing of the two solutions. High-velocity impingement promotes rapid mixing within the chamber to facilitate rapid particle precipitation. Reprinted with permission from Zhu et al. (2007). Copyright (2007) American Chemical Society

jet velocities of the fluid stream, and chamber size have been optimized (Johnson and Prud'homme 2003a, b, c). According to Johnson and Prud'homme, optimal performance of the FN) process is achieved when τ_{mix} values are less than 100 ms (Johnson et al. 2006). These low τ_{mix} values promote nanoparticle production, as seen in (12.10), as well as narrow PSDs. In FN studies, Johnson and Prud'homme stress the importance of not only comparing τ_{prec} of the drug to τ_{mix} but also matching τ_{prec} of the drug with τ_{prec} of the stabilizer, especially in the case of polymeric stabilizers. When the precipitation times for the drug and stabilizer are manipulated to match one another, the hydrophobic portion of the stabilizer is designed to precipitate onto the surface of the drug particle at the onset of nucleation, thus deterring further particle growth beyond nucleation sizes. Moreover, the proper selection of stabilizers can act as a nucleation initiator to further control nanoparticle production. Characteristic precipitation times may be adjusted by tuning stabilizer properties, such as molecular weight (MW) and the size ratio of hydrophilic to hydrophobic moieties, as well as the drug feed concentration. To demonstrate the importance of stabilizer selection in FN, β-carotene particles stabilized by polystyrene (PS) (2 K)-*b*-polyethylene glycol (PEG) (5 K) and polycapralactone (PCL) (3.6 K)-*b*-PEG (6 K) were compared. Particles stabilized with PS-*b*-PEG, possessing a drug potency of 66 % w/w, were ~100 nm in diameter, while those stabilized with PCL-*b*-PEG required higher stabilizer levels to achieve an average particle size of 100 nm, reducing the drug potency to 18 % w/w. The reduced effectiveness of the PCL-*b*-PEG polymer to stabilize the β-carotene particles was attributed to the lower melting point of the PCL, which may have facilitated aggregation between the particles (Zhu et al. 2007). Polyelectrolytes such as poly (ethylene imine) or chitosan can also stabilize nanoparticles of β-carotene to an average diameter <100 nm and a drug loading >80 %. Besides steric stabilization, polyelectrolytes also provided electrostatic stabilization of the amorphous nanoparticles as demonstrated by zeta potential measurements. Amorphous state of the nanoparticles was due to fast precipitation (Zhu et al. 2010). FN has also reported the successful production of CsA nanoparticles (~300 nm) stabilized by a combination of dextrose monohydrate and lecithin at a drug potency of 30 % w/w (Chiou et al. 2008a, b). Methods, such as vacuum distillation or spray drying, or dialysis were required to remove the organic solvent from the final suspension in order to minimize aggregation of particles after precipitation Putsulka et al. investigated on the impact of block copolymer, solute and API on the FN process. The results were in agreement with a model developed by Johnson and Prud'homme (2003a). They demonstrated that log P was a good indication of the stability of hydrophobic drugs in nanoparticles. Manufacturing of 100 nm particles with at least 50 % drug loading was reported preferable with small molecules having a log P<6 and >1 % solubility in water miscible solvent. Nonety percent of drug loaded particles were achievable if drug log P was ~10, but the size of the resulting particles were around 200 nm showing the impact of loading on the particle size. Equal mass ratio of small molecule and polymer led to particle size of ~100 nm independent of solid concentration (Pustulka et al. 2013). Log P has also been correlated with particle stability; indeed, log P>12 showed good stability and log P<2 was very

difficult to generate nanoparticles due to its high solubility. Later, Zhu et al. confirmed the importance of drug insolubility to prevent interparticulate migration. They also mentioned the use of log P to predict particle stability, enabling therefore a fast and easy pre-clinical drug screening (Zhu 2014).

The necessity of hand operation for the FNP process was eliminated by modification of the design of the CIJ mixer and by adding a second antisolvent dilution step. These two changes allowed for fast quenching with a high antisolvent concentration enhancing therefore nanoparticle stability. Stable and reproducible nanoparticles (55 nm) of β-carotene were obtained using CIJ with dilution. Because it overcomes the equal volume ratios of original CIJ design, CIJ-D enables a decrease in the volume needed, making it an inexpensive technique (Han et al. 2012).

Recent research on the FN process has focused on the addition of a multi-inlet-vortex mixer (MIVM) to FN (schematic shown in Fig. 12.23) to allow for efficient mixing of multiple streams with unequal flow rates, which has been found to be a requirement for some systems to achieve optimal nano-precipitation conditions. To validate that sufficient mixing is achieved within the MIVM, Liu et al. developed a computation fluid dynamics (CFD) simulations program to emulate flow behavior within the MIVM (Liu et al. 2008; Shen et al. 2011). The simulation was validated using a model experiment, involving a parallel, competing reaction system, in which product yields were measured to give an indication of mixing intensity. Excellent correlation between the simulation and experimental data was found, providing validation of mixing performance within the MIVM, as well as a useful tool to optimize process parameters for nanoparticle production in future studies (Liu et al. 2008). Shen et al. confirmed the rapid micromixing and high supersaturation leading to nanoparticle formation. High Re was important to produce nanoparticles with controlled size distribution as previously mentioned by Liu et al. (2008). MIVM demonstrated the ability to encapsulate at high efficiency a wide variety of materials such as model drug, b-carotene, hydrophilic charged polymers (Shen et al. 2011). In the case of the production of paclitaxel nanoparticles by FN, submicron particles could not be produced using only PCL(3 K)-*b*-PEG (5 K) as the stabilizer. However, the introduction of a PCL homopolymer in addition to the block copolymer using the MIVM-modified CIJ mixer yielded particles ranging from 80 to 145 nm in diameter,

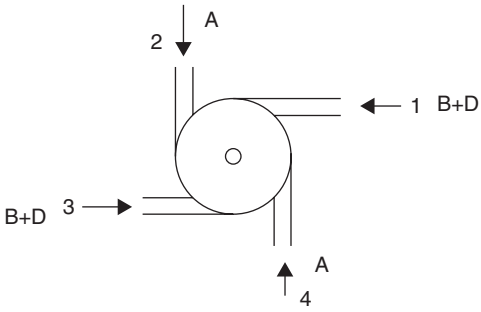

Fig. 12.23 Schematic of a multi-inlet-vortex mixer (MIVM), used to facilitate efficient mixing of multiple feed streams with unequal flow rates into the confined impinging jet (CIJ) mixer. Reprinted from Liu et al. (2008). Copyright 2008 with permission from Elsevier

depending on the MW of the PCL homopolymer (Johnson et al. 2006). The scalability of this new mixer was demonstrated for different chamber geometries and sizes (Johnson et al. 2006). The benefit of highly stabilized nanoparticles of curcumin processed by FN (mean particle size <80 μm) compared to unprocessed particles was demonstrated in vivo in mice with improved clinical efficacy at low dose and much higher bioavailability (Cheng et al. 2013). Recently, Chow et al. also compared the performance of MIVM with a two stream)confined impinging jet with dilution mixer (CIJ-D-M). They showed that both mixers enable particle sizes below 100 nm and high encapsulation efficiency (>99.9%). Particles produced with MIVM displayed better short-term stability as well as roughly spherical particles compared to the irregular nanoaggregates obtained with CIJ-D-M. However, smaller particle size was obtained with the CIJ-D-M; these results were explained by the differences in the configuration of the mixing chambers (Chow et al. 2014). In order to overcome the short-term stability they co-formulated the product with polyvinylpyrolidone (PVP); PVP surrounded the particle in a protective barrier thus preventing the leaking of cucurmin and extended the stability of the nanosuspension (Chow et al. 2015).

12.3.1.2 Controlled Precipitation (CP) Process

To minimize particle growth after precipitation, the controlled precipitation (CP) process incorporates a semicontinuous solvent removal step, such as vacuum distillation, after the solvent and antisolvent are mixed together (Fig. 12.24). By incorporating the solvent removal step in-line with the process to remove excess solvent immediately after precipitation instead of in a separate step, substantial levels of particle growth may be minimized. In CP, solvent removal is typically performed within a wiped film evaporator to maximize the available surface area over which solvent evaporation may occur, as well as to reduce any foaming that might have occurred during processing, given the high amounts of surfactants required for stabilization in some cases (Rogers et al. 2004; Hitt et al. 2003, 2006).

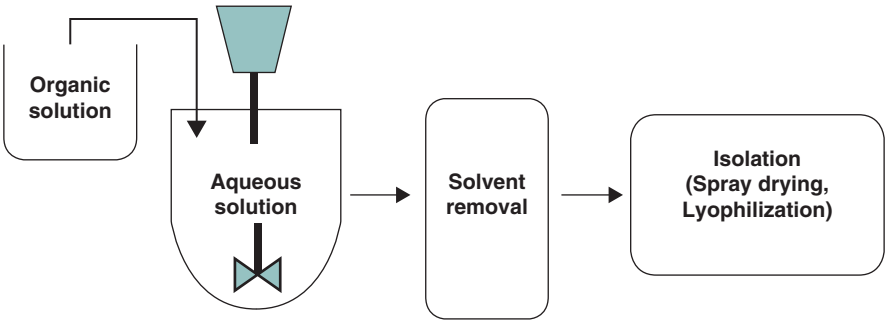

Fig. 12.24 Schematic of controlled precipitation process. Adapted from Rogers et al. (2004)

Rapid removal of a significant portion of the solvent markedly reduces the solubility of the drug in the mixed solvent. Thus, particle growth by condensation of dissolved drug molecules and Ostwald ripening may be greatly minimized.

Danazol and naproxen particles prepared by CP were well below 1 μm in diameter, 200 and 270 nm, respectively, as long as the operating temperature was kept at 3 °C (Rogers et al. 2004). Measured residual solvent levels, methanol for both cases, in the aqueous suspension after the solvent removal step ranged between 70 and 380 ppm, well below the International Conference on Harmonization (ICH) guidelines for pharmaceuticals for human use (Rogers et al. 2004). Lower precipitation temperatures corresponded to lower residual methanol levels, in addition to favoring nanoparticle production. A significant increase in particle size (up to an order of magnitude) and polydispersity (from unimodal to bi- and tri-modal distributions) was observed when the precipitation temperature was increased to 25 and 50 °C (Rogers et al. 2004), consistent with the AP work by Matteucci et al. (2006). Additionally, the ability of the CP process to produce high-potency nanoparticles has been demonstrated for several poorly water-soluble drugs, including Itz stabilized by HPMC (up to 94 % w/w drug potency for particles 90–355 nm in diameter) (Matteucci et al. 2007), cyclosporin A (CsA) stabilized using Tween 80 (91 % w/w drug potency for particles 300 nm in diameter) (Tam et al. 2008), and repaglinide (REP) stabilized with HPMC (50 % w/w drug potency for particles 650 nm in diameter) (Sinswat et al. 2007), as expected since the particle formation and stabilization mechanism for CP are similar to those of AP. Scalability of the CP process was also demonstrated by the successful production of a 1-kg batch of naproxen particles (Rogers et al. 2004). The impingement mixer can be combined with an on-line spray-dryer for a continuous process suitable for industrial scale production of nanoparticles (Dong et al. 2011).

Another important aspect of the CP process is its high propensity to produce amorphous particles, due to the rapid nucleation and stabilization rates generated during the precipitation process. As seen in the Noyes–Whitney equation (12.1), higher metastable solubilities of high-energy amorphous compounds, C_{sat}, relative to crystalline compounds, provide a larger concentration gradient to drive particle dissolution. Production and stabilization of an amorphous morphology require rapid particle stabilization during the precipitation process, similar to the conditions required for stabilization of small particle sizes. The same principles are applied to control particle morphology, as the goal is to stabilize the particle before the molecules can arrange into a crystal structure. Controlled precipitation of Itz (Matteucci et al. 2007), CsA (Tam et al. 2008), and REP (Sinswat et al. 2007) have yielded nanoparticles possessing an amorphous morphology, which contributed to their enhanced dissolution rates over the bulk, crystalline drug particles.

12.4 Precipitation into Acid: Microprecipitated Bulk Powder (MBP) Formulations

Scientists at Roche have recently presented a modified approach to AP, in which a poorly water-soluble drug compound is stabilized by an ionic polymer via precipitation in an acid bath (Albano et al. 2002; Shah et al. 2012). A simplified process flow diagram is illustrated in Fig. 12.25. The setup, which is patent protected (Desai et al. 2010) and described by Shah et al., consists of two vessels with temperature control, one containing a cooled acidic aqueous phase (+5 °C) and the other one containing an organic solution where a drug and a polymer are dissolved. Both vessels contain automatic stirrers, the acidic aqueous phase is circulated in a closed loop and passes through a high shear mixing unit where the organic phase is added via an injection nozzle at a defined flow rate. Addition of the organic solution to the cooled acid phase where both drug and polymer are highly insoluble initiate nucleation of the drug particles and a precipitate, which is a mixture of API and ionic polymer, is formed. After complete addition of the drug-polymer phase the suspension is passed through the shear-mixing unit to adjust the particle size. The suspension is then filtered and washed with the acidic aqueous phase and then with water to remove the organic solvent. Once washed, the precipitate is dried to a desired water content (e.g., 2 % w/w). The ionic nature of the stabilizer is critical for effective "microprecipitation" of "nanosized" drug domains, which are claimed to be molecularly dispersed throughout a polymer matrix. Therefore, polymers such as hypromellose acetate succinate, polymethacrylate, polymethylmethacrylate,

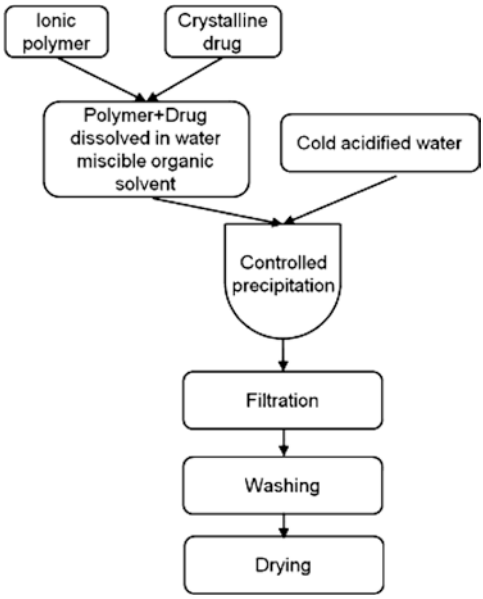

Fig. 12.25 Process train for production of microprecipitated bulk powder (MBP) formulation. Adapted and published with permission from Shah et al. (2010)

hypromellose phthalate, polyvinylphtalate and cellulose acetate phthalate are applicable. The resultant powder has been termed a "microprecipitated bulk powder" (MBP). Amorphous morphologies have also been formed under sufficiently rapid stabilization conditions. Ionic polymers with a MW of at least 80,000 Da and a glass transition temperature, T_g, >50 °C have been found to promote efficient stabilization of submicron, amorphous drug domains by this precipitation technique. The acidic aqueous bath is likely needed to elicit the desired charge on the polymer to promote a strong interaction between the polymer and the newly formed drug surfaces (Shah et al. 2010). Shah et al. described the manufacturing of two proprietary compounds using MBP technology. HPMC-AS and Eudragit® L100 were investigated as carriers. Both compounds were characterized as amorphous after processing. However, under the conditions tested only one of them was in a single-phase system as demonstrated by the single Tg observed by DSC. These results demonstrated that depending on the interaction and miscibility between the drug and polymer, a dispersion of amorphous drug in the polymer, or molecular dispersion of the drug could be obtained. The dissolution of solid dispersions manufactured with MBP was dependent on the lipophilicity of the drug but was optimized using additional excipients and led to rapid and complete dissolution of the compounds with up to 20-fold supersaturation in aqueous environment. These in-vitro results were confirmed in beagle dogs where a 20-fold increase in bioavailability compared to micronized crystalline drug was demonstrated. Accelerated stability studies indicated assay values higher than 99 % and a maintained amorphous state. The high Tg of the polymer, its low affinity for water and a good miscibility with the drug was responsible for product stability. This manufacturing process appears to be a good alternative when hot-melt-extrusion and spray-drying technologies cannot be used to improve solubility of poorly water-soluble compounds. Vemurafenib falls into this category, indeed its high melting point and low solubility in organic solvent renders hot –melt-extrusion or spray drying unsuitable techniques. Consequently solvent controlled precipitation was investigated and precipitated amorphous solid dispersion in HPMC-AS were manufactured. Vemurafenib amorphous MBP was incorporated into tablets and exhibited enhanced stability and clinical efficacy in human (Shah et al. 2013).

This technology has demonstrated scalability and vemurafenib has recently been approved for commercialization under the trade name of Zelboraf® (EMA assessment report 2012).

12.5 Nanoparticle Recovery

Whereas a wide variety of techniques have been developed to produce aqueous dispersions of nanoparticles, the recovery of the nanoparticles in the solid state remains a formidable challenge. Common techniques for solvent removal include spray drying, freeze drying (i.e., lyophilization), and ultrafiltration (Limayem et al. 2004; Torino et al. 2010; Matteucci et al. 2008). Particle growth may occur in these

processes, as the nanoparticles are concentrated during solvent removal. Concentration of nanoparticles may occur by various pathways, depending on the state of solvation of the polymeric stabilizer during solvent removal, as shown in Fig. 12.26. Process conditions, such as temperature, salinity of the nanoparticle dispersion, or rate of solvent removal, may be manipulated to influence flocculation behavior of the nanoparticles. In spray drying, dense flocs, which do not redisperse well back to primary nanoparticles, may be produced because the increase in nanoparticle concentration within the shrinking, evaporating droplet raises collision rates and the propensity for Ostwald ripening. Additionally, the high temperatures required for sufficient solvent evaporation, typically greater than 90 °C, have been shown to desolvate some polymeric stabilizers and can further facilitate the formation of large, dense flocs (Heimenz and Rajagopalan 1997; Larson 1999; Napper 1983). Similarly, for freeze drying and ultrafiltration, the increase in nanoparticle concentration and potential changes in solvent quality with solvent removal may also produce dense flocs with the same limitations. These particle recovery techniques are energy intensive and may require long processing times (freeze drying and ultrafiltration).

An alternative approach to nanoparticle recovery is to form large, open flocs of primary nanoparticles that may be more efficiently filtered than isolated primary particles, dried, and then redispersed upon dosing (Matteucci et al. 2008; Chen et al.

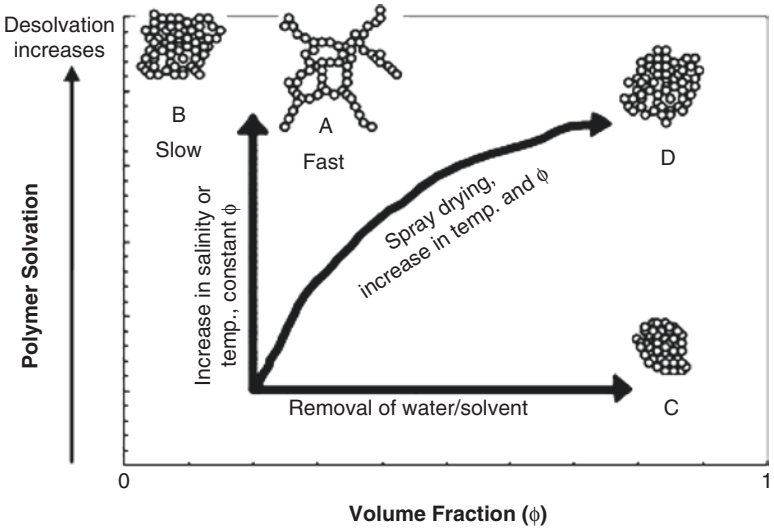

Fig. 12.26 Floc structure as a function of polymer solvation and particle volume fraction, Φ. Polymer solvency diminishes with an increase in salinity or temperature. Adapted and reprinted with kind permission from Springer Science+Business Media: Matteucci et al. (2008), copyright 2008

2009; Miller et al. 2012). Aqueous suspensions (500 mg drug in 50 mL solution) of large, open flocs can been filtered in minutes to obtain a dry powder (Matteucci et al. 2008; Chen et al. 2009), compared to hours for recovery of primary nanoparticles by filtration (typically ~0.03 mL/min cm^2) (Matteucci et al. 2008). Flocculation of primary particles may be induced by adding a salt to raise the ionic strength of the solution (Matteucci et al. 2008; Chen et al. 2009) or by changing the pH (Miller et al. 2012), in each case to desolvate the polymer stabilizer on the particle surface. In the case of flocculation with salt, the loss of hydration of the polymer leads to a loss in steric stabilization of the nanoparticles. At the cloud point of the polymer, steric stabilization becomes weak and the polymer-coated nanoparticles flocculate. Solvation of polyethylene oxide (PEO)-, PVP-, and HPMC-based stabilizers are known to decrease with an increase in salinity or temperature (Pandit et al. 2000; Xu et al. 2006; Pang and Englezos 2002). Sodium sulfate (Na_2SO_4) has been used to flocculate crystalline naproxen nanoparticles stabilized by PVP- or PEO-based polymers (Chen et al. 2009) and Itz nanoparticles stabilized by mixtures of poloxamer 407 (P407) and HPMC (Matteucci et al. 2008). This process is best illustrated by "Path A" in Fig. 12.26, where the addition of salt rapidly decreases the polymer solvation and sticky collisions between unstabilized nanoparticles produce open flocs. The strong van der Waals attraction between particles "locks in" the open floc structure and inhibits rearrangement of the particles, as indicated by microscopy images (Fig. 12.27) and calculated fractal dimensions <2. The flocs are essentially formed by diffusion-limited colloid aggregation. In contrast, slow induction of polymer desolvation ("Path B") allows particles to rearrange into more energetically favorable dense flocs. Recovery methods in which nanoparticle volume fractions increase via solvent reduction, as in spray ("Path D") and freeze drying ("Path C") and ultrafiltration ("Path C"), also tend to form denser flocs that may not readily redisperse to primary particles after drying, as compared to flocs produced by "Path

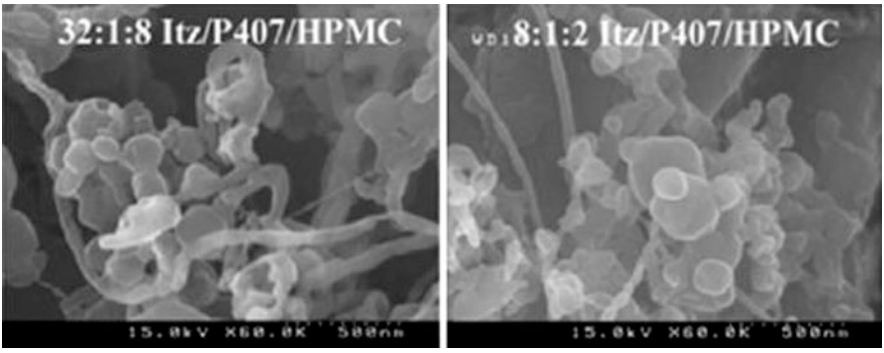

Fig. 12.27 Scanning electron microscopy (SEM) images of salt-flocculated Itz nanoparticle dispersions stabilized with different amounts of excipient. Reprinted with kind permission from Springer Science + Business Media: Matteucci et al. (2008), copyright 2008

A." Moreover, flocculate formation may be tuned to balance requirements for drug loading (drug/excipient ratio within the particles) versus process yields by controlling the nature and composition of the polymer stabilizers and the amount of salt used to induce flocculation, which was demonstrated during flocculation of naproxen (Chen et al. 2009) and Itz nanoparticles (Matteucci et al. 2009).

Upon redispersion of the flocs in a good solvent, or during drug administration in physiological fluids, the primary nanoparticles within the floc are highly accessible to the solvent and thus readily redisperse, a behavior indicative of loose, open flocs. Itz and naproxen powders that were dried after salt flocculation have been shown to redisperse to their original freshly precipitated particle sizes (~300 nm diameter) (Matteucci et al. 2008, 2009; Chen et al. 2009) and drug yields after filtration were as high as 99 % (w/w recovered/input drug), compared to typical recoveries of 50–70 % for spray-dried materials (Nguyen et al. 2004; Maa et al. 1999). Furthermore, salt-flocculated Itz particles maintained their amorphous morphology from the original precipitated dispersions, as shown by differential scanning calorimetry (DSC) and dissolution studies, whereas the Itz particles crystallized when recovered by spray drying (Matteucci et al. 2008).

By a similar principle, electrosteric stabilization of nanoparticles coated with charged polymers may be manipulated by adjusting pH to neutralize a sufficient fraction of the charges. Itz nanoparticles stabilized by a by adjusting pH-sensitive methacrylate-based polymer, Eudragit L100-55, were flocculated rapidly by lowering the solution pH to 2.5 with hydrochloric acid (HCl) to protonate the carboxylate groups on the polymer (Miller et al. 2012). As described above, the rapid and strong increase in interparticle attraction due to the pH reduction under constant volume fraction resulted in relatively large open flocs (Matteucci et al. 2008; Chen et al. 2009). As observed for salt flocculation of Itz nanoparticles, crystallization of Itz was minimal, since the large flocs were rapidly filtered at room temperature (Matteucci et al. 2008, 2009). Upon redispersion at pH 6.8, solvation of the enteric polymer resulted in only a slight increase in size of the EL100-55-stabilized nanoparticles (Miller et al. 2012). Preservation of the amorphous morphology after the pH-flocculation process was verified by the achievement of higher in vivo bioavailability in rats upon oral administration of the flocculated powders relative to a commercial Itz solid dispersion (Sporanox) (Miller et al. 2012). An advantage of the pH flocculation process, relative to previous salt flocculation studies, is the potential for a decrease in salt impurities in the final product.

For the flocculation/filtration process, the ability to operate at low temperatures and constant particle volume fractions (flocculation induced without solvent reduction), as well as rapid removal of solvent, inhibited both growth and crystallization of the amorphous primary nanoparticles and promoted the preservation of the highly open floc structures. Another advantage of this technique is that large amounts of stabilizer may be used in the particle formation stage to promote the production of nanoparticles without impacting final drug loadings because any excess, unadsorbed stabilizers are removed during filtration, thus facilitating high drug/polymer ratios in

the powder, with drug loadings in the range of 80–99 % (Matteucci et al. 2008, 2009; Chen et al. 2009; Miller et al. 2012). Thus, the flocculation/filtration recovery process offers a simple, efficient alternative to traditional nanoparticle recovery techniques capable of yielding nanoparticle assemblies with high drug loadings and process yields while preserving amorphous morphologies.

Conclusion

Precipitation processes possess several advantages for nanoparticle production over conventional top-down approaches, such as milling and homogenization, as they offer enhanced control of morphology and PSD with minimal complications of contamination and product degradation. The ability of different precipitation processes, in which SCFs and organic solvents were utilized as both solvents and antisolvents, to reproducibly yield nanoparticles for a wide range of pharmaceutical materials has been demonstrated. The strengths and weaknesses of the different precipitation processes have also been highlighted to aid in screening the suitability of a particular process for different drug systems. Another important trend in precipitation research that has been highlighted in this chapter is the emphasis on understanding the fundamental mechanisms that drive these precipitation processes, in order to facilitate successful scale-up of the precipitation techniques and promote their utility in commercial settings. A product utilizing a solvent controlled precipitation technology has recently been commercialized. Increased knowledge of these precipitation technologies benefits not only the microparticle/nanoparticle production fields but also areas of drug encapsulation (Rodrigues et al. 2004; Li et al. 2005; Young et al. 1999) and cocrystallization (Padrela et al. 2009) and will be of general interest for all sectors involving particle engineering. Novel particle recovery processes, based on controlled flocculation/filtration of primary nanoparticles, have also been discussed as an efficient means to harvest nanoparticles after precipitation, making precipitation processes more attractive and feasible for industrial production.

Method Capsule 1
Precipitation by GAS

Based on the method reported by Muhrer et al. (2003).

Objective

- To obtain nanoparticles using GAS precipitation

Materials and Equipment

- Poorly water-soluble drug (proprietary)
  - MW = 600 g/mol
  - T_{melt} = 200 °C
  - Solubility (T = 25 °C): 3 mg/mL in water; 18.5 mg/mL in acetone or acetonitrile; insoluble in CO_2
- Solvent: Ethanol
- Antisolvent: CO_2
- Cryostat to subcool CO_2 from reservoir tank
- Pump to transfer CO_2 from reservoir tank to precipitator
  - Gilson HPLC pump (low/intermediate flow rates)/Haskel pneumatic piston pump (high flow rates)
- Heater coil (via water bath) to preheat CO_2 feed to process temperature before entering precipitator
- Precipitation vessel (1 L)
  - Equipped with a mechanical stirrer
  - Sinter metal filter connected to the outlet tube
- Pump to transfer organic solution to precipitation vessel
- Oil bath (T = 80 °C) to heat the fluid line exiting the precipitation vessel (to avoid blockage)

Method

- The poorly water-soluble drug was dissolved in 75–150 mL in ethanol at concentrations between 50 and 90 % of the solubility at 25 °C
- Drug/ethanol solution was pumped into the precipitator
- CO_2 (preheated to 25 °C) was fed into the precipitator at 18–360 mL/min until the precipitator was full
- Contents in precipitator stirred at 500 rpm during CO_2 filling and for 30 min after the precipitator was filled
- Exit valve on precipitator was opened to flush out solvents and fresh CO_2 was pumped through (20 mL/min) for at least 5 h to remove any residual organic solvent from powder
- Dry powder harvested from metal filter

Results

- SEM indicated that spherical particles with a moderate level of agglomeration were produced
- Lower CO_2 flow rates (2–18 mL/min):
- Produced bimodal particle-size distributions (PSD)
- 1–6-μm diameter
- Higher CO_2 flow rates (240–360 mL/min):
- Produced unimodal PSDs
- 500–720-nm diameter
- X-ray powder diffraction indicated that the resultant particles were amorphous
- Gas chromatography determined residual solvent levels were below 0.01 wt%

Method Capsule 2
Precipitation by PCA

Based on the method reported by Reverchon et al. (2003b).

Objective

- To obtain nanoparticles using PCA precipitation

Materials and Equipment

- Amoxicillin
- Solvent: *N*-methyl 2-pyrrolidone (NMP)
- Antisolvent: CO_2
- Shell-and-tube heat exchanger to cool feed to CO_2 reservoir
- Diaphragm pump to transfer CO_2 from reservoir to dryer
- CO_2 dryer (113 L) with silica gel as the drying medium to remove trace amounts of water from CO_2 reservoir, prior to entering precipitator
- Heat exchanger to heat CO_2 to supercritical conditions
- Piston pump to transfer organic solution to precipitator
- Precipitation vessel (5.2 L)
  - Internal stainless steel basket to collect powder
  - Temperature maintained by a water jacket
- Coaxial injector: internal tube i.d. = 3 mm fitted with a 0.5-mm diameter nozzle; annulus i.d. = 8.5 mm
- Liquid separator (13 L) heated with water jacket to separate and collect solvent and antisolvent

Method

- PCA operation conducted in a continuous mode, where CO_2 exiting the precipitator was recirculated and the solvent exiting the liquid separator was purged and stored
- CO_2 was pumped into the precipitator at a constant flow rate (0.6–2.0 kg/h), passing through a heat exchanger to heat the CO_2 to 40 °C, until steady-state conditions were achieved. The precipitator pressure was set to 150 bar
- Pure NMP was fed into the chamber through the coaxial injector for a few minutes
- ~100 mL of the amoxicillin/NMP solution (20–100 mg/mL amoxicillin) was then fed into the chamber at the same flow rate as the pure NMP
- Pure CO_2 continued to flow through the precipitator for a predetermined amount of time, correlating to the calculated time required for 99 wt% elimination of NMP
- Dry powder was harvested from the internal basket inside precipitator

Results

- 90 wt% drug recovery, as calculated compared to initial drug amount in organic feed solution
- Amorphous particles produced
- SEM indicated that spherical particles were produced
  - Lower drug feed concentrations (20 mg/mL):
    Produced more narrow particle-size distributions (PSD)
    200–600-nm diameter
  - Higher drug feed concentrations (100 mg/mL):
    Produced more broad PSDs
    500–1800-nm diameter

Method Capsule 3

Precipitation by RESS

Based on the method reported by Turk et al. (2002).

Objective

- To obtain nanoparticles using RESS precipitation

Materials and Equipment

- β-sitosterol
- Solvent: CO_2
- Extraction column
- Diaphragm pump to transfer CO_2 into extraction column
- Water bath to heat extraction column
- Capillary nozzle (i.d. of 50 μm, length of 50 μm)—heated to 115–145 °C to prevent clogging during atomization

Method

- CO_2 from the reservoir was pressurized to a pre-expansion pressure of 20–30 MPa
- The $scCO_2$ was then pumped through a water bath heated to 75–145 °C (pre-expansion temperature) to the extraction column
- The extraction column, which was also immersed in the water bath (T = 75–145 °C), was packed with the drug and the CO_2 solution became saturated with the drug
- The $scCO_2$–drug solution was then expanded through a heated, capillary nozzle into an expansion chamber, for powder collection

Results

- SEM indicated that roughly spherical particles with moderate agglomeration were produced. Primary particles were ~150 nm in diameter
- Particle size was independent of pre-expansion temperature

Method Capsule 4

Precipitation by EPAS

Based on the method reported by Chen et al. (2002).

Objective

- To obtain nanoparticles using EPAS precipitation

Materials and Equipment

- Cyclosporin A (CsA)
- Stabilizers: Myrj 52, Tween 80, polyvinylpyrrolidone (PVP 40 T)
- Solvent: dichloromethane (DCM)
- Antisolvent: deionized water
- EPAS apparatus: stainless-steel coiled tube (3 m length, 1/16″ o.d. × 0.030″ i.d.) housed within a plastic water jacket (24″ length, 1–1/2″ o.d.)
- Temperature controller to circulate and heat water through the EPAS apparatus's water jacket
- Nozzle: stainless-steel tube (10″ length, 1/16″ o.d. × 0.030″ i.d.) that was cut with a wire cutter to produce a thin, elliptical slit. The tapered section of the orifice was ~0.5 mm in length and the tip was filed down (to adjust the thickness of the slit) until desired atomization was achieved, generally characterized by a pressure drop across the nozzle orifice of ~20 MPa for flow rates of 1 mL/min
- HPLC pump to feed solvent into the antisolvent
- Water bath to heat aqueous surfactant solution
- Separatory funnel (125 mL)
- Lyophilizer

Method

- Solutions of 1–5 % w/v CsA in DCM and aqueous solutions of 1 % w/v surfactant were prepared
- The aqueous surfactant solution (50 mL) was poured into the separatory funnel, which was then submerged in a water bath ($T = 75$ °C)
- The nozzle of the EPAS apparatus was submerged ~2 cm below the surface of the aqueous solution
- The organic drug solution was fed into the aqueous surfactant solution at a flow rate of 1 mL/min until a drug concentration of 1 % w/v CsA (10 mg/mL) was achieved in the aqueous suspension
  - Turbulence from the atomization of the organic solution was sufficient to facilitate mixing with the aqueous phase
  - To suppress the surfactant foam produced by the intense mixing of the organic and aqueous phases, nitrogen was blown across the top of the separatory funnel
- To dry the particles, the suspensions were flash frozen in liquid nitrogen and lyophilized to powders

Results

- Particle sizing results were determined by dynamic light scattering
  - Block copolymer (Myrj 52, Tween 80) versus homopolymer (PVP 40 T) stabilizers
    Myrj and Tween-stabilized particles were about half the size of PVP-stabilized particles (530–630 nm vs. 1080 nm, respectively)
  - 1 % w/v versus 5 % w/v drug concentration in organic feed
    Higher drug concentrations in the feed yielded smaller particles (~340 nm for Mryj and Tween-stabilized particles and ~600 nm for PVP-stabilized particles)
- 86–96 % drug recoveries achieved, as calculated compared to the initial drug amount in feed solution
- X-ray powder diffraction indicated that the resultant particles were amorphous
- Gas chromatography determined residual solvent levels in powders were below 0.0004 wt%

Method Capsule 5

Flash Nanoprecipitation (FN)

Based on the method reported by Chiou et al. (2008b).

Objective

- To obtain nanoparticles using FN

Materials and Equipment

- Cyclosporin A (CsA)
- Stabilizers: lecithin and dextrose monohydrate
- Solvent: ethanol
- Antisolvent: deionized (DI) water
- Two syringe pumps (50 mL syringe)
- Confined liquid impinging jet (CLIJ) mixer

Method

- CsA (0.7 g) was dissolved in ethanol (10 mL) and loaded into one of the syringe pumps
- An aqueous solution (30 mL) of lecithin (0.3 g) and dextrose monohydrate (1.5 g) was prepared and loaded into the other syringe pump
- The syringe pumps containing the organic and aqueous solutions were fed into the CLIJ mixer at 40 mL/min and 120 mL/min, respectively, until a total of 10 mL of organic solution and 30 mL of aqueous solution had been dispensed
- The resultant aqueous suspension was quenched in 50 mL of DI water

Results

- Particle sizing results were determined by laser light scattering
  - Average particle diameter: 294 nm (span 1.017, GSD 1.46)
  - After drying, the particles were a mean diameter of approximately 260 nm
- Scanning electron microscopy demonstrated that the particles were spherical

Method Capsule 6

Precipitation by CP

Based on the method reported by Matteucci et al. (2007).

Objective

- To obtain nanoparticles using CP

Materials and Equipment

- Itraconazole (Itz)
- HPMC E5
- Solvent: 1,3 dioxolane
- Antisolvent: deionized water
- Syringe to inject organic solution into a mixer
- Mixing apparatus to mix organic and aqueous phase
- Vacuum distillation apparatus equipped with a wiped film evaporator
- Pump to transfer aqueous suspension from mixing apparatus to vacuum distillation apparatus
- Lyophilizer

Method

- Solutions of Itz (3.3 % w/w) in 1,3 dioxolane and aqueous solutions of HPMC (various concentrations) were prepared
- The aqueous phase was maintained at $T_{precip} = 3$ °C
- The organic phase was rapidly introduced to the aqueous phase using a mixing apparatus (may be accomplished by using a syringe to inject the organic phase into the aqueous phase, as the aqueous phase is being stirred by a magnetic stir bar)
- The newly formed aqueous suspension was pumped to the vacuum distillation apparatus, where the methanol content in the slurry was reduced
- To dry the drug particles, the aqueous suspensions were frozen in liquid nitrogen and then lyophilized to powders

Results

- Particle sizing results were inferred from BET surface area measurements
  - Lower drug/stabilizer ratios resulted in smaller particle sizes
    Average particle sizes were 90, 200, 270, and 355 nm for a 1/2, 1/1, 2/1, and 4/1 Itz/HPMC ratio, respectively
- Scanning electron microscopy demonstrated that the particles were spherical and confirmed particle-size estimates from BET surface area measurements
- Contact-angle measurements demonstrated that the HPMC was primarily concentrated on the particle surface, and not within the interior of the particle
- X-ray powder diffraction and differential scanning calorimetry indicated that the resultant particles were amorphous

Method Capsule 7

Salt Flocculation for Nanoparticle Recovery

Based on the method reported by Matteucci et al. (2008).

Objective

- To recover nanoparticles produced by precipitation processes using salt flocculation

Materials and Equipment

- Aqueous suspension of itraconazole (Itz) nanoparticles, prepared by controlled precipitation, stabilized with a combination of both Pluronic F127 (P127) and HPMC E5 (8:1:2 Itz:P127:HPMC)
- Sodium sulfate salt, anhydrous (Na_2SO_4)
- Type P2 filter paper (area: 95 cm^2, pore size: 1–3 μm)
  - Filter paper cut into a circle with a 11-cm diameter
- Vacuum pump

Method

- At room temperature, a 1.5-M solution of Na_2SO_4 was added to an aqueous nanoparticle dispersion (10 mg/mL Itz) at a ratio of 12:5 v:v (salt solution:dispersion) and allowed to sit for 3 min
  - Within seconds, flocs formed and were observed to take up the entire volume of the nanoparticle dispersion/salt solution mixture.
  - After 3 min, larger flocs formed and the flocs creamed, taking up ~20 % of the original volume
- The flocculated suspension was filtered through the filter paper under vacuum until water was no longer observed on top of the filter cake (typically <8 min for ~200 mL of the nanoparticle suspension/salt solution mixture)
- An aqueous HPMC solution (30 mL at the same concentration as the aqueous phase during nanoparticle precipitation) was cooled in an ice bath. Immediately after filtration, the chilled HPMC solution was used to rinse the filter cake
  - For the 8:1:2 Itz:P127:HPMC particles, a 2.5-mg/mL HPMC solution was used
- The filter cake was dried at room temperature and atmospheric pressure overnight
- Dried powders were gently scraped off the filter paper with a spatula

Results

- Static light scattering results showed that the flocculated nanoparticles redispersed back down to near-original particle sizes in DI water
  - Before flocculation: $D_{10}/D_{50}/D_{90}$ were 110/340/2260 nm
  - After salt flocculation and redispersion in water with 5 min of sonication: $D_{10}/D_{50}/D_{90}$ were 120/370/1480 nm
- Scanning electron microscopy images confirm the ~300-nm primary particle sizes reported by light scattering (see Fig. 12.27)
- 94 wt% drug loading (% of drug in dried powder)
- Drug yields of ~90 % were obtained, as calculated compared to the amount of drug in the initial dispersion
- Contact-angle measurements indicated that the stabilizers were concentrated on the particle surface, not within the particle interior
- Temperature-modulated differential scanning calorimetry (mDSC) indicated that primary nanoparticles remained amorphous after salt flocculation

Method Capsule 8

Microprecipitated Bulk Powder (MBP)

Based on the method reported by Shah et al. (2012).

Objective

- To obtain stable amorphous particles using MBP technology

Materials and Equipment

- Poorly water soluble drug (proprietary)
  - MW = 536.6 g/mol
  - T_{melt} = 120 °C
  - Solubility: <0.05 mg/mL in water, >200 mg/mL in dimethylacetamide
- Stabilizing polymer: HPMC-AS-LF
- Solvent: Dimethylacetamide
- Anti-solvent: Aqueous solution maintained between pH 1 and 3 and temperature at 5 ± 2 °C
- Vessel containing cooled, pH controlled anti-solvent
- Vessel containing drug and polymer solution
- Vacuum filtration capabilities
- Forced air oven or fluid bed dryer

Method

- A solution containing 20 % (w/w) API and polymer (ratio API to polymer 4:6) was dissolved in dimethylacetamide
- The solution was then added to the chilled aqueous acidic vessel (ratio of solvent to antisolvent to be maintained as 1:10 during precipitation) allowing for rapid co-precipitation
- The precipitate was washed using the same acidic aqueous solution followed by water washings
- Once washed, the precipitate was collected as a wet cake by a vacuum filtration device
- The wet cake was dried in a forced air oven or fluid bed dryer at 45 ± 5 °C
- MBP was then de-lumped using a hammer mill to achieve the desired particle size

Results

- Differential Scanning Calorimetry indicated that compound exhibited a single Tg indicating a single-phase system demonstrating a molecular dispersion of the drug within the carrier
- XRD demonstrated the amorphous nature of the MBP product

- Transmission Electron Microscopy showed uniform material across an area of 0.2 μm
- The dissolution testing demonstrated a fast release rate and extent of supersaturation with a 20-fold supersaturation maintained
- Animal studies in rats confirmed the in vitro results with exposures ~40 fold higher as compared to nanosuspensions of the drug
- Stability studies demonstrated the unusually stable character of this amorphous formulation under accelerated conditions
- Critical process conditions leading to a robust process have been identified as follows:
  - Precipitation rate
  - Solvent/Anti-solvent ratio
  - Temperature
  - Hydrodynamic conditions
  - Washing cycles
  - Drying
- Drug yields of 90 % were calculated

Method Capsule 9

Rapid Expansion from Supercritical to Aqueous Solution

Based on the method reported by Tozuka et al. (2010).

Objective

- To obtain nanoparticles using RESAS precipitation

Materials and Equipment

- Indomethacin
- Ethanol
- Poly-Vinyl-Alcohol
- RESAS apparatus comprising:
  - CO_2 pump
  - Solution pump a reaction vessel and a
  - Pressure regulator
  - Reaction vessel
  - Precipitation unit
- Freeze drier
- Stainless steel container

Method

- Indomethacin was dissolved into a 10 mL ethanol to a 20 mg/mL solution
- Liquefied CO_2 was added to the vessel at 14 mL/min
- Solvent CO_2 was added to the reaction vessel
- Once the pressure reached the desired value, the drug solution and CO_2 fluid were co-sprayed via a co-axial nozzle
- After co-spraying, the CO_2 fluid containing IMC and ethanol was expanded from the reaction vessel to an aqueous media of 30 mL using the back pressure regulator
- Once the expansion was finished, the suspension was dispersed by sonication
- The suspension was added to a 200 mL stainless steel container and freeze-dried at -120 °C for 72 h

Results

- Production of spherical nanoparticles of indomethacin was achieved
  - Pressure and temperature affected yield (26.7–47.7 %) and particle size 25 MPa and 40 °C appeared as optimal conditions
  - In the high pressure vessel the particle size increase with temperature increase. Nozzle geometry, solubility and nature of solute sovent interaction affect particles properties
  - Freeze dried samples reproduced submicron particles when dispersed in water

- Scanning electron microscopy indicated that spherical shape particle were obtained with pressure of 25–40 MPa
- X-ray diffraction demonstrated low crystallinity in the samples with amorphous component of indomethacin
  - The stable γ form and metastable α crystalline forms are obtained depending on processing parameters
- Dissolution profile indicated that $scCO_2$ treated samples dissolved 90 % of the drug in 10 min which was significantly faster than commercial indomethacin
  - This was attributed to the nano-range particles leading to increase surface area and formation of a metastable form having higher solubility

References

Albano AA, Phuapradit W, Sandhu HK, Shah NH (2002) Stable complexes of poorly soluble compounds in ionic polymers, US 6,350,786

Bakhbakhi Y, Rohani S, Charpentier PA (2005) Micronization of phenanthrene using the gas antisolvent process: Part 2. Theoretical study. Ind Eng Chem Res 44(19):7345–7351

Baldyga J, Czarnocki R, Shefeunov BY, Smith KB (2010) Particle formation in supercritical fluids—scale-up problem. Chem Eng Res Des 88:331–341

Blankschtein D, Thurston GM, Benedek GB (1986) Phenomenological theory of equilibrium thermodynamic properties and phase separation of micellar solutions. J Chem Phys 85(12):7268–7288

Bosselmann S, Nagao M, Chow KT, Williams RO III (2012) Influence of formulation and processing variables on properties of itraconazole nanoparticles made by advanced evaporative precipitation into aqueous solution. AAPS PharmSciTech 13(3):949–960

Bristow S, Shekunov T, Shekunov BY, York P (2001) Analysis of the supersaturation and precipitation process with supercritical CO_2. J Supercrit Fluids 21(3):257–271

Bustami R, Chan H-K, Dehghani F, Foster N (2000) In: International symposium on supercritical fluids, Generation of protein microparticles using high pressure modified carbon dioxide, Atlanta, GA

Carl LY (1999) Chemical properties handbook. McGraw-Hill, New York

Chan H-K, Chew NYK (2003) Novel alternative methods for the delivery of drugs for the treatment of asthma. Adv Drug Deliv Rev 55(7):793–805

Chang SA, Gray DG (1978) The surface tension of aqueous hydroxypropyl cellulose solutions. J Colloid Interface Sci 67:255–265

Cheng KK, Yeung CF, Ho SW, Chow SF, Chow AHL, Baum L (2013) Highly stabilized curcumin nanoparticles tested in an in vitro blood–brain barrier model and in Alzheimer's disease Tg2576 mice. AAPS J 15(2):324–336

Charoenchaitrakool M, Dehghani F, Foster NR, Chan HK (2000) Micronization by rapid expansion of supercritical solutions to enhance the dissolution rates of poorly water-soluble pharmaceuticals. Ind Eng Chem Res 39(12):4794–4802

Chattopadhyay P, Gupta RB (2001a) Production of griseofulvin nanoparticles using supercritical CO_2 antisolvent with enhanced mass transfer. Int J Pharm 228(1–2):19–31

Chattopadhyay P, Gupta RB (2001b) Production of antibiotic nanoparticles using supercritical CO_2 as antisolvent with enhanced mass transfer. Ind Eng Chem Res 40(16):3530–3539

Chattopadhyay P, Gupta RB (2002) Protein nanoparticles formation by supercritical antisolvent with enhanced mass transfer. AICHE J 48(2):235–244

Chen X, Young TJ, Sarkari M, Williams RO, Johnston KP (2002) Preparation of cyclosporine A nanoparticles by evaporative precipitation into aqueous solution. Int J Pharm 242(1–2):3–14

Chen X, Vaughn JM, Yacaman MJ, Williams RO, Johnston KP III (2004a) Rapid dissolution of high-potency danazol particles produced by evaporative precipitation into aqueous solution. J Pharm Sci 93(7):1867–1878

Chen X, Ill Benhayoune Z, Williams RO, Johnston KP (2004b) Rapid dissolution of high potency itraconazole particles produced by evaporative precipitation into aqueous solution. J Drug Deliv Sci Technol 14(4):299–304

Chen X, Lo CY-L, Sarkari M, Williams RO, Johnston KP III (2006) Ketoprofen nanoparticle gels formed by evaporative precipitation into aqueous solution. AICHE J 52(7):2428–2435

Chen XX, Matteucci ME, Lo CY, Johnston KP, Williams RO (2009) Flocculation of polymer stabilized nanocrystal suspensions to produce redispersible powders. Drug Dev Ind Pharm 35(3):283–296

Chiou H, Chan H-K, Heng D, Prud'homme RK, Raper JA (2008a) A novel production method for inhalable cyclosporine A powders by confined liquid impinging jet precipitation. J Aerosol Sci 39(6):500–509

Chiou H, Chan H-K, Prud'homme RK, Raper JA (2008b) Evaluation on the use of confined liquid impinging jets for the synthesis of nanodrug particles. Drug Dev Ind Pharm 34(1):59–64
Chow HF, Sun CC, Chow AHL (2014) Assessment of the relative performance of a confined impinging jets mixer and a multi-inlet vortex mixer for curcumin nanoparticle production. Eur J Pharm Biopharm 88(2):462–471
Chow SF, Wan KY, Cheng KK, Wong KW, Sun CC, Baum L, Chow AHL (2015) Development of highly stabilized curcumin nanoparticles by flash nanoprecipitation and lyophilization. Eur J Pharm Biopharm 94:436–444
Crison JR (2000) Biopharmaceutical aspects of water-insoluble drugs for oral drug delivery. In: LIU R (ed) Water-insoluble drug formulation. CRC Press, Boca Raton
Daniels R, Barta A (1994) Pharmacopoeial cellulose ethers as oil-in-water emulsifiers I: Interfacial properties. Eur J Pharm Biopharm 40:128–133
de la Fuente Badilla JC, Peters CJ, de Swaan AJ (2000) Volume expansion in relation to the gas-antisolvent process. J Supercrit Fluids 17(1):13–23
de la Fuente JC, Shariati A, Peters CJ (2004) On the selection of optimum thermodynamic conditions for the GAS process. J Supercrit Fluids 32(1–3):55–61
Dearn AR (1994) Atovaquone pharmaceutical compositions. WO 9414426, 23 Dec 1993
Debenedetti PG (1990) Homogeneous nucleation in supercritical fluids. AICHE J 36(9):1289–1298
Debenedetti PG, Tom JW, Kwauk X, Yeo SD (1993) Rapid expansion of supercritical solutions (RESS): fundamentals and applications. Fluid Phase Equilibr 82:311–321
Desai D, Diodone R, Go Z, Ibrahim PN, Iyer R, Mair HJ, Sandhu HK, Shah NH, Visor G, Wyttenbach N, Lauper S, Pudewell J, Wierschem F (2010) Compositions and uses thereof. US20100310659 A1 (03.31.2010)
Dodds S, Wood JA, Charpentier PA (2007) Modeling of the gas-antisolvent (GAS) process for crystallization of beclomethasone dipropionate using carbon dioxide. Ind Eng Chem Res 46:8009–8017
Domingo C, Berends E, van Rosmalen GM (1997) Precipitation of ultrafine organic crystals from the rapid expansion of supercritical solutions over a capillary and a frit nozzle. J Supercrit Fluids 10(1):39–55
Dong Y, Ng WK, Shen S, Kim S, Tan RBH (2009) Preparation and characterization of spironolactone nanoparticles by antisolvent precipitation. Int J Pharm 375(1–2):84–88
Dong Y, Ng WK, Hu J, Shen S, Tan RBH (2010) A continuous and highly effective static mixing process for antisolvent precipitation of nanoparticles of poorly water-soluble drugs. Int J Pharm 386(1–2):256–261
Dong Y, Ng WK, Shen S, Kim S, Tan RH (2011) Controlled antisolvent precipitation of spironolactone nanoparticles by impingement mixing. Int J Pharm 410(1–2):175–179
Elvassore N, Parton T, Bertucco A, Di Noto V (2003) Kinetics of particle formation in the gas antisolvent precipitation process. AICHE J 49(4):859–868
Elvassore N, Cozzi F, Bertucco A (2004) Mass transport modeling in a gas antisolvent process. Ind Eng Chem Res 43(16):4935–4943
Engstrom JD, Simpson DT, Cloonan C, Lai ES, Williams RO III, Kitto GB, Johnston KP (2007) Stable high surface area lactate dehydrogenase particles produced by spray freezing into liquid nitrogen. Eur J Pharm Biopharm 65(2):163–174
Engstrom JD, Lai ES, Ludher B, Chen B, Milner TE, Kitto GB, Williams RO III, Johnston KP (2008) Formation of stable submicron protein particles by thin film freezing. Pharm Res 25(6):1334–1336
Erriguible A, Laugier S, Laté M, Subra-Paternault P (2013) Effect of pressure and non-isothermal injection on re-crystallization by CO_2 antisolvent: solubility measurements, simulation of mixing and experiments. J Supercrit Fluids 76:115–125
Erriguible A, Neurohr C, Revelli AL, Laugier S, Fevotte G, Subra-Paternault P (2015) Cocrystallization induced by compressed CO_2 as antisolvent: simulation of a batch process for the estimation of nucleation and growth parameters. J Supercrit Fluids 98:194–203
Esfandiari N, Ghoreishi SM (2013a) Synthesis of 5-fluorouracil nanoparticles via supercritical gas antisolvent process. J Supercrit Fluids 84:205–210

Esfandiari N, Ghoreishi SM (2013b) Kinetics modeling of ampicillin nanoparticles synthesis via supercritical gas antisolvent process of supercritical fluids. Chem Eng Technol 81:119–127
European Medicines Agency (2012) Zelboraf. Assessment report
Falk R, Randolph TW, Meyer JD, Kelly RM, Manning MC (1997) Controlled release of ionic compounds from poly(L-lactide) microspheres produced by precipitation with a compressed antisolvent. J Control Release 44(1):77–85
Franklin RK, Edwards JR, Chernyak Y, Gould RD, Henon F, Carbonell RG (2001) Formation of perfluoropolyether coatings by the rapid expansion of supercritical solutions (RESS) process. Part 2: Numerical modeling. Ind Eng Chem Res 40(26):6127–6139
Fusaro F, Mazzotti M, Muhrer G (2004) Gas antisolvent recrystallization of paracetamol from acetone using compressed carbon dioxide as antisolvent. Cryst Growth Des 4(5):881–889
Fusaro F, Haenchen M, Mazzotti M, Muhrer G, Subramaniam B (2005) Dense gas antisolvent precipitation: a comparative investigation of the GAS and PCA techniques. Ind Eng Chem Res 44(5):1502–1509
Gardner CR, Walsh CT, Almarsson O (2004) Drugs as materials: valuing physical form in drug discovery. Nat Rev Drug Discov 3(11):926–934
Gassmann P, List M, Schweitzer A, Sucker H (1994) Hydrosols—alternatives for the parenteral application of poorly water-soluble drugs. Eur J Pharm Biopharm 40(2):64–72
Gao L, Liu G, Wang X, Liu F, Xu Y, Ma J (2011) Preparation of a chemically stable quercetin formulation using nanosuspension technology. Int J Pharm 404(1–2):231–237
Gupta RB (2006) Nanoparticle technology for drug delivery, vol 53, 1st edn. Taylor & Francis, New York, pp 53–84
Hanna M, York P (1998) Method + apparatus for the formation of particles. WO 9836825, February 20
Han J, Zhu Z, Qian H, Wohl AR, Beaman CJ, Hoye TR, Macosko CW (2012) A simple confined impingement jets mixer for flash nanoprecipitation. J Pharm Sci 101(10):4018–4023
Heimenz PC, Rajagopalan R (1997) Principles of colloid and surface chemistry. Marcel Dekker, New York
Helfgen B, Turk M, Schaber K (2003) Hydrodynamic and aerosol modelling of the rapid expansion of supercritical solutions (RESS-process). J Supercrit Fluids 26(3):225–242
Hiendrawan S, Veriansyah B, Tjandrawinata RR (2014) Micronization of fenofibrate by rapid expansion of supercritical solution. J Ind Eng Chem 20(1):54–60
Hitt JE, Tucker CJ, Evans JC, Curtis CA, Svenson S (2003) Process to precipitate drug particles. US 20030049323, 08/27/2002
Hitt JE, Rogers TL, Gillespie IB, Scherzer BD, Garcia PC, Beck NS, Tucker CJ, Young TJ, Hayes DA, Williams RO III, Johnston KP, McConville JT, Peters JI, Talbert R, Burgess D (2006) Enhanced delivery of pharmaceutical compositions to treat life threatening infections. WO 2006026502, 08/26/2005
Hu J, Johnston KP, Williams RO III (2004) Nanoparticle engineering processes for enhancing the dissolution rates of poorly water soluble drugs. Drug Dev Ind Pharm 30(3):233–245
Hu J, Ng W-K, Dong Y-C, Shen S-C, Tan RBH (2011) Continuous and scalable process for water-redispersible nanoformulation of poorly aqueous soluble APIs by antisolvent precipitation and spray-drying. Int J Pharm 404(1–2):198–204
Jacobs C, Kayser O, Muller RH (2000) Nanosuspensions as a new approach for the formulation for the poorly soluble drug tarazepide. Int J Pharm 196:161–164
Jarmer DJ, Lengsfeld CS, Randolph TW (2003) Manipulation of particle size distribution of poly(L-lactic acid) nanoparticles with a jet-swirl nozzle during precipitation with a compressed antisolvent. J Supercrit Fluids 27(3):317–336
Jarmer DJ, Lengsfeld CS, Randolph TW (2004) Nucleation and growth rates of poly(L-lactic acid) microparticles during precipitation with a compressed-fluid antisolvent. Langmuir 20(17):7254–7264
Jarmer DJ, Lengsfeld CS, Randolph TW (2006) Scale-up criteria for an injector with a confined mixing chamber during precipitation with a compressed-fluid antisolvent. J Supercrit Fluids 37(2):242–253

Johnson BK, Prud'homme RK (2003a) Flash nanoprecipitation of organic actives and block copolymers using a confined impinging jets mixer. Aust J Chem 56(10):1021–1024
Johnson BK, Prud'homme RK (2003b) Chemical processing and micromixing in confined impinging, jets. AIChE J 49(9):2264–2282
Johnson BK, Prud'homme RK (2003c) Mechanism for rapid self-assembly of block copolymer nanoparticles. Phys Rev Lett 91(11):118302/1–118302/4
Johnson BK, Saad W, Prud'homme RK (2006) Nanoprecipitation of pharmaceuticals using mixing and block copolymer stabilization. In: ACS symposium series, polymeric drug delivery II, vol 924, pp 278–291
Jouyban A, Rehman M, Shekunov BY, Chan H-K, Clark BJ, York P (2002) Solubility prediction in supercritical CO_2 using minimum number of experiments. J Pharm Sci 91(5):1287–1295
Kayrak D, Akman U, Hortaçsu Ö (2003) Micronization of Ibuprofen by RESS. J Supercrit Fluids 26(1):17–31
Keck CM, Mueller RH (2006) Drug nanocrystals of poorly soluble drugs produced by high pressure homogenization. Eur J Pharm Biopharm 62(1):3–16
Keshavarz A, Karimi-Sabet J, Fattahi A, Golzary AA, Rafiee-Tehrani M, Dorkoosh FA (2012) Preparation and characterization of raloxifene nanoparticles using Rapid Expansion of Supercritical Solution (RESS). J Supercrit Fluids 63:169–179
Kikic I, De Zordi N, Moneghini M, Solinas D (2010) Solubility estimation of drugs in ternary systems of interest for the antisolvent precipitation processes. J Supercrit Fluids 55(2):616–622
Kim MS, Kim JS, Park HJ, Cho WK, Cha KH, Hwang SJ (2011) Enhanced bioavailability of sirolimus via preparation of solid dispersion nanoparticles using a supercritical antisolvent process. Int J Nanomedicine 6:2997–3009
Kipp JE (2004) The role of solid nanoparticle technology in the parenteral delivery of poorly water-soluble drugs. Int J Pharm 284(1–2):109–122
Ksibi H, Subra P, Garrabos Y (1995) Formation of fine powders of caffeine by RESS. Adv Powder Technol 6(1):25–33
Larson RG (1999) The structure and rheology of complex fluids. Oxford University Press, New York
Lengsfeld CS, Delplanque JP, Barocas VH, Randolph TW (2000) Mechanism governing microparticle morphology during precipitation by a compressed antisolvent: atomization vs nucleation and growth. J Phys Chem B 104(12):2725–2735
Li J, Rodrigues M, Paiva A, Matos HA, Gomes de Azevedo E (2005) Modeling of the PGSS process by crystallization and atomization. AIChE J 51(8):2343–2357
Li S, Liu Y, Liu T, Zhao L, Zhao J, Feng N (2011) Development and in-vivo assessment of the bioavailability of oridonin solid dispersions by the gas anti-solvent technique. Int J Pharm 411(1–2):172–177
Lim RTY, Ng WK, Tan RBH (2010) Amorphization of pharmaceutical compound by co-precipitation using supercritical anti-solvent (SAS) process (Part I). J Supercrit Fluids 53(1–3):179–184
Limayem I, Charcosset C, Fessi H (2004) Purification of nanoparticle suspensions by a concentration/diafiltration process. Sep Purif Technol 38:1–9
Lin C, Muhrer G, Mazzotti M, Subramaniam B (2003) Vapor-liquid mass transfer during gas antisolvent recrystallization: modeling and experiments. Ind Eng Chem Res 42(10):2171–2182
Lipinski CA (2001) Avoiding investment in doomed drugs. Is poor solubility an industry wide problem? Curr Drug Discov 1:17–19
Lipinski C (2002) Poor aqueous solubility—an industry wide problem in drug discovery. Am Pharm Rev 5:82–85
Liu G-T, Nagahama K (1996) Application of rapid expansion of supercritical solutions in the crystallization separation. Ind Eng Chem Res 35:4626–4634
Liu Y, Cheng C, Liu Y, Prud'homme RK, Fox RO (2008) Mixing in a multi-inlet vortex mixer (MIVM) for flash nano-precipitation. Chem Eng Sci 63(11):2829–2842

Liu G, Zhang D, Jiao Y, Zheng D, Liu Y, Duan C, Jia L, Zhang Q, Lou H (2012) Comparison of different methods for preparation of a stable riccardin D formulation via nano-technology. Int J Pharm 422(1–2):516–522

Liversidge GG, Cundy KC (1995) Particle size reduction for improvement of oral bioavailability of hydrophobic drugs: I. Absolute oral bioavailability of nanocrystalline danazol in beagle dogs. Int J Pharm 125(1):91–97

Liversidge EM, Liversidge GG, Cooper ER (2003) Nanosizing: a formulation approach for poorly-water-soluble compounds. Eur J Pharm Sci 18:113–120

Maa Y-F, Nguyen P-A, Sweeney T, Shire SJ, Hsu CC (1999) Protein inhalation powders: spray drying vs spray freeze drying. Pharm Res 16(2):249–254

Martin A, Cocero MJ (2004) Numerical modeling of jet hydrodynamics, mass transfer, and crystallization kinetics in the supercritical antisolvent (SAS) process. J Supercrit Fluids 32(1–3):203–219

Martin A, Cocero MJ (2008) Micronization processes with supercritical fluids: fundamentals and mechanisms. Adv Drug Deliv Rev 60(3):339–350

Martin A, Bouchard A, Hofland GW, Witkamp GJ, Cocero MJ (2007) Mathematical modeling of the mass transfer from aqueous solutions in a supercritical fluid during particle formation. J Supercrit Fluids 41(1):126–137

Martin A, Pham H, Kilzer A, Kareth S, Weidner E (2010) Micronization of polyethylene glycol by PGSS (particles from gas saturated solutions)-drying of aqueous solutions. Chem Eng Process 49:1259–1266

Matteucci ME, Hotze MA, Johnston KP, Williams RO III (2006) Drug nanoparticles by antisolvent precipitation: mixing energy versus surfactant stabilization. Langmuir 22(21):8951–8959

Matteucci ME, Brettmann BK, Rogers TL, Elder EJ, Williams RO, Johnston KP (2007) Design of potent amorphous drug nanoparticles for rapid generation of highly supersaturated media. Mol Pharm 4(5):782–793

Matteucci ME, Paguio JC, Miller MA, Williams RO, Johnston KP III (2008) Flocculated amorphous nanoparticles for highly supersaturated solutions. Pharm Res 25(11):2477–2487

Matteucci ME, Paguio JC, Miller MA III, Williams RO, Johnston KP (2009) Highly supersaturated solutions from dissolution of amorphous itraconazole microparticles at pH 6.8. Mol Pharm 6(2):375–385

Mendez-Santiago J, Teja AS (1999) The solubility of solids in supercritical fluids. Fluid Phase Equilibr 158–160:501–510

Miller MA, DiNunzio J, Matteucci ME, Ludher BS III, Williams RO, Johnston KP (2012) Flocculated amorphous itraconazole nanoparticles for enhanced in vitro supersaturation and in vivo bioavailability. Drug Dev Ind Pharm 38(5):557–570

Mueller M, Meier U, Kessler A, Mazzotti M (2000) Experimental study of the effect of process parameters in the recrystallization of an organic compound using compressed carbon dioxide as antisolvent. Ind Eng Chem Res 39(7):2260–2268

Muhrer G, Mazzotti M (2003) Precipitation of lysozyme nanoparticles from dimethyl sulfoxide using carbon dioxide as antisolvent. Biotechnol Prog 19(2):549–556

Muhrer G, Lin C, Mazzotti M (2002) Modeling the gas antisolvent recrystallization process. Ind Eng Chem Res 41(15):3566–3579

Muhrer G, Mazzotti M, Muller M (2003) Gas antisolvent recrystallization of an organic compound. Tailoring product PSD and scaling-up. J Supercrit Fluids 27(2):195–203

Muller RH, Bohm BHL (1997) Colloidal drug carriers expert meeting, 3rd meeting, Berlin, Germany, May 29–31, 1997. In: Mueller RH, Benita S, Boehm BHL (eds) Nanosuspensions. Medpharm Scientific, Berlin, pp 149–174

Muller RH, Jacobs C, Kayser O (2001) Nanosuspensions as particulate drug formulations in therapy. Rationale for development and what we can expect for the future. Adv Drug Deliv Rev 47(1):3–19

Mullers K, Paisana M, Wahl MA (2015) Simultaneous Formation and Micronization of Pharmaceutical Cocrystals by Rapid Expansion of Supercritical Solutions (RESS). Pharm Res 32(2):702–713

Napper DH (1983) Polymeric stabilization of colloidal dispersions. Academic, New York
Nguyen XC, Herberger JD, Burke PA (2004) Protein powders for encapsulation: a comparison of spray-freeze drying and spray drying of darbepoetin alfa. Pharm Res 21(3):507–514
Noyes AA, Whitney WR (1897) The rate of solution of solid substances in their own solutions. J Am Chem Soc 19:930–934
Okamoto H, Danjo K (2008) Application of supercritical fluid to preparation of powders of high-molecular weight drugs for inhalation. Adv Drug Deliv Rev 60(3):433–446
Overhoff KA, Engstrom JD, Chen B, Scherzer BD, Milner TE, Johnston KP, Williams RO (2007a) Novel ultra-rapid freezing particle engineering process for enhancement of dissolution rates of poorly water-soluble drugs. Eur J Pharm Biopharm 65(1):57–67
Overhoff KA, Moreno A, Miller DA, Johnston KP, Williams RO (2007b) Solid dispersions of itraconazole and enteric polymers made by ultra-rapid freezing. Int J Pharm 336(1):122–132
Overhoff KA, Johnston KP, Tam J, Engstrom J, Williams RO III (2009) Use of thin film freezing to enable drug delivery: a review. J Drug Deliv Sci Technol 19(2):89–98
Padrela L, Rodrigues MA, Velaga SP, Matos HA, de Azevedo EG (2009) Formation of indomethacin-saccharin cocrystals using supercritical fluid technology. Eur J Pharm Sci 38(1):9–17
Padrela L, Rodrigues MA, Velaga SP, Fernandes AC, Matos HA, Gomes de Azevedo E (2010) Screening for pharmaceutical cocrystals using the supercritical fluid enhanced atomization process. J Supercrit Fluids 53(1–3):156–164
Pandit N, Trygstad T, Croy S, Bohorquez M, Koch C (2000) Effect of salts on the micellization, clouding, and solubilization behavior of pluronic F127 solutions. J Colloid Interface Sci 222:213–220
Pang P, Englezos P (2002) Phase separation of polyethylene oxide (PEO)-water solution and its relationship to the flocculating capability of the PEO. Fluid Phase Equilibr 194–197:1059–1066
Pathak P, Meziani MJ, Desai T, Sun Y-P (2004) Nanosizing drug particles in supercritical fluid processing. J Am Chem Soc 126(35):10842–10843
Pathak P, Meziani MJ, Desai T, Sun Y-P (2006) Formation and stabilization of ibuprofen nanoparticles in supercritical fluid processing. J Supercrit Fluids 37(3):279–286
Pathak P, Prasad GL, Meziani MJ, Joudeh AA, Sun Y-P (2007) Nanosized paclitaxel particles from supercritical carbon dioxide processing and their biological evaluation. Langmuir 23(5): 2674–2679
Park J, Cho W, Cha KH, Ahn J, Han K, Hwang SJ (2013) Solubilization of the poorly water soluble drug, telmisartan, using supercritical anti-solvent (SAS) process. Int J Pharm 441(1–2):50–55
Perez de Diego Y, Wubbolts FE, Jansens PJ (2006) Modelling mass transfer in the PCA process using the Maxwell–Stefan approach. J Supercrit Fluids 37(1):53–62
Perrut M, Jung J, Leboeuf F (2005) Enhancement of dissolution rate of poorly-soluble active ingredients by supercritical fluid processes: Part I: Micronization of neat particles. Int J Pharm 288(1):3–10
Pestieau A, Krier F, Lebrun P, Brouwers A, Streel B, Evrard B (2015) Optimization of a PGSS (particles from gas saturated solutions) process for a fenofibrate lipid-based solid dispersion formulation. Int J Pharm 485(1–2):295–305
Pratsinis SE (1988) Simultaneous nucleation, condensation, and coagulation in aerosol reactors. J Colloid Interface Sci 124(2):416–427
Pustulka KM, Wohl AR, Lee HS, Michel AR, Han J, Hoye TR, McCormick AV, Panyam J, Macosko CW (2013) Flash nanoprecipitation: particle structure and stability. Mol Pharm 10(11):4367–4377
Rabinow BE (2004) Nanosuspensions in drug delivery. Nat Rev Drug Discov 3(9):785–796
Rasenack N, Muller BW (2002) Dissolution rate enhancement by in situ micronization of poorly water-soluble drugs. Pharm Res 19(12):1894–1900
Reverchon E, Della Porta G (1999) Production of antibiotic micro- and nano-particles by supercritical antisolvent precipitation. Powder Technol 106(1–2):23–29
Reverchon E, Pallado P (1996) Hydrodynamic modeling of the RESS process. J Supercrit Fluids 9(4):216–221

Reverchon E, Donsi G, Gorgoglione D (1993) Salicylic acid solubilization in supercritical CO_2 and its micronization by RESS. J Supercrit Fluids 6(4):241–248
Reverchon E, Della Porta G, Falivene MG (2000) Process parameters and morphology in amoxicillin micro and submicro particles generation by supercritical antisolvent precipitation. J Supercrit Fluids 17(3):239–248
Reverchon E, Caputo G, De Marco I (2003a) Role of phase behavior and atomization in the supercritical antisolvent precipitation. Ind Eng Chem Res 42(25):6406–6414
Reverchon E, De Marco I, Caputo G, Della Porta G (2003b) Pilot scale micronization of amoxicillin by supercritical antisolvent precipitation. J Supercrit Fluids 26(1):1–7
Reverchon E, De Marco I, Torino E (2007) Nanoparticles production by supercritical antisolvent precipitation: a general interpretation. J Supercrit Fluids 43(1):126–138
Reverchon E, De Marco I (2011) Mechanisms controlling supercritical antisolvent precipitate morphology. Chem Eng J 169(1–3):358–370
Rodrigues M, Peiriço N, Matos H, Gomes de Azevedo E, Lobato MR, Almeida AJ (2004) Microcomposites theophylline/hydrogenated palm oil from a PGSS process for controlled drug delivery systems. J Supercrit Fluids 29(1–2):175–184
Rodrigues MA, Li J, Padrela L, Almeida A, Matos HA, de Azevedo EG (2009) Anti-solvent effect in the production of lysozyme nanoparticles by supercritical fluid-assisted atomization processes. J Supercrit Fluids 48(3):253–260
Rogers TL, Johnston KP, Williams RO III (2001a) Solution-based particle formation of pharmaceutical powders by supercritical or compressed fluid CO_2 and cryogenic spray-freezing technologies. Drug Dev Ind Pharm 27(10):1003–1015
Rogers TL, Gillespie IB, Hitt JE, Fransen KL, Crowl CA, Tucker CJ, Kupperblatt GB, Becker JN, Wilson DL, Todd C, Broomall CF, Evans JC, Elder EJ (2004) Development and characterization of a scalable controlled precipitation process to enhance the dissolution of poorly water-soluble drugs. Pharm Res 21(11):2048–2057
Rossmanna M, Braeuerb A, Leipertz A, Schluecker E (2013) Manipulating the size, the morphology and the polymorphism of acetaminophen using supercritical antisolvent (SAS) precipitation. J Supercrit Fluids 82:230–237
Sarkari M, Brown J, Chen X, Swinnea S, Williams RO, Johnston KP (2002) Enhanced drug dissolution using evaporative precipitation into aqueous solution. Int J Pharm 243(1–2):17–31
Sekhon BS (2010) Supercritical fluid technology: an overview of pharmaceutical applications. Int J PharmTechnol Res 2(1):810–826
Shah N, Sandhu H, Phuapradit W, Lyer R, Albano A, Desai D, Choi D, Tang K, Tian H, Chokshi H, Go Z, Malick W, Radinov R, Shankar A, Wolff S, Mair H (2010) Solid complexes with ionic polymers. Pharm Technol 32(12):46–47
Shah N, Sandhu H, Phuapradit W, Pinal R, Iyer R, Albano A, Chatterji A, Anand S, Choi DS, Tang K, Tian H, Chokshi H, Singhal D, Malick W (2012) Development of novel microprecipitated bulk powder (MBP) technology for manufacturing stable amorphous formulations of poorly soluble drugs. Int J Pharm 438(1–2):53–60
Shah N, Iyer RM, Mair HJ, Choi DS, Tian H, Diodone R, Fahnrich K, Pabst-PAvot A, Tang K, Scheubel E, Grippo JF, Moreira SA, Go Z, Mouskountakis J, Louie T, Ibrahim PN, Sandhu H, Rubia L, Chokshi H, Singhal D, Malick W (2013) Improved human bioavailability of vemurafenib, a practically insoluble drug, using an amorphous polymer-stabilized solid dispersion prepared by a solvent-controlled coprecipitation process. J Pharm Sci 102(3):967–981
Shen H, Hong S, Prud'homme RK, Liu Y (2011) Self-assembling process of flash nanoprecipitation in a multi-inlet vortex mixer to produce drug-loaded polymeric nanoparticles. J Nanopart Res 13(9):4109–4120
Shariati A, Peters CJ (2002) Measurements and modeling of the phase behavior of ternary systems of interest for the GAS process: I. The system carbon dioxide + 1-propanol + salicylic acid. J Supercrit Fluids 23(3):195–208

Shekunov BY, Hanna M, York P (1999) Crystallization process in turbulent supercritical flows. J Crystal Growth 198/199(Pt. 2):1345–1351

Shoyele SA, Cawthorne S (2006) Particle engineering techniques for inhaled biopharmaceuticals. Adv Drug Deliv Rev 58(9–10):1009–1029

Sinswat P, Gao X, Yacaman MJ, Williams RO, Johnston KP (2005) Stabilizer choice for rapid dissolving high potency itraconazole particles formed by evaporative precipitation into aqueous solution. Int J Pharm 302(1–2):113–124

Sinswat P, Matteucci ME, Johnston KP, Williams RO III (2007) Dissolution rates and supersaturation behavior of amorphous repaglinide particles produced by controlled precipitation. J Biomed Nanotechnol 3(1):18–27

Sohnel O, Garside J (1992) Precipitation: basic principles and industrial applications. Butterworth-Heinemann, Newton

Sporanox Package Insert (Janssen Pharmaceutica Products, L.P.)

Subramaniam B, Rajewski RA, Snavely K (1997) Pharmaceutical processing with supercritical carbon dioxide. J Pharm Sci 86(8):885–890

Tam JM, McConville JT, Williams RO, Johnston KP III (2008) Amorphous cyclosporin nanodispersions for enhanced pulmonary deposition and dissolution. J Pharm Sci 97(11):4915–4933

Thakur R, Gupta RB (2005) Rapid expansion of supercritical solution with solid cosolvent (RESS-SC) process: formation of griseofulvin nanoparticles. Ind Eng Chem Res 44(19):7380–7387

Thakur R, Gupta RB (2006a) Rapid expansion of supercritical solution with solid cosolvent (RESS-SC) process: formation of 2-aminobenzoic acid nanoparticle. J Supercrit Fluids 37(3):307–315

Thakur R, Gupta RB (2006b) Formation of phenytoin nanoparticles using rapid expansion of supercritical solution with solid cosolvent (RESS-SC) process. Int J Pharm 308(1–2): 190–199

Thote AJ, Gupta RB (2005) Formation of nanoparticles of a hydrophilic drug using supercritical carbon dioxide and microencapsulation for sustained release. Nanomedicine 1(1):85–90

Torino E, Marco ID, Reverchon E (2010) Organic nanoparticles recovery in supercritical antisolvent precipitation. J Supercrit Fluids 55:300–306

Tozuka Y, Miyazaki Y, Takeuchi H (2010) A combinational supercritical CO_2 system for nanoparticle preparation of indomethacin. Int J Pharm 386(1–2):243–248

Turk M (2000) Influence of thermodynamic behaviour and solute properties on homogeneous nucleation in supercritical solutions. J Supercrit Fluids 18(3):169–184

Turk M (2009) Manufacture of submicron drug particles with enhanced dissolution behaviour by rapid expansion processes. J Supercrit Fluids 47(3):537–545

Turk M, Bolten D (2010) Formation of submicron poorly water-soluble drugs by rapid expansion of supercritical solution (RESS): results for naproxen. J Supercrit Fluids 55:778–785

Turk M, Lietzow R (2008) Formation and stabilization of submicron particles via rapid expansion processes. J Supercrit Fluids 45:346–355

Turk M, Hils P, Helfgen B, Schaber K, Martin HJ, Wahl MA (2002) Micronization of pharmaceutical substances by the rapid expansion of supercritical solutions (RESS): a promising method to improve bioavailability of poorly soluble pharmaceutical agents. J Supercrit Fluids 22(1):75–84

Uchida H, Nishijima M, Sano K, Demoto K, Sakabe J, Shimoyama Y (2015) Production of theophylline nanoparticles using rapid expansion of supercritical solutions with a solid cosolvent (RESS-SC) technique. J Supercrit Fluids 105:128–135

Vaughn JM, Gao X, Yacaman M-J, Johnston KP, Williams RO (2005) Comparison of powder produced by evaporative precipitation into aqueous solution (EPAS) and spray freezing into liquid (SFL) technologies using novel Z-contrast STEM and complimentary techniques. Eur J Pharm Biopharm 60(1):81–89

Vemavarapu C, Mollan MJ, Needham TE (2009) Coprecipitation of pharmaceutical actives and their structurally related additives by the RESS process. Powder Technol 189(3):444–453

Weber M, Thies M (2002) Understanding the RESS process. In: Sun Y-P (ed) Supercritical fluid technology in materials science and engineering. Marcel Dekker, New York, pp 387–437
Weber A, Weiss C, Tschernjaew J, Kummel R (1999) Gas antisolvent crystallization.From fundamentals to industrial applications. Fraunhofer Institut Umwelt- Sicherheits- Energietechnik, Oberhausen, pp 235–238
Weber M, Russell LM, Debenedetti PG (2002) Mathematical modeling of nucleation and growth of particles formed by the rapid expansion of a supercritical solution under subsonic conditions. J Supercrit Fluids 23(1):65–80
Werling JO, Debenedetti PG (1999) Numerical modeling of mass transfer in the supercritical antisolvent process. J Supercrit Fluids 16(2):167–181
Werling JO, Debenedetti PG (2000) Numerical modeling of mass transfer in the supercritical antisolvent process: miscible conditions. J Supercrit Fluids 18(1):11–24
Westesen K, Siekmann B (1998) Solid lipid particles, particles of bioactive agents and methods for the manufacture and use thereof. US 5785976, 12 April 1994
Wubbolts FE, Bruinsma OSL, van Rosmalen GM (1999) Dry-spraying of ascorbic acid or acetaminophen solutions with supercritical carbon dioxide. J Crystal Growth 198/199(Pt. 1):767–772
Xu XM, Song YM, Ping QN, Wang Y, Liu XY (2006) Effect of ionic strength on the temperature-dependent behavior of hydroxypropyl methylcellulose solution and matrix tablet. J Appl Polym Sci 102:4066–4074
Yildiz N, Tuna S, Döker O, Çalimli A (2007) Micronization of salicylic acid and taxol (paclitaxel) by rapid expansion of supercritical fluids (RESS). J Supercrit Fluids 41(3):440–451
Young TJ, Johnston KP, Mishima K, Tanaka H (1999) Encapsulation of lysozyme in a biodegradable polymer by precipitation with a vapor-over-liquid antisolvent. J Pharm Sci 88(6):640–650
Young TJ, Mawson S, Johnston K (2000) Rapid expansion from supercritical to aqueous solution to produce submicron suspensions of water-insoluble drugs. Biotechnol Prog 16:402–407
Young TJ, Johnston KP, Pace GW, Mishra AK (2003) Phospholipid-stabilized nanoparticles of cyclosporine A by rapid expansion from supercritical to aqueous solution. AAPS PharmSciTech 5(1):1–16
Young TJ, Johnston KP, Pace GW, Mishra AK (2004) Phospholipid-stabilized nanoparticles of cyclosporin A by rapid expansion from supercritical to aqueous solution. AAPS PharmSciTech 5(1):70–85
Zhu Z, Anacker JL, Ji S, Hoye TR, Macosko CW, Prud'homme RK (2007) Formation of block copolymer-protected nanoparticles via reactive impingement mixing. Langmuir 23(21): 10499–10504
Zhu Z, Margulis-Goshen K, Magdassi S, Talmon Y, Macosko CW (2010) Polyelectrolyte stabilized drug nanoparticles via flash nanoprecipitation: a model study with β-carotene. J Pharm Sci 99(10):4295–4306
Zhu Z (2014) Flash nanoprecipitation: prediction and enhancement of particle stability via drug structure. Mol Pharm 11(3):776–786